LEVEL II (12)

DNA 5395F

CHARACTERIZATION OF PHOTOELECTRON EMISSION FOR SGEMP ANALYSIS

AD A095172

Melvin J. Bernstein

Advanced Research & Applications Corporation

1223 East Arques Avenue

Sunnyvale, California 94086

1 May 1980

Final Report for Period 1 January 1979—30 April 1980

CONTRACT No. DNA 001-79-C-0101

APPROVED FOR PUBLIC RELEASE;
DISTRIBUTION UNLIMITED.

1981

A

FILE COPY

Prepared for

Director

DEFENSE NUCLEAR AGENCY

Washington, D. C. 20305

81 2 19 036

Destroy this report when it is no longer
needed. Do not return to sender.

REPORT DOCUMENTATION PAGE		READ INSTRUCTIONS BEFORE COMPLETING FORM
1. REPORT NUMBER DNA 5395F	2. GOVT ACCESSION NO. AD-A095 172	3. RECIPIENT'S CATALOG NUMBER
4. TITLE (and Subtitle) CHARACTERIZATION OF PHOTOELECTRON EMISSION FOR SGEMP ANALYSIS		5. TYPE OF REPORT & PERIOD COVERED Final Report for Period 1 Jan 79—30 Apr 80
		6. PERFORMING ORG. REPORT NUMBER ARACOR-TR-38-2
7. AUTHOR(s) Melvin J. Bernstein		8. CONTRACT OR GRANT NUMBER(s) DNA 001-79-C-0101
9. PERFORMING ORGANIZATION NAME AND ADDRESS Advanced Research & Applications Corporation 1223 East Arques Avenue Sunnyvale, California 94086		10. PROGRAM ELEMENT, PROJECT, TASK AREA & WORK UNIT NUMBERS Subtask R99QAXEE502-23
11. CONTROLLING OFFICE NAME AND ADDRESS Director Defense Nuclear Agency Washington, D.C. 20305		12. REPORT DATE 1 May 1980
		13. NUMBER OF PAGES 122
14. MONITORING AGENCY NAME & ADDRESS(if different from Controlling Office)		15. SECURITY CLASS (of this report) UNCLASSIFIED
		15a. DECLASSIFICATION DOWNGRADING SCHEDULE

16. DISTRIBUTION STATEMENT (of this Report)

Approved for public release; distribution unlimited.

17. DISTRIBUTION STATEMENT (of the abstract entered in Block 20, if different from Report)

18. SUPPLEMENTARY NOTES

19. KEY WORDS (Continue on reverse side if necessary and identify by block number)

System Generated Electromagnetic Pulse (SGEMP)
SGEMP Photoemission
Photoelectron Yield
Primary Electron Energy Spectra
Primary Electron Yields
Secondary Electron Yields
X-ray Photoemission

20. ABSTRACT (Continue on reverse side if necessary and identify by block number)

Photoelectron emission characteristics from SGEMP-relevant materials have been determined using both pulsed and steady-state x radiation in the 1-6 keV range. The photoemission parameters determined were spectral yields of primary electrons and total yields of secondary electrons. A magnetic spectrometer was developed to determine the time-resolved spectral yields of primary electrons generated by pulsed plasma radiation; the total yields were measured using X-ray diodes. To determine the yields of primary and secondary

DD FORM 1473   EDITION OF 1 NOV 65 IS OBSOLETE

20. ABSTRACT (Continued)

electrons generated by steady-state monochromatic X-rays, a retarding poten-
tial method was used. The spectral yields generated by monochromatic radia-
tion were also determined using a magnetic spectrometer. Emitter materials
included the following conductors and dielectrics: aluminum, anodized
aluminum, gold, silver, copper, glass, silicon, graphite, Mylar, Kapton, Tef-
lon, solar-cell cover glass and white thermal paint. Those materials studied
using both the pulsed and steady-state radiation exhibited good agreement of
primary yields. Each primary-electron energy spectrum was consistent with
atomic absorption edges in the material.

PREFACE

1

TABLE OF CONTENTS

LIST OF ILLUSTRATIONS

LIST OF TABLES

I   INTRODUCTION

The exposure of an orbiting spacecraft to exoatmospheric
nuclear x radiation results in photoelectron emission from all
irradiated surfaces. This pulsed electron emission is the driving
mechanism for system generated electromagnetic pulse (SGEMP) ef-
fects which could cause unacceptable electronic problems in a
spacecraft. In order to analyze and predict SGEMP responses, it
is necessary to know the energy distribution and the yield of the
emitted photoelectrons. This report gives the results of a set
of studies to characterize photoemission from materials used on
satellites and/or during SGEMP experiments. These studies in-
cluded the use of both pulsed and steady-state x radiation.

The interaction of x radiation with material generates photo-
electrons, Auger electrons and Compton electrons, all referred to
here as primary electrons, that have energies extending from the
incident x-ray energies down to nearly zero. These primary elec-
trons then produce in the material secondary electrons with ener-
gies averaging only a few eV. For the irradiation intensities of
interest to system responses, space-charge effects are expected
to limit the emission of low-energy electrons. However, when
satellites are highly charged by the ambient electrons in space,
the SGEMP responses could be enhanced significantly by the
secondary-electron emission. Therefore, the present studies were
directed at identifying the characteristics of both primary and
secondary electrons. The characteristics of photoelectron emis-
sion include the yield (number of electrons per incident photon),
the energy distribution of these electrons and the angular distri-
bution.

There are many programs directed at developing means to predict SGEMP responses. One of these, denoted the SKYNET series, has used the intense pulsed radiation generated by the OWL II' exploding-wire plasma radiation source (PRS) at Physics International Company (PI). To obtain the photoelectron spectral yields needed for the analysis of these results, one could measure the x-ray spectral intensity and apply an empirical/theoretical photo-emission computer code.[1,2] Unfortunately, besides the uncertainties inherent in the x-ray measurements themselves, there have been sub-stantial uncertainties in the characterization of surface materials and in the accuracy of available computer codes, especially at low photon energies. Therefore, a magnetic photoelectron spectrometer system (PESS) was designed and developed to give direct measurements of the photoelectron spectral yields generated by the PRS x radiation incident on materials of interest to these SKYNET SGEMP tests. In addition to the PESS instrument used for determining the energy spectra of pulsed photoelectron emission, auxilliary instrumenta-tion was used during these SKYNET experiments. Thermopile calori-meters were used to measure the x-ray fluence and an array of x-ray diodes (XRD) was used for total photoemission measurements.

Complementary to the SKYNET pulsed photoelectron measurements were photoemission studies using low-energy, steady-state mono-chromatic x rays. Such steady-state studies provided an accurate data set of photoemission spectral yields as a function of x-ray energy from materials of interest. These data can also be used to verify photoemission computer codes being developed under DNA contract. The steady-state portion of this program was subdivided into two experimental parts: a) determination of primary and secondary electron yields and b) determining the energy distribu-tion of primary electrons.

Section II of this report gives the design considerations and
engineering aspects of the PESS instrumentation plus the auxilliary
equipment used during the pulsed studies. Section III gives the
results of the pulsed measurements with an analysis of the results
in Section IV. The experimental techniques and results of the
steady-state yield measurements are described in Section V while
the steady-state spectral measurements and results are given
in Section VI. Section VII provides a summary of supporting com-
putations by Systems Sciences and Software (SSS) to calibrate the
PESS by determining the effects of space charge and applied electric
fields on electron orbits. A comparison of pulsed and steady-state
results is given in Section VIII along with a comparison of DNA-
supported theoretical yields to the measured values. Conclusions
and recommendations are given in Section IX.

II. SKYNET INSTRUMENTATION

The instrumentation required for diagnostic support to the
SKYNET experiments consisted of the following: photoelectron spec-
trometer, calorimeters, x-ray diodes, and associated data-recording
equipment.

A. PHOTOELECTRON SPECTROMETER SYSTEM (PESS)

1. Spectrometer Design:

The primary objective of the SKYNET Diagnostic support was to
develop instrumentation for determining the energy distribution of
photoelectron emission generated by the OWL II' exploding-wire x-ray
spectrum. The transient nature of the x-ray source required that
the emitted photoelectrons be separated according to their energies
and detected simultaneously by an array of detectors having suitable
time resolution. In order to use an array of detectors and have a
good electron-collection efficiency, it was decided to use a magne-
tic field for energy resolution rather than an electrostatic field.

The original design goals were to use eight detectors to cover
a factor of twenty in electron energy and to have a time resolution
of 3 nanoseconds. For the OWL II' x-ray spectrum, the electron
energies of interest were under 5 keV. Therefore, the required mag-
netic field for deflecting the electrons through 180° could be
much less than 10^{-2} Tesla (100 Gauss). For this range of fields,
it was preferable to use an air-core magnetic solenoid which has
several advantages over the use of a permanent magnet. First of
all, the magnetic field could be varied easily by changing the
current flowing through the coil. In addition, the geometry permit-
ted use of a larger divergence in the electron trajectories. Other
advantages of the air-core solenoid were: lighter weight, lower
cost, and faster procurement time.

The designed instrument is referred to as the photoelectron spectrometer system (PESS). A cross section of the magnetic spectrometer is shown schematically in Figure 1. X radiation entered the spectrometer through a port on the side arm and was incident onto the photoemitter at 60° to the surface normal. A fraction of the emitted photoelectrons passed through a set of defining apertures into the spectrometer chamber. There the axial magnetic field provided energy resolution and guided the electrons to a set of eight electromagnetically-shielded Faraday cups. In an ideal configuration, the electrons would follow 180° orbits from aperture to cups. However, the constraint of a large energy range led to placing the cup array at a lesser angle. Two Faraday cup arrays were used and the electrons followed orbits averaging 157° or 168°.

The entrance port on the sidearm of the spectrometer had a 2.5-cm-diameter collimating aperture so that the x radiation was incident only on the photoemitter face. The shank of the emitter was undercut so it was shadowed from the x rays while the mounting flange at the rear was sufficiently remote that photoelectrons could not reach the aperture. A set of aperture plates were placed in the channel to the main chamber to minimize the number of scattered electrons passing into the chamber. The photoemitter was originally mounted on a grounded support. Subsequently, this mounting was changed to a coaxial feedthrough so that the photoemitter could be biased and/or the total photoemission current could be monitored.

A photograph of the spectrometer is shown in Figure 2. The vacuum chamber and side arm were constructed of aluminum. A magnet coil 20 cm in diameter by 25 cm long was wound on the cylindrical chamber leaving a 2 cm gap for the electron aperture. The coil current i_B was generated by an adjustable power supply. For the spectrometer geometry and range of i_B, electron energies could be measured within the limits of 0-15 keV.

13

COAXIAL FEEDTHROUGH

PHOTOEMITTER

MAGNET COIL
ON VACUUM
CHAMBER

METAL
POSTS

ELECTRON
APERTURE

A
B
C
D
E
F
G
H

e

e

$\odot B_z$

├── 5 cm ──┤

R.F. SHIELDED
FARADAY CUPS
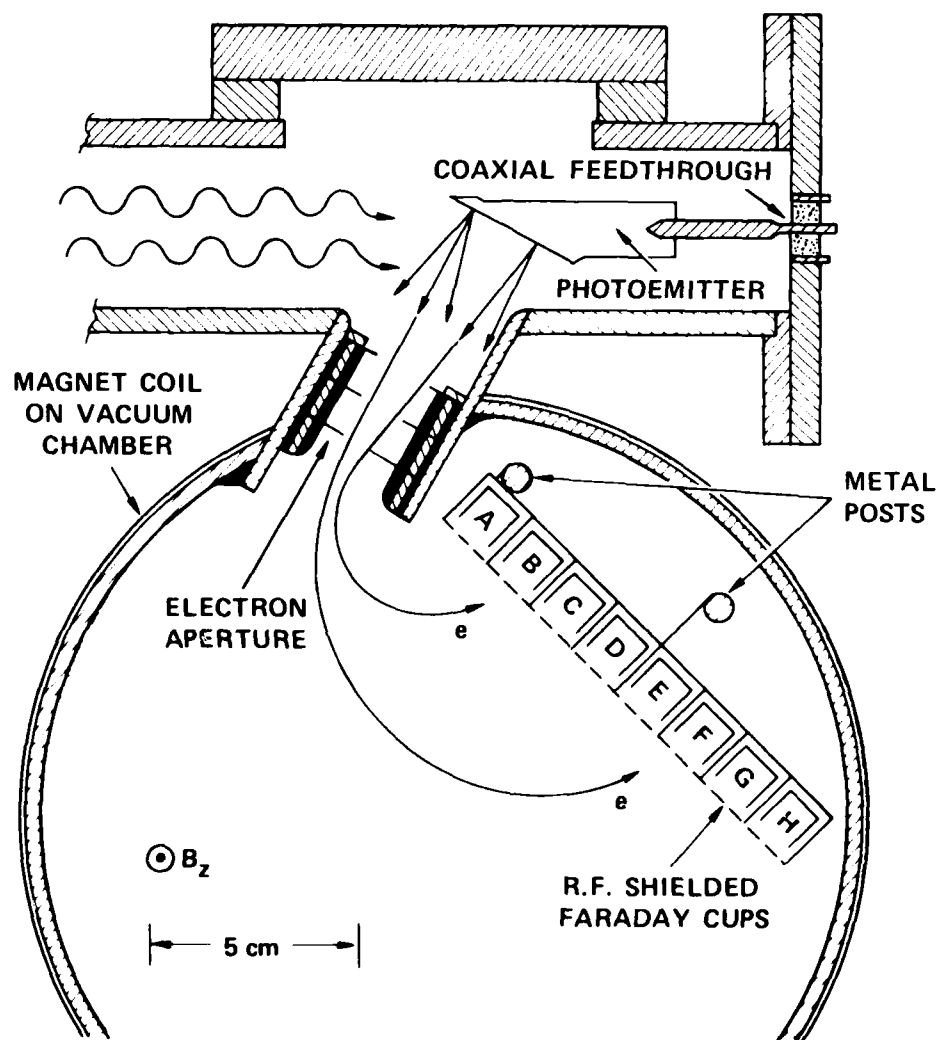
Figure 1   Cross section of magnetic photoelectron spectro-
            meter, PESS

14
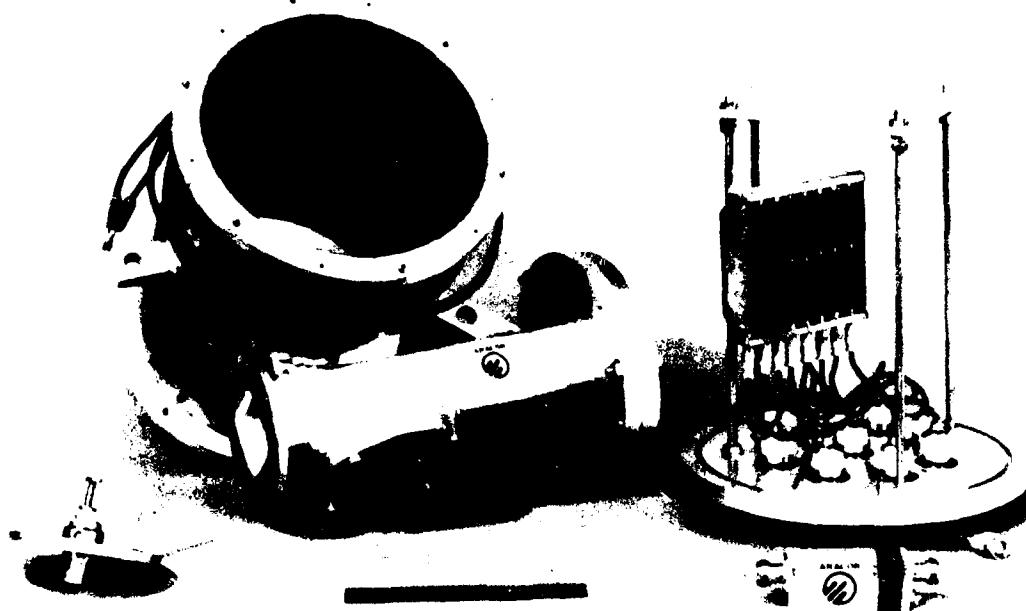
Figure 2   Photograph of magnetic photoelectron spectrometer,
           PESS.   Clockwise, components are photoemitter mounting,
           chamber, Faraday-cup array and a pulse amplifier

15

2. Magnetic-Field Calibration

A Hall probe was used to measure the axial component of the magnetic field, B_z, as a function of radius at three axial heights $Z = 0$ (midplane), 2 and 4 cm. The results are given in Figure 3. At the center of the coil, the measured value of 11.7 gauss/ampere agrees well with a value of 11.85 gauss/ampere calculated for the coil geometry. The last electron aperture was at 9.2 cm from the coil center while the photoemitter surface was about 14 cm from the axis. In this region, the magnetic field was an order-of-magnitude lower than the field inside the chamber. Thus, we could neglect curvature of the electron trajectories between the emitter and aperture.

Calibration of the magnetic field was confirmed also by subsequent operation of the PESS with the photoemitter biased negatively. In this case, low-energy secondary electrons were accelerated and detected in the Faraday cup corresponding to the appropriate energy.

3. Electron Detectors

The electron detectors were a set of Faraday cups formed of sheet brass. These cups were enclosed and electromagnetically isolated from each other by a grounded structure covered on the front by a semi-transparent brass screen. The cup dimensions were 10 mm wide, 10 mm deep and 70 mm high (parallel to magnetic field) with a 14.5 mm center-to-center spacing. This depth-to-width ratio for each cup minimized electron backscatter and a carbon coating in the form of Aquadag[3] further reduced the electron backscatter.
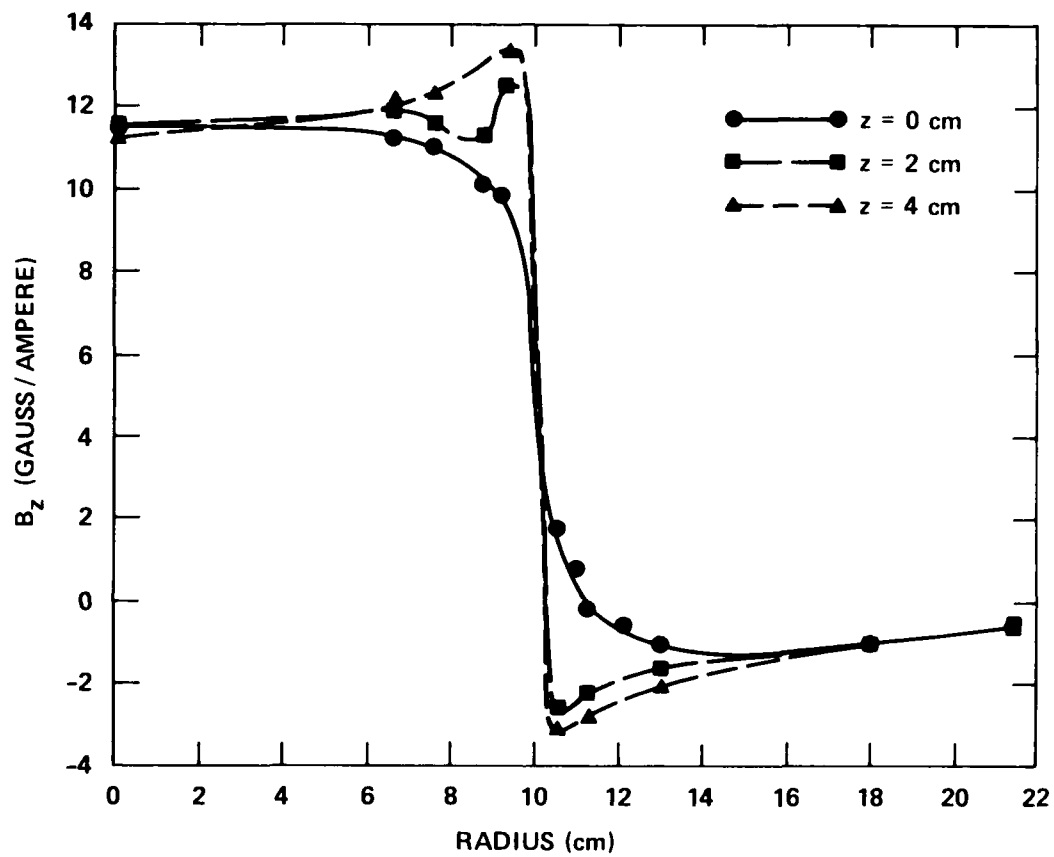
Figure 3   Axial magnetic field of PESS as a function of radius and distance from midplane

The electron signal from each Faraday cup was transmitted on
a RG-174 coaxial cable to a vacuum feedthrough. Since each cup
would detect only a small fraction of the emitted photoelectrons,
pulse amplifiers were used to increase the signal levels before
transmission on long cables to the recording instrumentation.
Each Faraday cup was directly grounded through 50 ohms to provide
the proper input for the amplifier. These pulse amplifiers, had
gains measured to be 28 to 31 dB when driven by a 50-ohm source.[4]
The gains of these amplifiers were routinely measured at the begin-
ning and end of each test series. The frequency response of these
units were within 3 dB from about 20 kHz to better than 600 MHz and
the output noise was less than 2 mV at full bandwidth.

Crosstalk between the Faraday cups was checked by injecting
a fast-rising narrow pulse onto one cup and observing the pickup
on adjacent cups. The electromagnetic isolation was found to be
better than 80 dB. The RF shielding on each cup also attenuated
sufficiently the pickup of fields accompanying the electron pulse.

4. Calibration of PESS

Calibration factors were needed to determine the electron
energy, energy resolution and electron collection efficiency in
the magnetic photoelectron spectrometer (PESS). Using the basic
laws of physics, these calibration factors were derived from the
geometry of the system, specifically the shapes and positions of
the photoemitter, electron aperture and Faraday cups, and from the
magnetic field. From the field plots in Figure 3, the magnetic
field was considered to be uniform between the aperture and the
cups, while the much weaker field between the photoemitter and the
aperture was assumed to have negligible effect on electron trajec-
tories.

The calculated calibration factors for the electron energy and energy resolution depended primarily on the sizes and orientation of the electron aperture and Faraday cups. A secondary factor was the angular distribution of electron trajectories through the aperture.

The electron aperture was 10 mm wide by 8 mm high and each Faraday cup was 10 mm wide. Distances, y, from the center of the aperture to the centers of the eight cups were: 35, 50, 64, 78, 93, 107, 122 and 136 mm. The energy of an electron is proportional to the square of its cyclotron radius and to the square of the magnetic field. For 180° focusing of electrons, the mean energy, E_o, of detected electrons is given in terms of the applied magnet coil current, i_B, and the diameter of the orbit, y, by the following expression,

$$E_o = 3.01 \ (i_B y)^2 \ eV$$

where i_B is in ampere and y in cm. The mean electron energies given by this expression are plotted in Figure 4 as a function of solenoid current for the eight Faraday cups. At any given magnetic field, the eight cups spanned about a factor of 20 in energy. On the average, the electrons appeared to have energies a few percent lower than was actual because of several factors: non-180° focusing, divergence of the electrons through the aperture and curvature of electron trajectories in the magnetic field ahead of aperture. Some of these effects partially offset one another. These calculated values of the energy calibration factors were in good agreement with measurements of accelerated secondary electrons described later in the report.

The beveled surface of the photoemitter mounting used for most of these measurements had dimensions of 19.5 mm wide by 9.5 mm high, giving an irradiated area of 1.81 cm^2. A few of the mounted

19
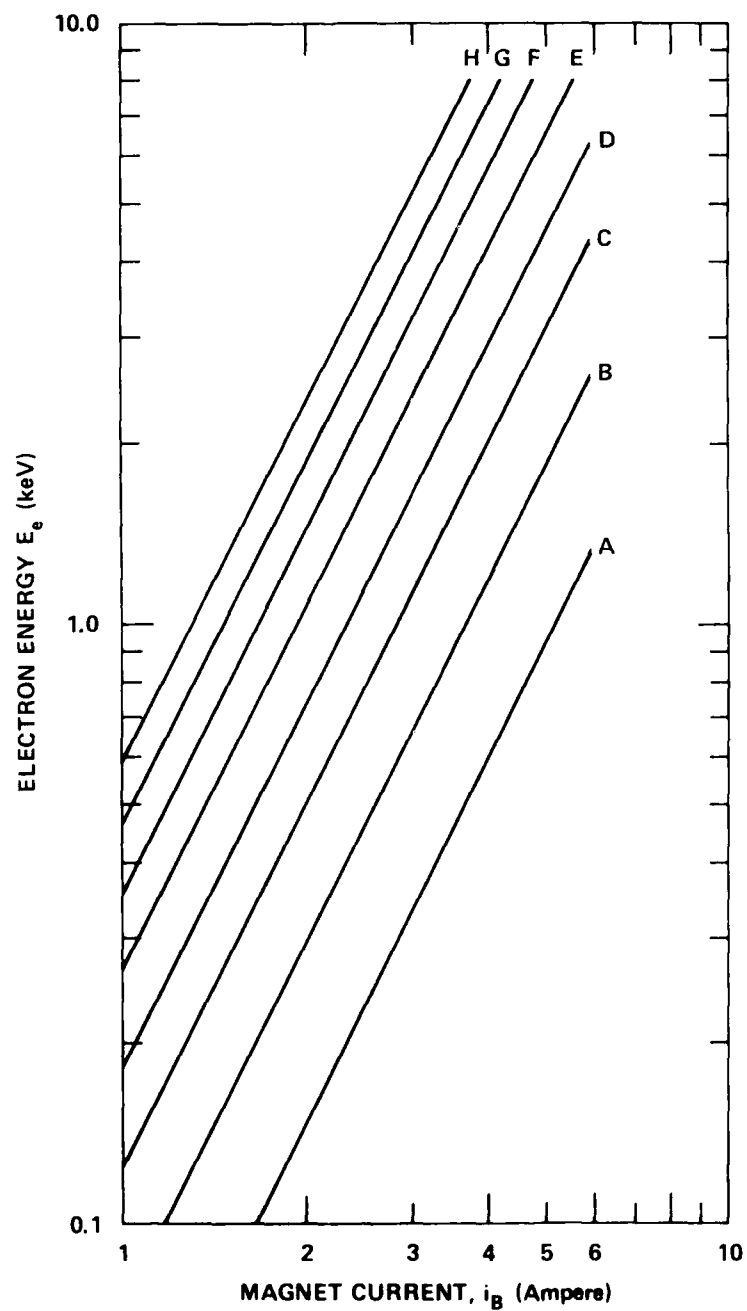
Figure 4   Calculated values of average electron energy, E_e to each Faraday cup as a function of magnet coil current I_B

emitter materials had slightly larger irradiated areas up to 2.0 cm^2; a larger emitter of 3.2 cm^2 was used in 1976 and at the beginning of the March 1977 series. The distance from the photo-emitter to the electron aperture was 59 mm so that the aperture subtended a solid angle of .023 sterradian relative to the photo-emitter. The geometry of the photoemitter and aperture resulted in an angular distribution of electron velocities through the aperture ranging up to $\pm 14^{\circ}$.

The energy spread, ΔE, of electrons collected by each Faraday cup depended on the cup width, aperture width, separation y and mean electron energy E_o. The angular divergence of the electrons and the location of the Faraday cups (166° or 156° orbits) added slightly to ΔE, but these were neglected since their effect fell within the experimental accuracy of the measurements. Electron scatter off the RF screen in front of the cups could also degrade the energy resolution, but did not appear to be a problem. In general, usage of a rectangular aperture and a rectangular detector results in a trapezoidal energy distribution for the collected electrons in a magnetic spectrometer. Since the aperture and cup widths were all 10 mm in PESS, the energy distribution was triangular peaked at E_o. However, because of the energy dependence on y^2, this triangular distribution is skewed slightly to higher energies. This effect is most pronounced for the cups nearest the aperture. The full base width of the energy distribution detected by each cup was $\Delta E/E_o = 2/y$ with y in cm, while the full width at half maximum was half the base width.

The fraction of the emitted electrons which were detected by the cups depended on three factors: angular distribution of the emitted electrons, the solid angle subtended by the aperture, and the fraction of transmitted electrons collected by the cups. The

21

angular distribution of the primary electrons is discussed in
Section IV of this report and the aperture subtended a solid angle
of 0.023 sterradian. With regard to the last factor, the primary
electrons were assumed to be smoothly distributed over the array
of Faraday cups. In this case, a collection efficiency of 45% was
obtained from the ratio of cup width to cup spacing (0.69) and the
transparency of the RF Screen (0.66).

B.   CALORIMETRY

The x-ray fluence needed to be measured on every shot, since
the output from the source varied greatly. Thermopile calorimeters
were used to measure the x-ray fluences transmitted through standard
windows onto the photoemitting surfaces. Each unit consisted
of 100 gold-foil calorimeters connected in series to give a much
larger signal than obtained with a single-foil calorimeter and
therefore a better signal-to-noise ratio. A photograph of one is
shown in Figure 5. A pair of thermopiles were sometimes used moun-
ted side by side on one diagnostic port to gain increased precision
in the measurements.

The response of these calorimeters had been determined to have
an accuracy of ±10%. However, the accuracy of the fluence measure-
ments was degraded on some shots by excessive electrical noise or
variations in the filter thicknesses. Comparison was also made
with the fluences measured by PI personnel using other calorimeters.

C.   X-RAY DIODES

Total photoemission yields were measured using a 7-channel
array of x-ray diodes (XRD), which is shown in Figure 6. This
unit had been developed for other DNA programs to study the plasma
radiation from pulsed-power facilities. The use of this instrument

22
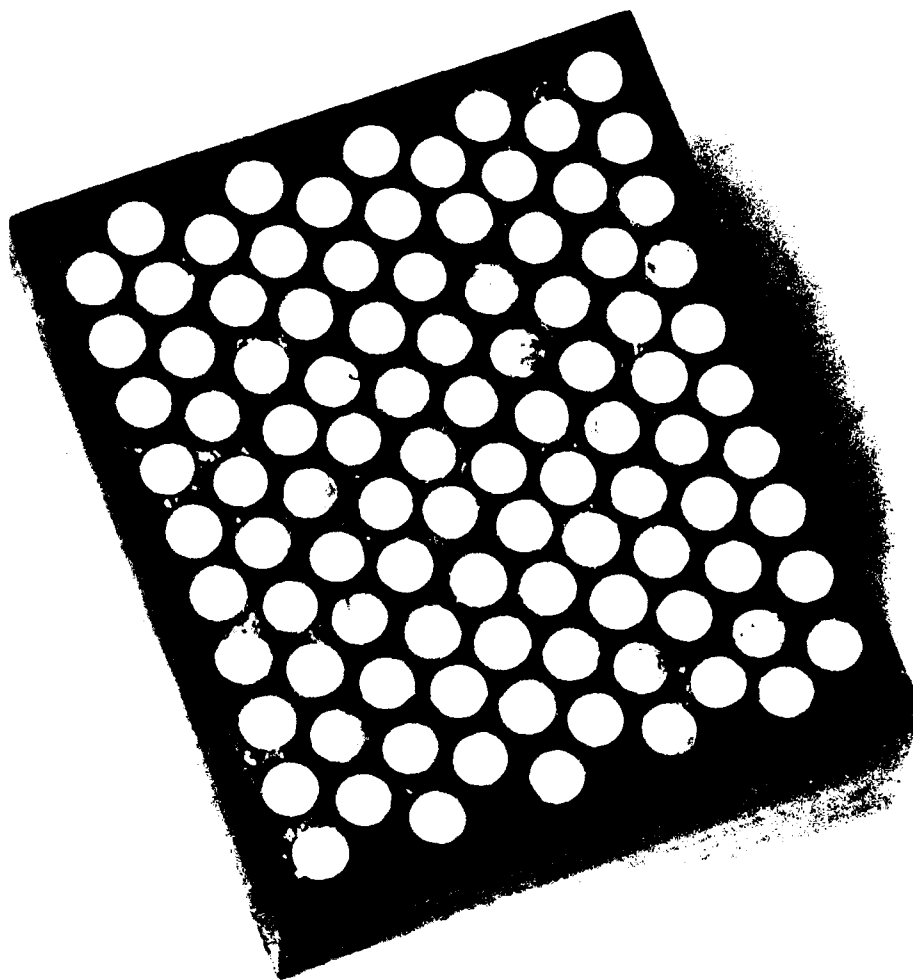
Figure 5   Photograph of 100 - junction thermopile calorimeter

23

Figure 6   Photograph of 7-channel XRD array.   From left to right
            components are: photocathode array, anode screens,
            filter holder, mounting ring

24

during the SKYNET experiments had the three goals of determining:
1) time variations in the x-ray flux with a resolution better than
1 nanosecond, 2) time variations in the x-ray spectrum, 3) total
photoemission yields from different materials.

D.   EXPERIMENTAL SETUP

The OWL II' exploding-wire facility at Physics International
Company (PI) had a horizontal axis with a cylindrical vacuum cham-
ber. A large number of diagnostic ports on the circumference of the
chamber allowed observation of the radially-emitted plasma radia-
tion. A picture of the facility is shown in Figure 7. Tests per-
formed by PI early in the SKYNET SGEMP program showed that the x-ray
flux was the same at all diagnostic ports. Distances from the
source axis to the various detectors were measured.

The diagnostic ports were provided with special fixtures having
thin sealed x-ray windows to isolate the diagnostic instrumentation
from the plasma environment. A separate vacuum system was used to
pump out all the diagnostic instruments. Because of the long pump-
out lines to the individual ports and the short pumping times (15-
20 minutes), the pressure in the instrumentation was typically 10^{-3}
to 10^{-2} Torr.

The x radiation was normally filtered by two layers of alumin-
ized Kapton, one of which was the sealed window. During any given
series of experiments, the same thickness of Kapton was used on all
ports. However, the Kapton obtained for each series had substantial
variations in thickness, ranging from 6.9 to 9.5 m (1.00-1.35 mg/cm^2).
This variation in thickness caused less change in transmitted x-ray
hardness than the shot-to-shot variations. In addition to the two
layers of Kapton, the x-rays were sometimes attenuated using fine-
mesh stainless-steel screen to avoid space-charge effects. A few
measurements were also made using extra layers of Kapton or Mylar
to harden the spectrum.

25
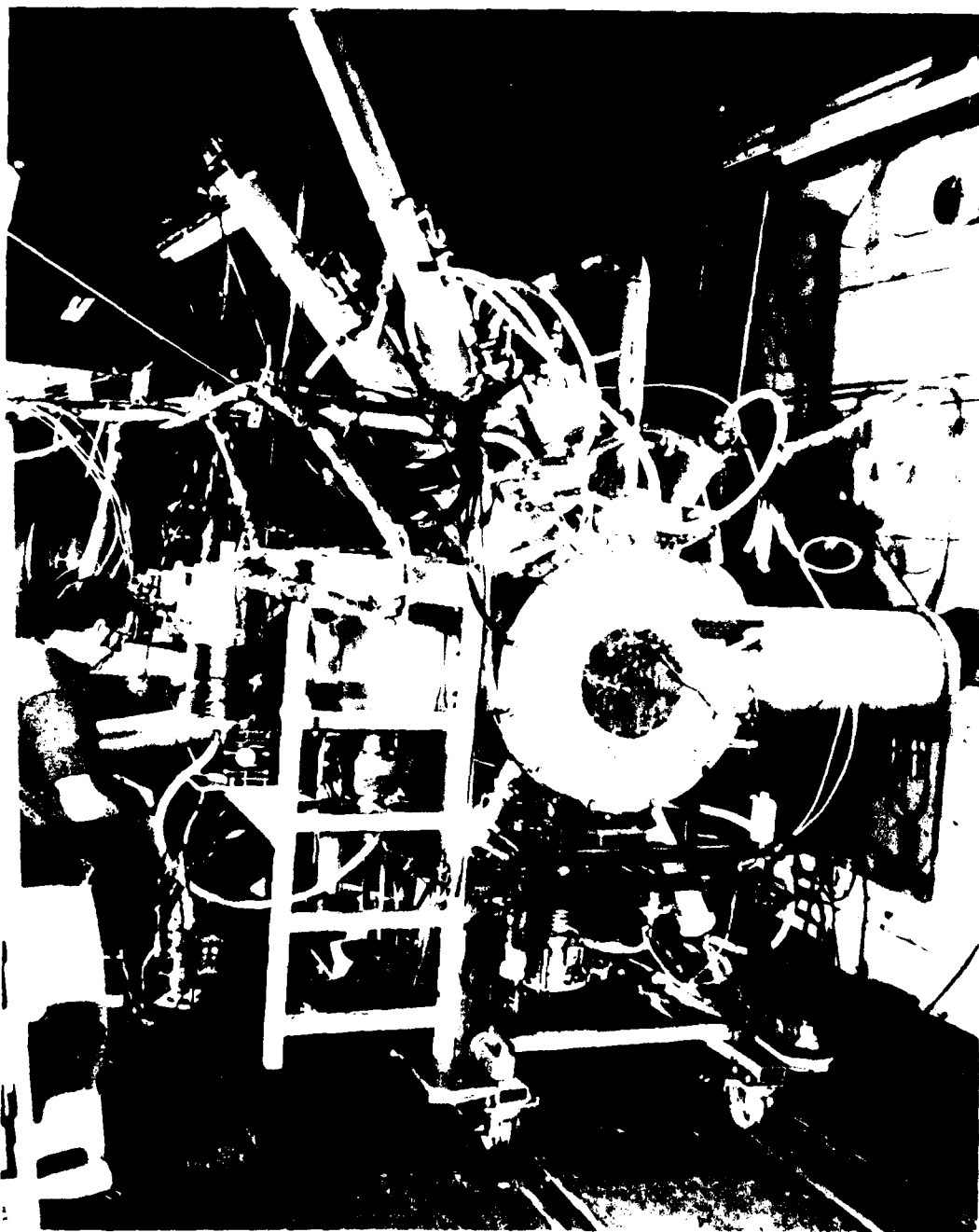
Figure 7   Photograph of diagnostic instrumentation mounted on
            OWL II' plasma facility

E.   SIGNAL RECORDING

1.   Signal Cables

Electrical signals from the eight Faraday cups in the PESS
the photoemitter, seven XRDs and two calorimeters were transmitted
on coaxial cables to the PI OWL II screen room. Because of the
large size and design of this particular screen room, some of the
electrical noise generated by pulsing of the OWL II facility pene-
trated the recording room and was often observed on low-level
signals. The magnitude of this electrical noise varied widely on
different test series.

The coaxial cables used for these measurements were RG-223 and
RG-214, both of which have double braided shields. It was antici-
pated that several of the PESS signals would be very low in ampli-
tude even after the 30-times amplification. Therefore, the eight
amplifiers and the associated bundle of cables were enclosed in an
aluminum can and a large braided-wire conduit connected to the
screen room. Many of the other coaxial cables were also enclosed
in braided-wire shields to ensure minimal noise pickups.

The length of the RG-223 cables was 45 feet (13.7 meters) so
that the attenuation was 2.2 db at 100 MHz increasing to 4.7 db at
400 MHz. The 15.2 meter RG-214 cables had RG-223 extensions in
the screen room, but the overall attenuation was still substantially
lower than the above values.

2.   Recording Instrumentation

The electrical signals were recorded using Tektronix oscil-
loscopes equipped with cameras and Polaroid film. During the
several series of experiments, various oscilloscope models were
used. The fastest recording was on some DNA-provided 7903 units

which had a bandwidth of 500 MHz. Other models used were R7704,
485, 475, 465 and 454A. These units had bandwidths of 100 to 300
MHz. Under favorable conditions, signals were recorded with time
resolutions under 3 nanoseconds and a noise level under 1 mV.
At other times, when the ambient electrical noise was high, band-
width limitation was used that slightly integrated the signals.

On the last series of experiments, a computer-based CAMAC
system was added for additional recording capability. This sys-
tem, developed for use on DNA programs, electronically recorded
the integrals of the transient signals and processed the data.
A picture of the CAMAC equipment is shown in Figure 8. In addi-
tion, the calorimeter signals were recorded and processed. Since
the number of oscilloscopes was limited, this CAMAC system permit-
ted the simultaneous recording of all the signals. The PESS and
XRD signals were recorded simultaneously as much as possible using
"power tees" on the signal lines.
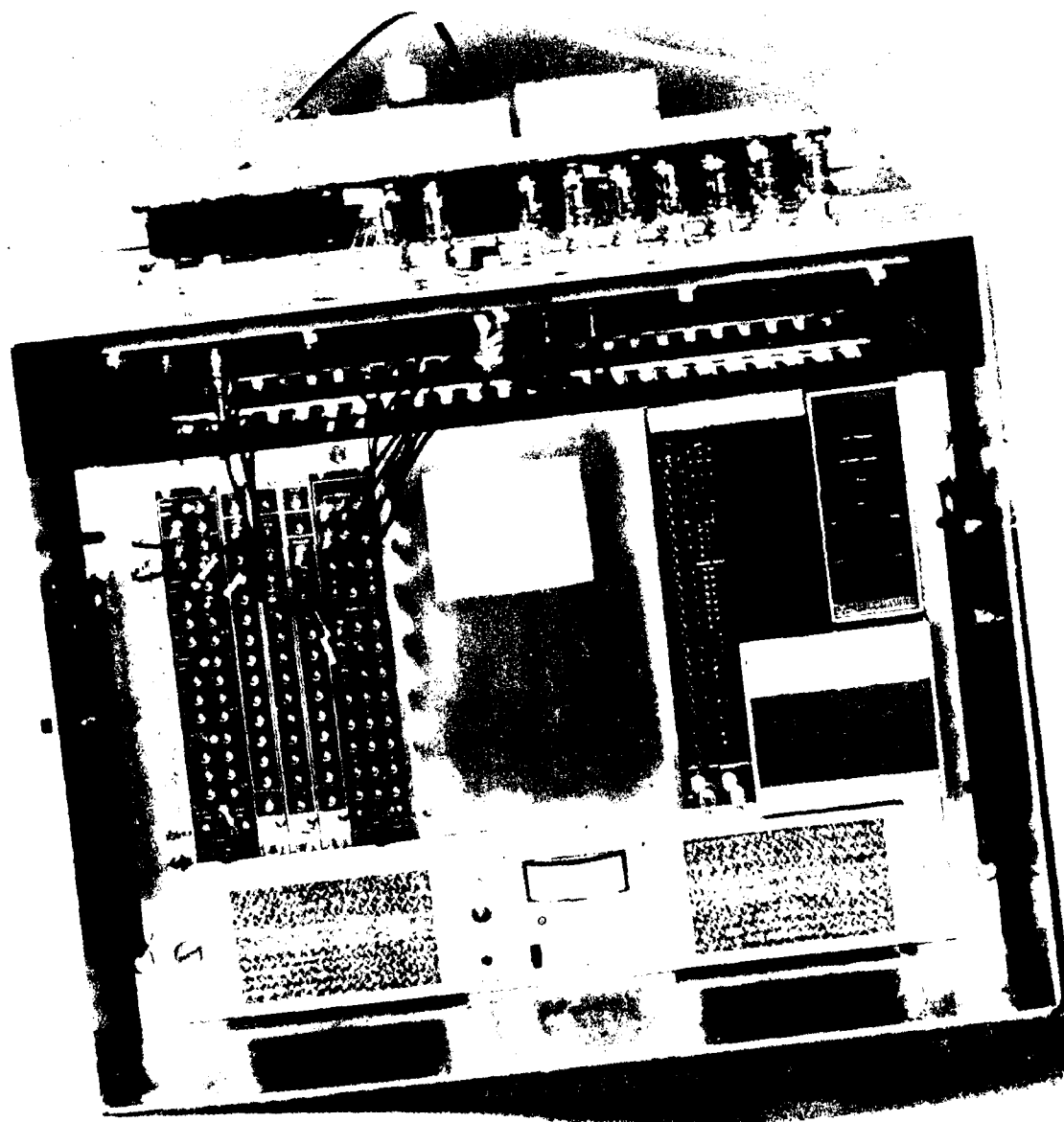
Figure 8. Photograph of CAMAC recording instrumentation

34

III.   SKYNET EXPERIMENTS

A.   X-RAY SOURCE

The results given in this report were obtained during four
SKYNET series of experiments on the PI OWL II' x-ray source, in
March-April 1977, August 1977, November 1977 and February - March
1979.   During these operations, a useful shot was one giving an
acceptable radiation output plus a properly-timed trigger pulse.
For the four series, the range of listed shot numbers and number
of useful shots were: No. 3602-3679 (64), No. 3903-3966 (56),
No. 4148-4188 (29), and No. 4759-4811 (29).   Some of these useful
shots provided only limited information because of various problems,
such as excessive noise on signals or improper vacuum in diagnostic
instrumentation.   For completeness, results for a silver emitter,
obtained during a SKYNET test series in 1976, are also included.
Some of the early results and analysis were published.[5]

The x-ray source in the PI OWL II' facility was formed from
magnesium-alloy aluminum wires and the output spectrum had been
measured by PI personnel during some early series of experiments.
This spectrum consisted of the following components: He-like Al
lines from 1.6 to 2.0 keV, H-like Al lines from 1.7 to 2.3 keV,
He-like recombination continuum above 2.0 keV, H-like recombination
continuum above 2.3 keV and magnesium lines from 1.3 to 1.9 keV.
Undoubtedly, there was also some hard bremsstrahlung radiation
extending up to over 100 keV.   The predominant lines were the
He-like and H-like Al lines at 1.60 and 1.72 keV, respectively.
About half of the recombination radiation was in the 2.0-2.3 keV
range although this continuum extended out beyond 4 keV.   The
radiation spectrum transmitted through the standard windows nor-
mally corresponded to an effective energy of about 1.8 keV and
could be modeled by assuming 40% at 1.65 keV, 50% at 2.0 keV and
10% at 2.5 keV.

The x-ray spectrum generated by the source was fairly repro-
ducible; the largest variations were in the higher-energy continuum
above 2 keV which ranged from 25 to 35% of the total. On the
other hand, the variation in thickness of the Kapton filters used
on different test series resulted in significantly different
x-ray transmission at the lowest x-ray energies. The x-ray
fluence and time history did exhibit large variations over the
course of the experiments; the fluence varied by up to an order of
magnitude and the pulse width varied by over a factor of three.

B.   PHOTOEMITTER MATERIALS

During the several test series, a large number of different
emitter materials were mounted in the PESS for measurements of
photoelectron energy spectra and yields. All the materials were
deemed relevant to understanding SGEMP responses. Several of
these materials were supplied by Mission Research Corporation (MRC)
as samples of what was mounted on models used in the SKYNET SGEMP
experiments; these included gold, silver, anodized aluminum, thick
Kapton, thick Teflon, white thermal paint and solar cell covers.
The other samples were selected as representative materials used
in the tests.

The samples were attached onto the beveled surface of the
photoemitter mounting using either small pieces of tape on the
back side or vacuum grease; the method depended on the thickness,
size and flexibility of the materials. Outgassing of the tape
was deemed to be inconsequential compared to that from other
components in the vacuum system.

Two or more samples of some materials were studied to deter-
mine reproducibility of the results. Cleanliness of the irradiated
surfaces was preserved as much as possible. It was found that the
primary yield was not sensitive to surface condition provided any
contamination from handling was wiped off. The following materials

31

were studied:

1. Aluminum foil (Al). Standard (18 m) and heavy-duty (25 m) Reynolds wrap.

2. Gold (Au). Two types of samples were used; one was gold-coated copper-clad PC board from MRC with the irradiated surface electrically connected to the mounting and the other sample was gold-coated copper foil.

3. Silver (Ag). A coating on PC board obtained from MRC.

4. Aluminum oxide (Al_2O_3). Anodized aluminum sheet obtained from MRC.

5. Copper foil (Cu).

6. Carbon (C). Two types of samples, graphite sheet and Aerodag.

7. Glass (SiO_2). A piece of a microscope slide 1 mm thick and a piece of microscope slide cover 0.2 mm thick were used. These glasses are assumed to have some small but significant percentages of sodium, potassium and/or calcium in their compositions.

8. Mylar ($C_{10}H_8O_4$). Thickness of 7 m with the backside in good electrical contract to the mounting.

9. Kapton ($C_{22}H_{10}N_2O_5$). Two sample types with thicknesses of 8 m and 125 m. Backsides of all samples were aluminized. Since the thin Kapton was obtained from rolls, there may have been some slight amount of aluminum on the front face. The thick sample was from MRC.

10. Teflon (CF_2). This sample from MRC was 125 m thick and the backside was coated with silver.

11. White Thermal Paint. Painted on aluminum foil from can provided by MRC, it contained an unknown amount of lead.

12. Solar Cell Cover (MgF_2). this photoemitter, obtained from MRC, was 0.3-mm-thick quartz (SiO_2) with an anti-reflection coating of MgF_2.

Samples of aluminum foil were studied on every test series to check the reproducibility of the PESS. The composition of some materials, notably dielectrics, were not well known. For instance, the glass microsocpe slides surely had some soda, lime or potash added to the silica. Polymers, such as Mylar and Kapton H, often have proprietary plasticizers added to the composition. Of course, the aluminum foil had the normal oxide layer with a thickness of 3-5 nanometers. In addition, all surfaces probably had a very thin layer of hydro-carbon contamination from the vacuum system.

All of these photoemitter materials were mounted on a beveled PESS mount with the surface normal pointed toward the electron aperture. In addition, a set of data was obtained with a gold emitter rotated about its support axis by angles of 60°, 90° and 180°. Data was also taken with an aluminum foil on a hemicylin-drical form 19 mm long with a radius of 5 mm.

Several of the above materials were used as photocathodes on the XRDs. These were aluminum foil, 0.2-mm glass, 6-μm Mylar, both thicknesses of Kapton (7 and 125 μm), 125-μm Teflon, white thermal paint and the 0.3 mm solar cell cover with its MgF_2 coating. In addition, graphite was used in the form of Aerodag and the brass mounting itself was used.

C.   GROUNDED PHOTOEMITTER RESULTS

The energy spectra of emitted primary electrons were deter-mined from the measurements using a grounded photoemitter (no applied bias) in the PESS. Data were obtained on several shots for a given photoemitter material. During these shots, the mag-net-coil current, i_B, was often set at different values to vary the energies of electrons detected by each Faraday cup. This permitted coverage of a broader range of electron energies from 0.1 to 5 keV, provided a smoother spectrum, and verified that all detector channels had the correct responses.

Three representative sets of signal traces are shown in
Figure 9-11 for photoemitters of gold and aluminum; the collected
electrons produced negative signals. The noise levels of 1-4 mV
on these signals is typical of half the usable shot data. On the
shots using a gold emitter, as in Figure 9, the time histories of
the signals were the same in the 0.6-2.4 keV range and exhibited
only a slight change in the relative peak amplitudes at higher
electron energies. At lower electron energies below 0.6 keV,
there was a significant smoothing in the structure of the time-
varying signals. Similar uniformity in the time history across
the electron energy spectrum was observed for most of the other
photoemitter materials. The largest time variations in the elec-
tron energy spectra were observed using an aluminum photoemitter,
as shown in Figures 10 and 11. On each of many such shots, the
electrons above 1.4 keV had a significantly different time his-
tory from that of electrons in the 0.7-1.4 keV range. A similar
result was observed in the emission from glass---electrons collected
on the channel centered at 1.82 keV had a smoother time history
than the electrons observed on the lower-energy channels.

The PESS data from each shot were used to derive a photoelec-
tron energy spectrum in the following fashion. From measurements on
the oscilloscope traces, values for the peak current, I_c, and
effective pulse width, τ, of each Faraday cup signal were obtained.
The accuracy of determining effective pulse widths was checked by
digitizing a few traces. In general, the pulse widths of all
signals for a given shot were nearly the same; variations were of
the types shown in Figures 9-11. The charge collected by each
cup was then $q = I_c \tau$ with an accuracy of $\pm$ 6%. Values for the
collected charges were also obtained during the last test series
from the integrated signals measured on the CAMAC system. XRD
signals were handled in the same way.
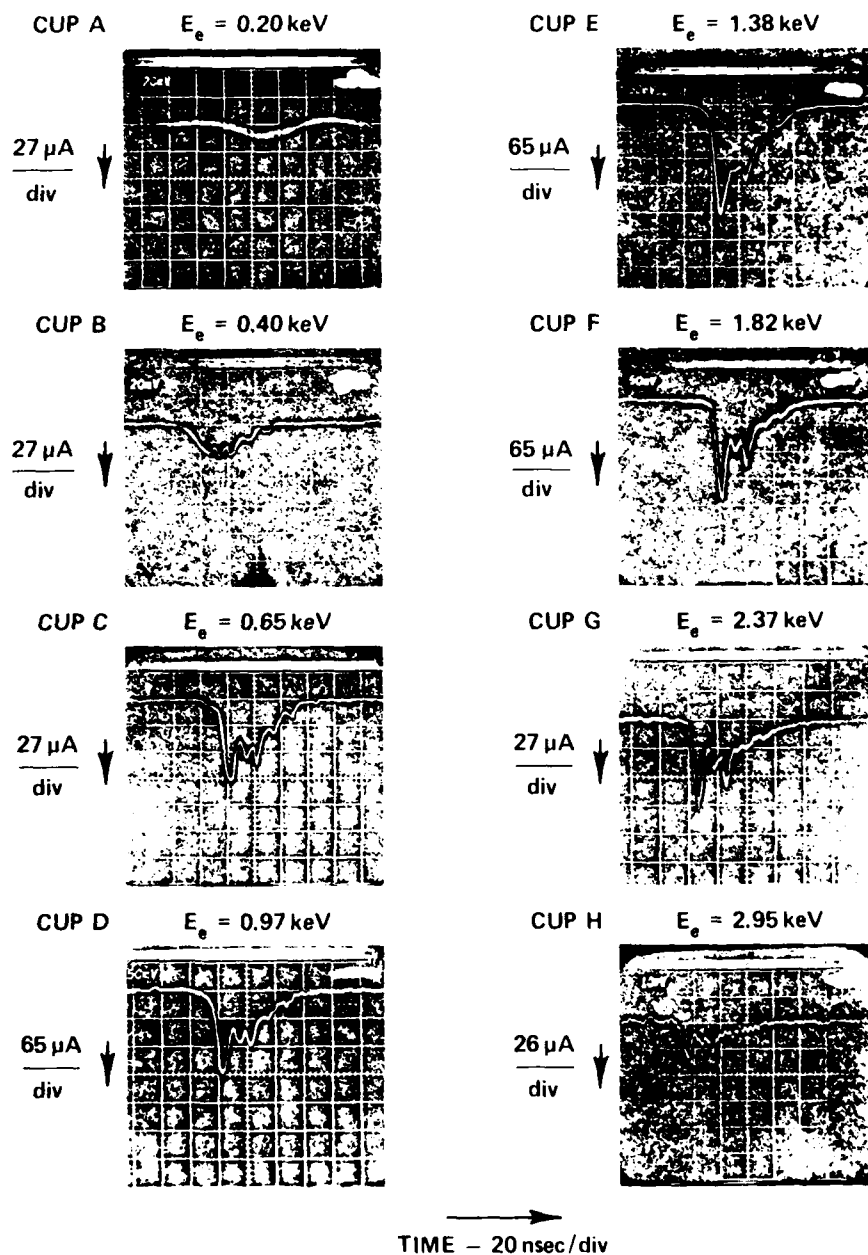
Figure 9   Photoelectron signals from gold on Shot No. 3621
            (grounded emitter). Magnet current was 2.3A and sweep
            was 20 nanoseconds per division

CUP A E_e = 0.14 keV

$\dfrac{27\,\mu A}{div}$ ↓

CUP E E_e = 1.03 keV

$\dfrac{65\,\mu A}{div}$ ↓

CUP B E_e = 0.30 keV

$\dfrac{27\,\mu A}{div}$ ↓

CUP F E_e = 1.37 keV

$\dfrac{65\,\mu A}{div}$ ↓

CUP C E_e = 0.50 keV

$\dfrac{27\,\mu A}{div}$ ↓

CUP G E_e = 1.78 keV

$\dfrac{27\,\mu A}{div}$ ↓

CUP D E_e = 0.73 keV

$\dfrac{65\,\mu A}{div}$ ↓

CUP H E_e = 2.22 keV

$\dfrac{26\,\mu A}{div}$ ↓
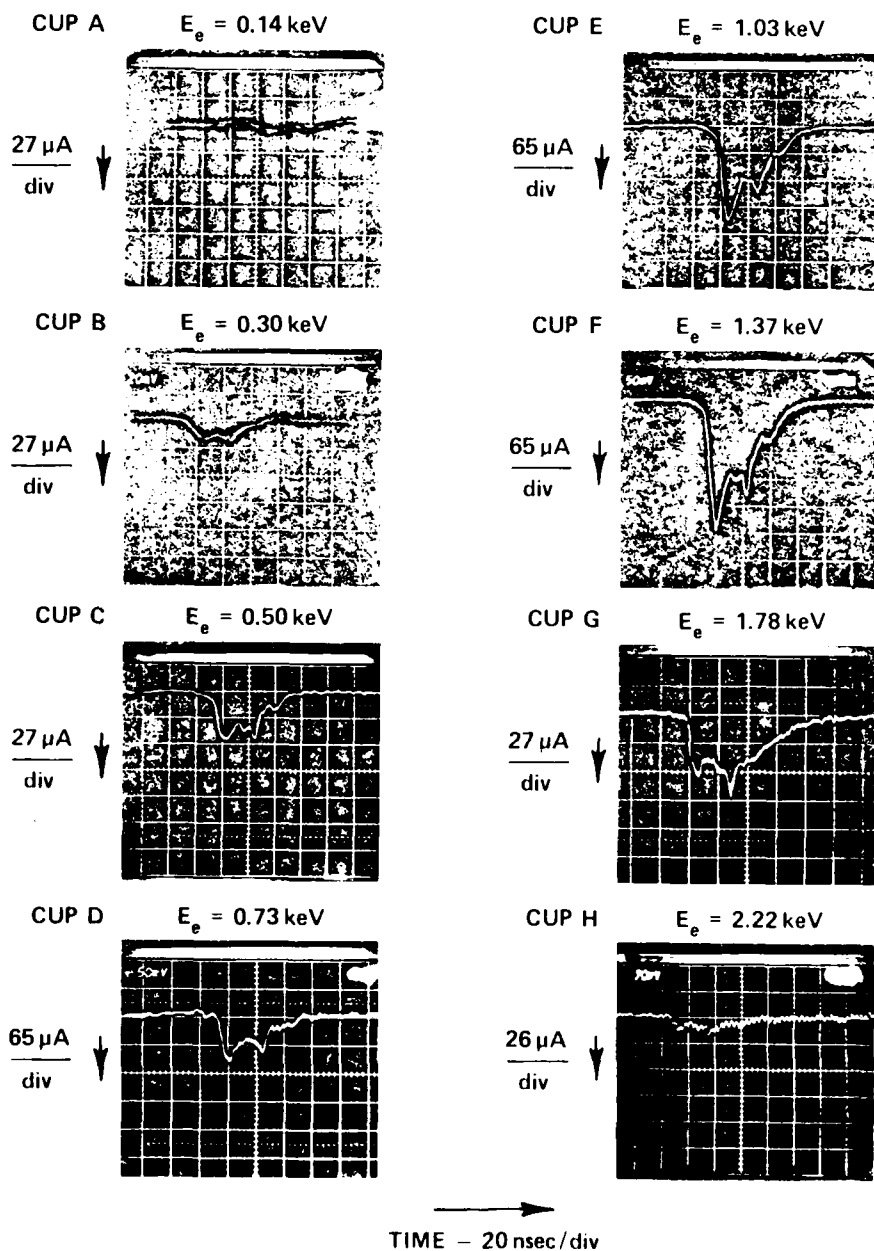
TIME — 20 nsec/div

Figure 10   Photoelectron signals from aluminum on Shot No. 3619 (grounded emitter). Magnet current was 2.0A and sweep was 20 nsec/division
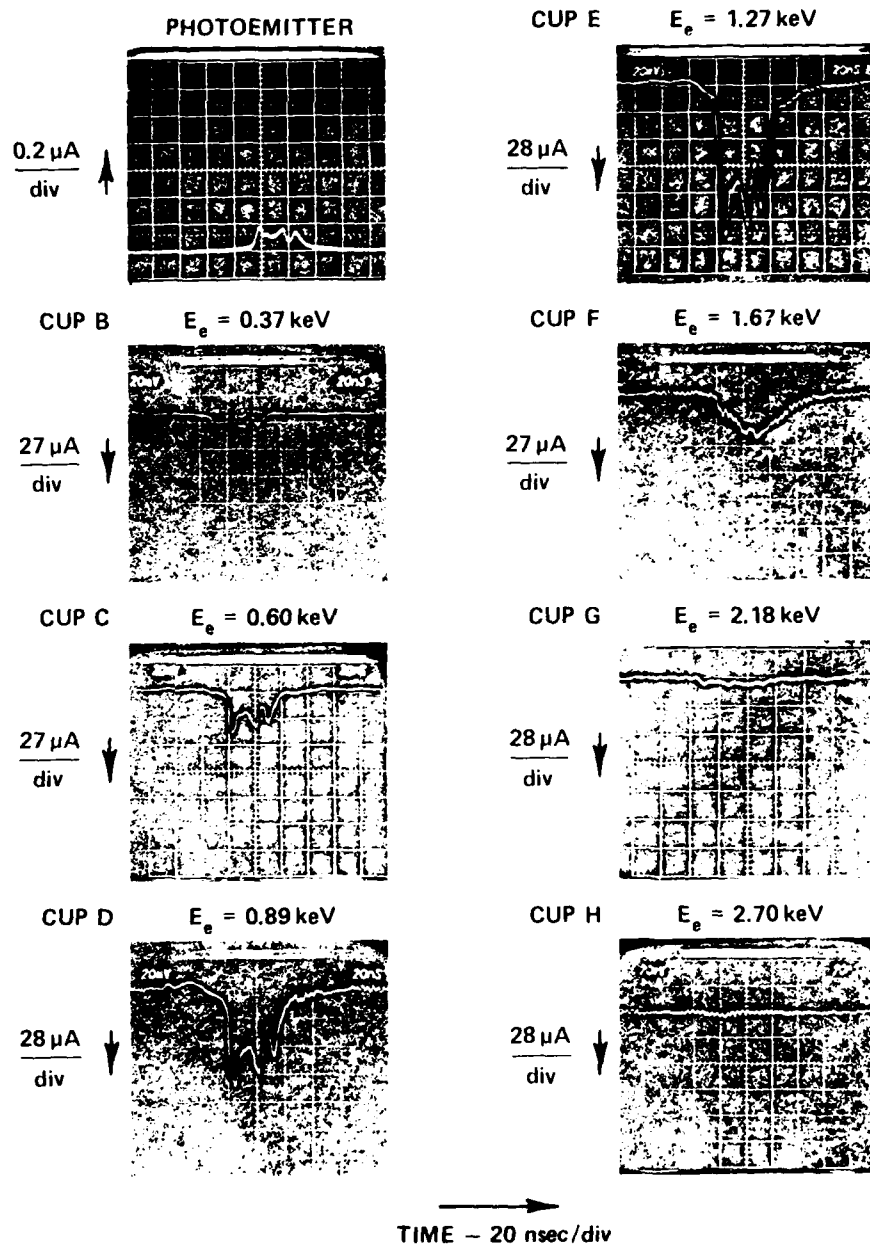
Figure 11 Photoelectron signal from aluminum on Shot No. 3672 (grounded emitter). Magnet current was 2.2A and sweep was 20 nsec/division

To obtain an energy spectrum from the charges collected by
the array of Faraday cups, each value of q was divided by the
corresponding value of ΔE and by the calorimeter signal, W, for
that shot. When applicable, the value of W was really TW where T
was the transmission of the added screen. Several sets of resulting
energy spectral data are given in Figures 12 to 17 with the spectral
intensity, $q/W\Delta E$, plotted as a function of the electron energy E_e.
All these data were multiplied by a common, arbitrary scale factor
for convenience in comparing the relative spectral yields. The
energy scale is that given in Section II.A.4. Small adjustments
in the energy scale, to account for the actual electron trajectories,
are included in Section IV.A.2, when values for the absolute spec-
tral yields are derived. Most of the individual data points in
these figures are identified by shot number. All of the data were
initially plotted in this form to determine if there were consis-
tent displacements between sets of data. It must be emphasized
that valid data for some materials were obtained on only one or
two shots. In those cases, there was less reliability in the nor-
malizations. Scatter and variations in the spectral data arose
from several sources: inaccuracies in measuring the signal inten-
sities and pulse widths, inaccuracies in the x-ray fluence, changes
in x-ray spectrum from shot to shot, an occasional incorrect set-
ting of the magnetic-coil current, i_B, and contamination of the
photoemitter surfaces. For clarity in these figures, the sizes of
most symbols are larger than the uncertainties in measuring the
collected charges. The largest errors were in measuring the small
signals at the low and high electron energies.

The data from a given set of shots generally exhibited good
consistency, such as those shown in Figures 12 and 15. On the
other hand, data from different test series sometimes exhibited
significant differences as shown in Figures 13 and 14. In parti-
cular, the aluminum-photoemission data from the three test series
in 1977 showed good agreement, but the February 1979 data were

38

1000

Aℓ – KLL

$\dfrac{q}{W\Delta E}$

$\left(\dfrac{C}{J-keV}\right)$

100

10

Shot	i_B
A	4160	2.3
B	4180	2.5
C	4182	2.5
D	4183	2.0
E	4184	2.2
F	4186	3.2

1

0   1.0   2.0   3.0

ELECTRON ENERGY, E_e (keV)
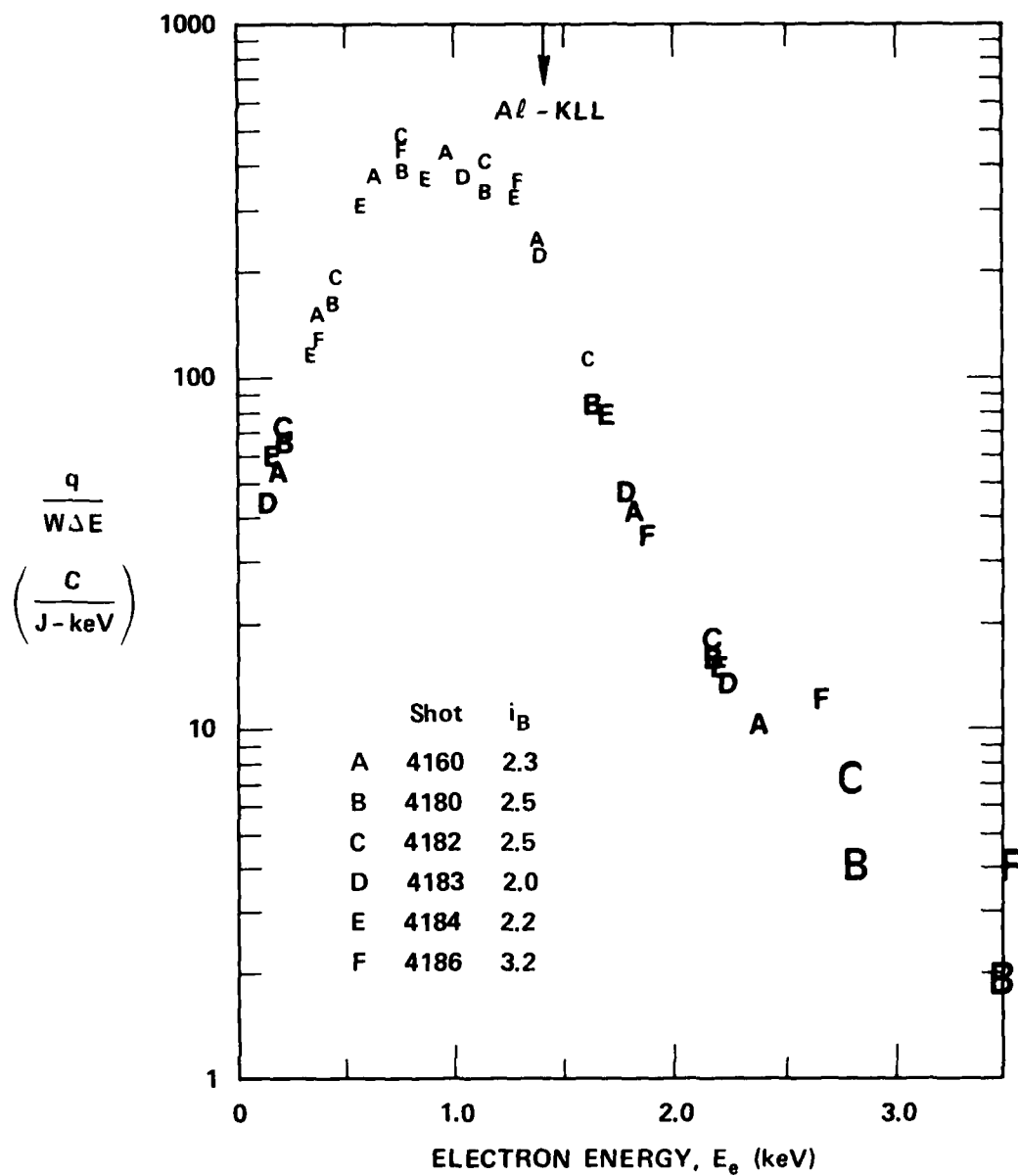
Figure 12   Photoelectron spectral data from aluminum mounted on
hemicylinder. Data normalized to incident x-ray
fluence with arbitrary scale factor

39
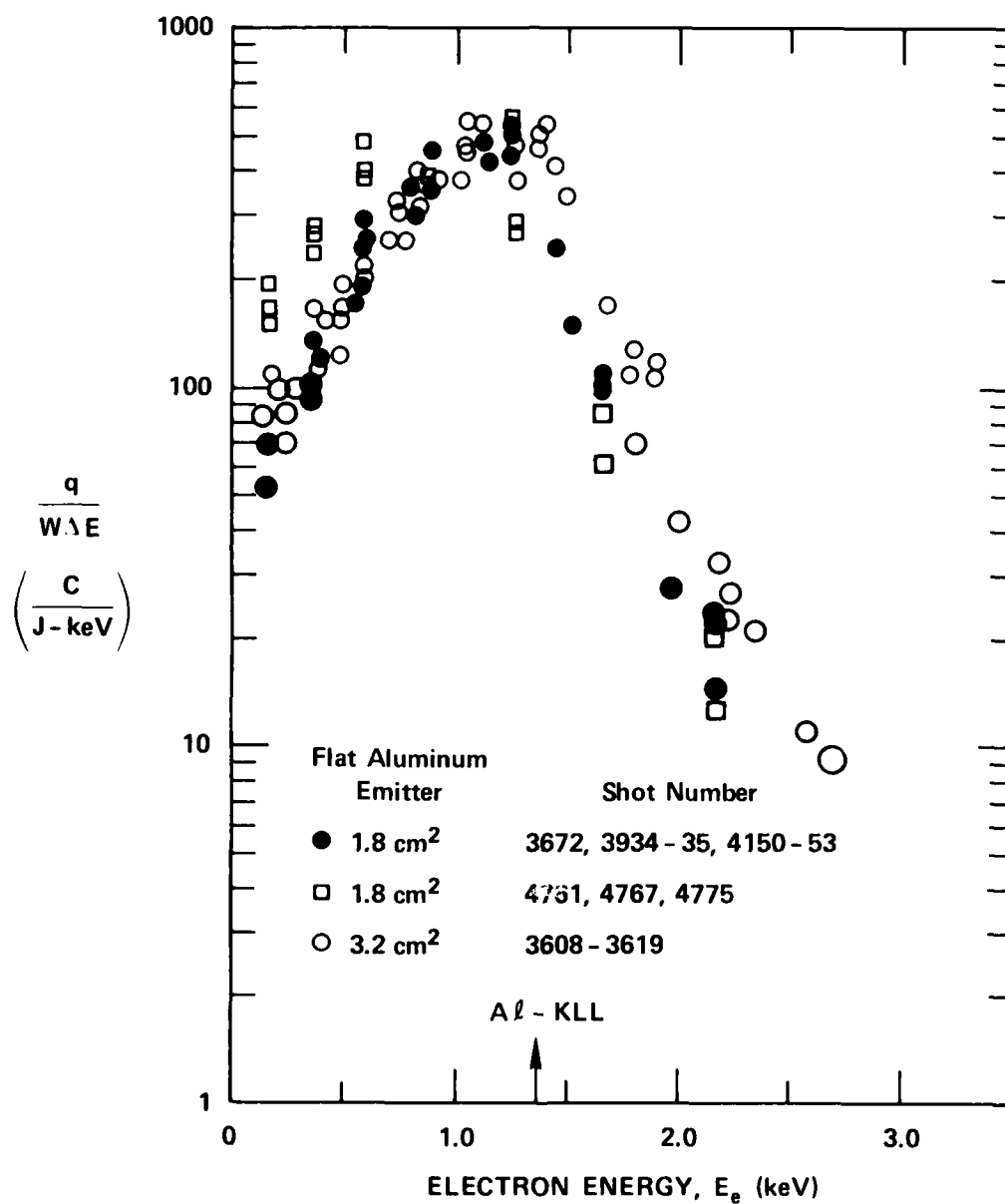
Figure 13   Normalized photoelectron spectral data from flat
aluminum emitter.   Data from four test series
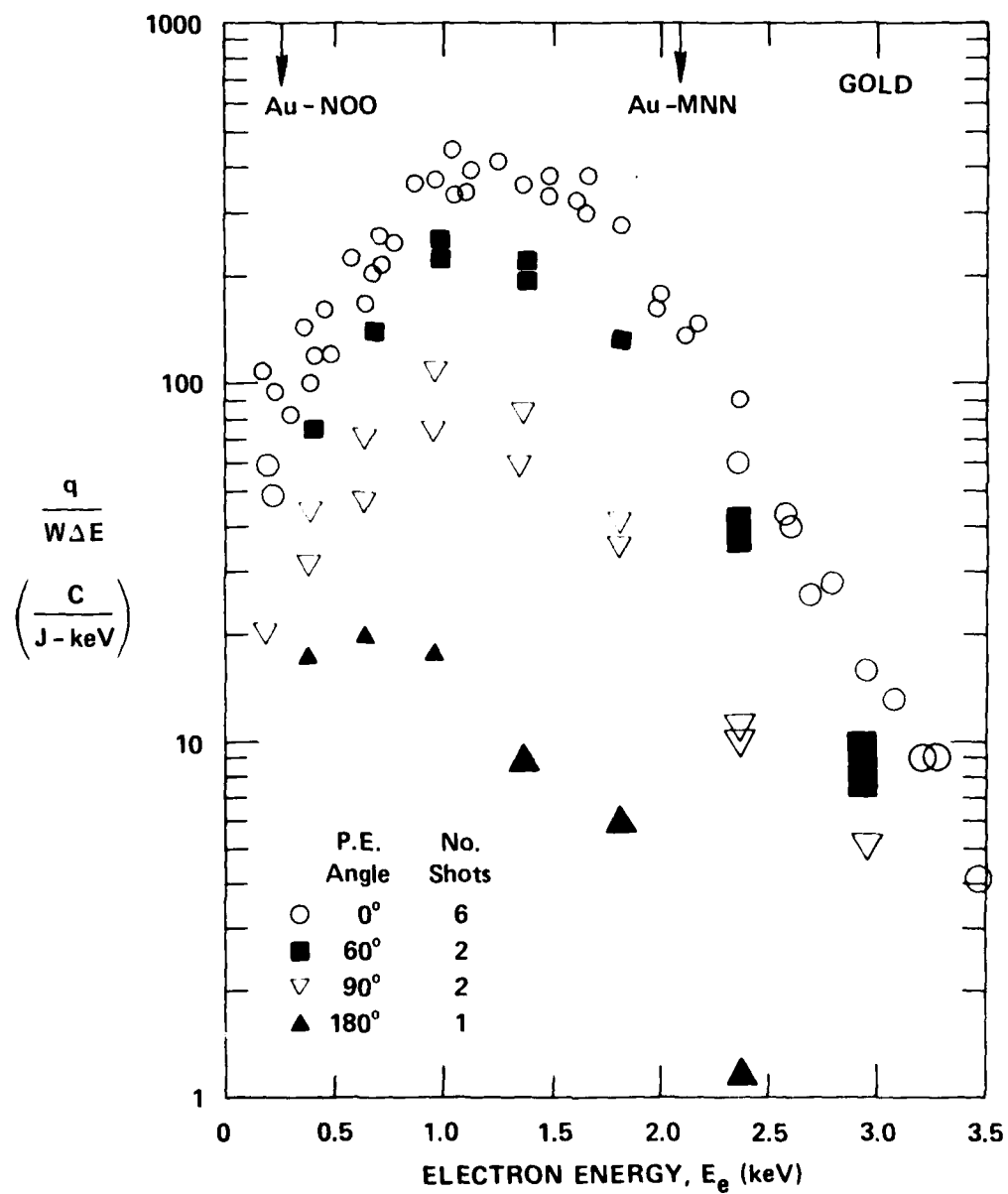
Figure 14 Normalized photoelectron spectral data from gold.
Emitter rotated on axis to different angles relative
to direction through aperture. Two sets of data at
90° obtained with emitter rotated in opposite direc-
tions

41
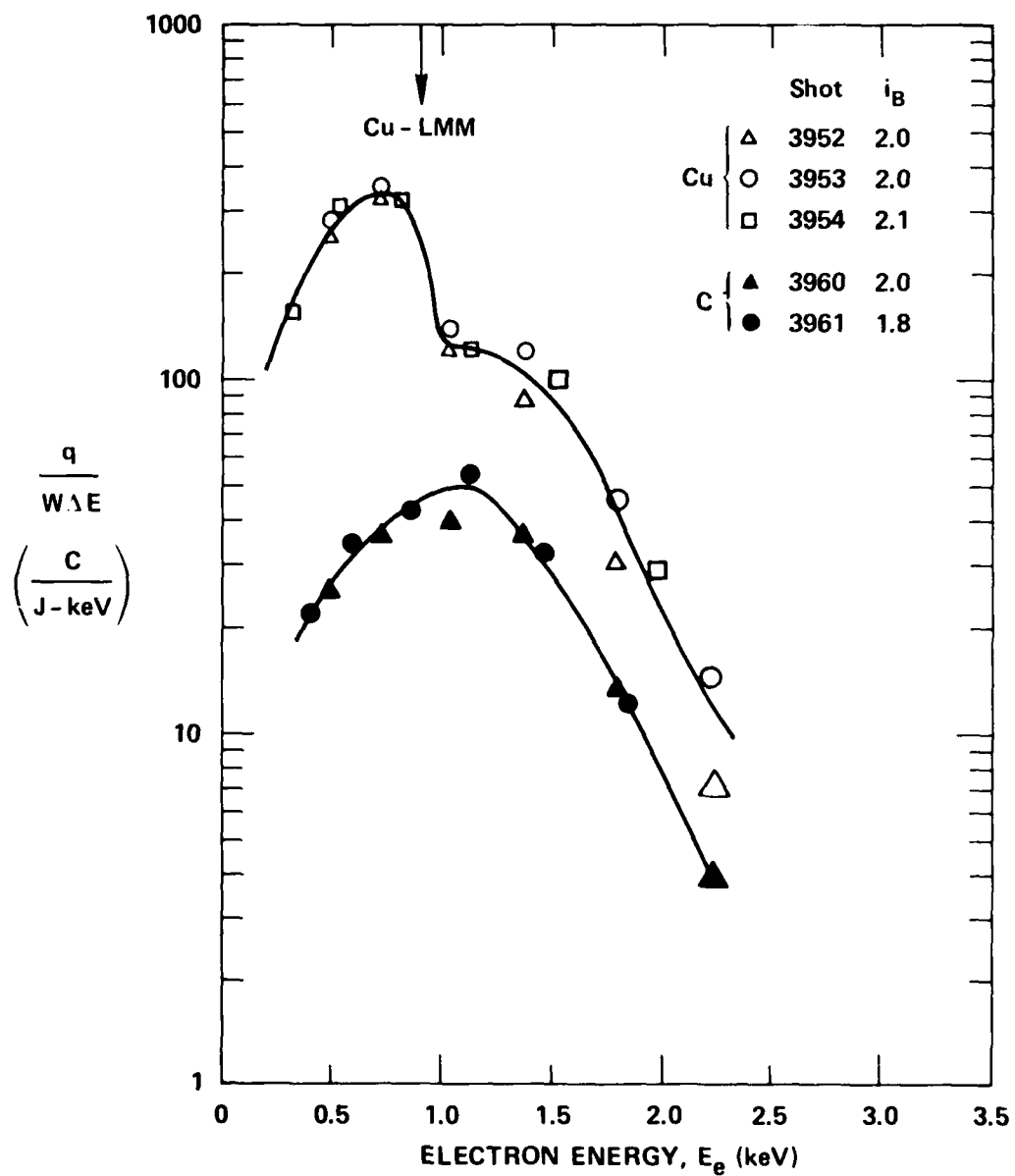
Figure 15 Normalized photoelectron spectral data from copper and graphite
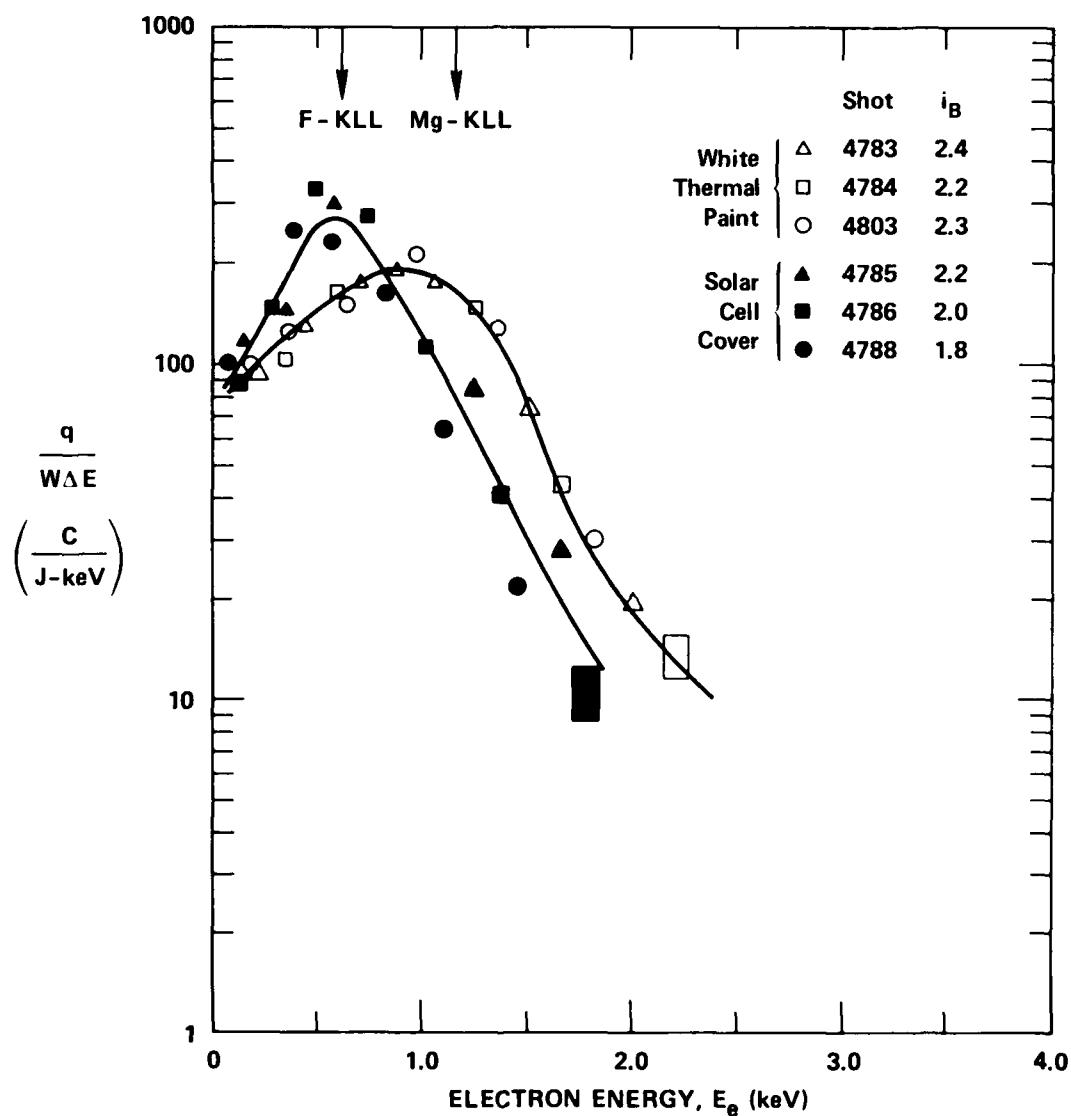
Figure 16   Normalized photoelectron spectral data from white
thermal paint and solar-cell cover glass

43
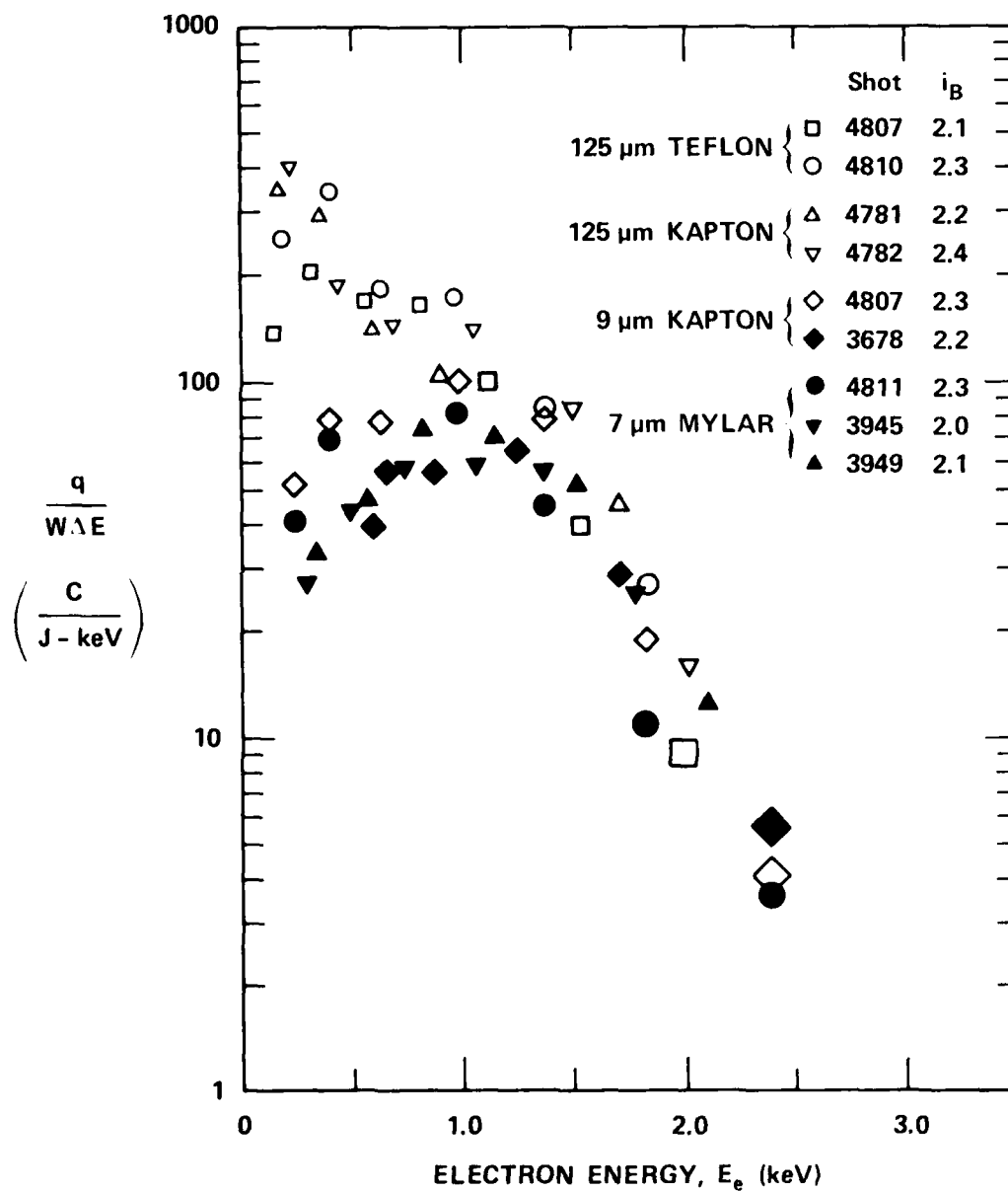
Figure 17   Normalized photoelectron spectral data from Mylar, Teflon and two thicknesses of Kapton

quite different. Similarly, the November 1977 data for gold differed substantially from the March 1977 results. Several possible explanations for these changes were considered including alteration of Faraday cup orientation, incorrect values of magnetic field, contamination of photoemitter surface and changes in irradiation spectrum. However, no one single phenomenon could account for all the observations.

Photoemission spectral yields from gold were also measured with the emitter mounting rotated about its axis and these results are shown in Figure 14. With the emitter at 60°, the signals were about half as large consistent with a cos θ angular distribution. The small signals observed with the emitter rotated to 90° arose from the finite size of the aperture so there was not an exact 90° emission angle. The rotation angle of the emitter was not exact as evidenced by the discrepancy between the two sets of data obtained with the emitter rotated in opposite directions. In addition, space-charge effects probably caused the electrons to diverge slightly. At 180° the very small signals are attributed to photoemission off the edges of the emitter.

Photoemission from the insulating materials exhibited almost the same reproducibility in the data as the conductors. The primary-electron energy spectra emitted from the thin samples of Mylar and Kapton were nearly the same, as shown in Figure 17. On the other hand, there was substantially more photoemission from the thick Kapton at energies below 1 keV than observed from samples of thin Kapton. In fact, the spectral yield from the 125-μm-thick Kapton was very similar to that of the thick Teflon. No explanation was found for the anomalous photoemission from this thick Kapton.

Photoemission from anodized aluminum was similar to that
from aluminum with a reduced spectral yield around the peak.
The primary-electron emission from the thick and thin sheets of
glass appeared to have the same energy spectrum but the yield
from the thick glass was about 40% lower.

D.   BIASED PHOTOEMITTER RESULTS

An additional goal was to determine the yield of secondary
electrons from the various emitters. To detect these low-energy
electrons, the emitter was biased negatively with respect to the
chamber so the low-energy electrons were accelerated to higher
energies and then were resolved by the magnetic field. These
biased-emitter measurements also served as an experimental energy
calibration of the system.

When the x radiation was filtered by only the normal two
layers of Kapton, the emission of secondary electrons from the
biased emitter was space-charge limited (s.c.l.). Therefore,
the majority of the data was obtained using one or two layers
of stainless-steel screen, with a transparency of 0.36, to atten-
uate the incident x-ray flux. Applied bias potentials ranged
from -320 to -1440 volts and the magnetic field was adjusted so
that the secondary electrons were collected by the second, third
or fourth cup from the aperture. A couple of measurements were
also made with the emitter biased positive to determine its effect
on the primary emission.

Representative sets of signal traces are shown in Figure 18-
21; the x-ray outputs were similar on all these shots. The first
two sets for flat gold and aluminum emitters, Figures 18 and 19,
were obtained with no x-ray attenuating screen and the secondary-
electron signals on cup C exhibited extreme space-charge limita-
tion. This is reflected by the signals going to zero just when

46

CUP A $E_e + V_A = -0.45\,keV$

$\dfrac{67\,\mu A}{div}$ ↓

CUP B $E_e + V_A = -0.25\,keV$

$\dfrac{67\,\mu A}{div}$ ↓

CUP C $E_e + V_A = 0$

$\dfrac{267\,\mu A}{div}$ ↓

CUP D $E_e + V_A = 0.32\,keV$

$\dfrac{68\,\mu A}{div}$ ↓

CUP E $E_e + V_A = 0.73\,keV$

$\dfrac{67\,\mu A}{div}$ ↓

CUP F $E_e + V_A = 1.17\,keV$

$\dfrac{66\,\mu A}{div}$ ↓

CUP G $E_e + V_A = 1.72\,keV$

$\dfrac{66\,\mu A}{div}$ ↓

CUP H $E_e + V_A = 2.30\,keV$

$\dfrac{27\,\mu A}{div}$ ↓

TIME   20 nsec / div
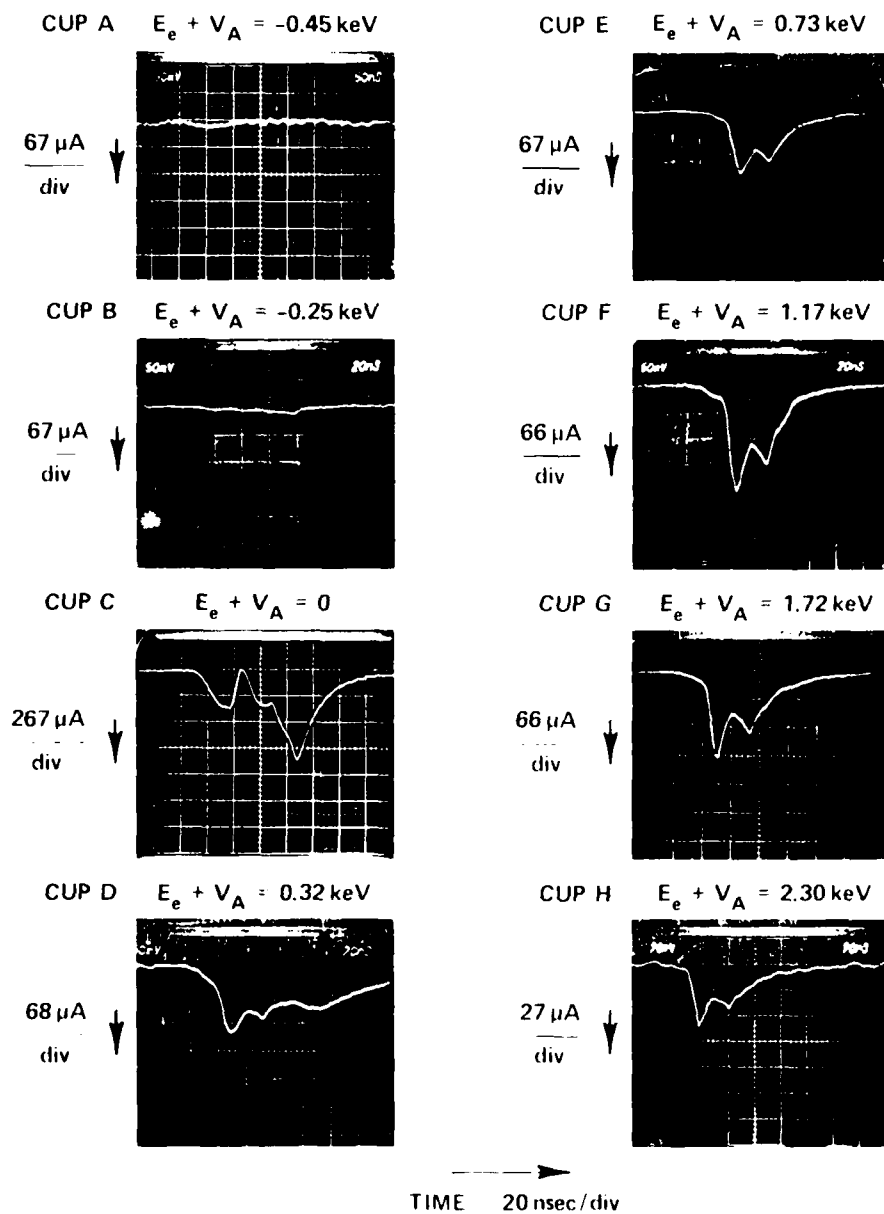
Figure 18   Photoelectron signals from flat gold biased at -650
volt; Shot No. 5632 with I_B - 2.3A

47

PHOTOEMITTER

$\dfrac{0.1\,A}{div}$

CUP E $\quad E_e + V_A = 0.67\,keV$

$\dfrac{68\,\mu A}{div}$

CUP B $\quad E_e + V_A = -0.23\,keV$

$\dfrac{27\,\mu A}{div}$

CUP F $\quad E_e + V_A = 1.07\,keV$

$\dfrac{67\,\mu A}{div}$

CUP C $\quad E_e + V_A = 0$

$\dfrac{117\,\mu A}{div}$

CUP G $\quad E_e + V_A = 1.58\,keV$

$\dfrac{66\,\mu A}{div}$

CUP D $\quad E_e + V_A = 0.29\,keV$

$\dfrac{27\,\mu A}{div}$

CUP H $\quad E_e + V_A = 2.10\,keV$

$\dfrac{13\,\mu A}{div}$

TIME   20 nsec/div
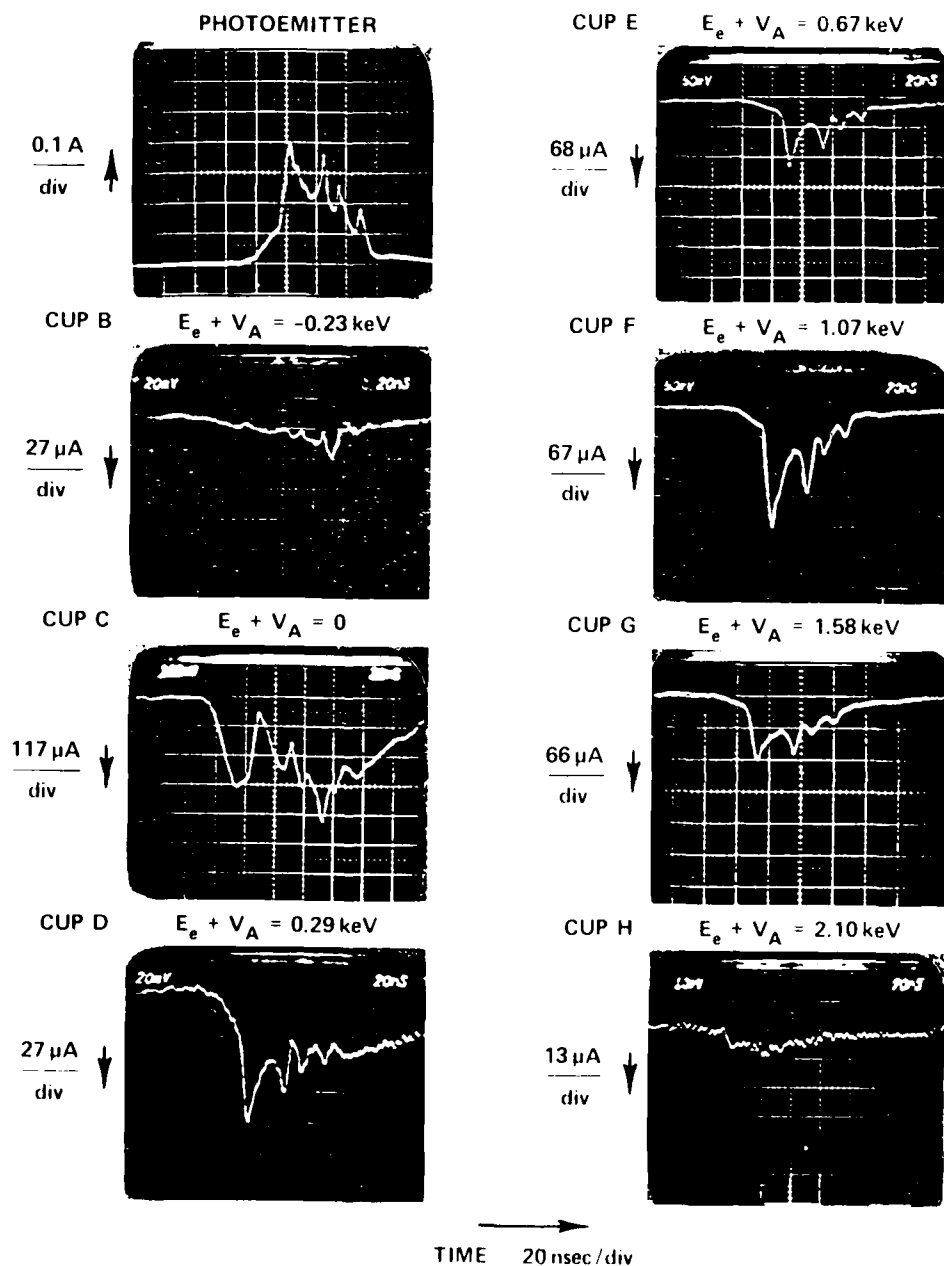
Figure 19   Photoelectron signals from flat aluminum biased at
−600 volt; Shot No. 3674 with I_B − 2.2A

48

the primary electron emission peaks. When the emitter was aluminum on a hemicylindrical mounting, the secondary-electron signals were moderately space-charge limited with no attenuating screen (Figure 20) and exhibited no limiting with one screen (Figure 21).

The biased-emitter signals had some important features. First of all, some electrons were detected in the cup corresponding to a lower energy than the one collecting the secondary electrons. These electrons were assumed to be accelerated secondaries that were scattered off a grounded surface that could be viewed by a small part of the aperture. For moderate space-charge limiting of the secondaries, as at 0.65 keV in Figure 20, the electrons detected in the lower-energy cup (0.40 keV) had the same time history as the primaries. In the results shown in Figure 21, the time history of the secondaries at 0.65 keV was the same as the accelerated primaries at 1.38 and 1.82 keV. However, the higher-energy electrons detected at 2.37 keV had a different time history and the electrons at 0.97 keV also followed this temporal history. Such photoemission from aluminum correlates with other observations such as shown in Figures 10 and 11.

Primary-electron energy spectra were derived from these data in the same way as for the grounded photoemitters. That is, the charges collected by the higher-energy cups were divided by the appropriate values of E and by the product, TW, of screen transmission and calorimeter signal. These values were plotted against the sum E_e + V for comparison of the energy spectra with the unbiased results. Sets of spectral data obtained from a biased flat gold emitter are shown in Figure 22.

These spectral results are representative of what was observed from biased emitters that were conductors on thin insulators. Compared to the grounded-emitter results, the spectral values with

CUP E $E_e + V_A$ = 0.73 keV

$\dfrac{67\,\mu A}{div}$ ↓

CUP B $E_e + V_A$ = -0.25 keV

$\dfrac{28\,\mu A}{div}$ ↓

CUP F $E_e + V_A$ = 1.17 keV

$\dfrac{117\,\mu A}{div}$ ↓

CUP C $E_e + V_A$ = 0

$\dfrac{267\,\mu A}{div}$ ↓

CUP G $E_e + V_A$ = 1.72 keV

$\dfrac{66\,\mu A}{div}$ ↓

CUP D $E_e + V_A$ = 0.32 keV

$\dfrac{67\,\mu A}{div}$ ↓

CUP H $E_e + V_A$ = 2.30 keV

$\dfrac{13\,\mu A}{div}$ ↓

TIME ──▶ CUPS C, E : 20 nsec/div
OTHERS : 50 nsec/div
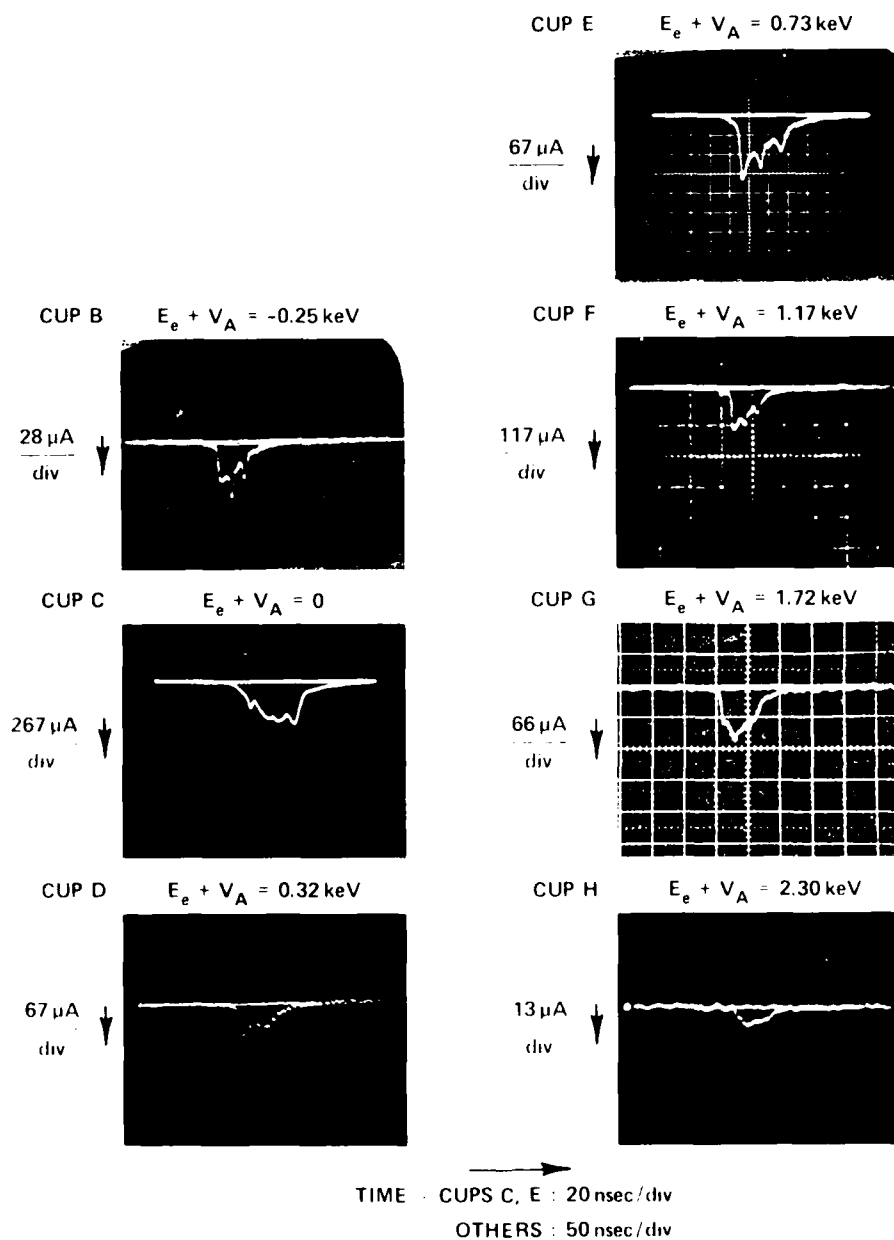
Figure 20   Photoelectron signals from cylindrical aluminum
biased at -650 volt; Shot No. 4159 with I_B - 2.3A

50

PHOTOEMITTER

CUP E $E_e + V_A = 0.73\,keV$

$\dfrac{0.14\,A}{div}$

$\dfrac{26\,\mu A}{div}$

CUP B $E_e + V_A = -0.25\,keV$

CUP F $E_e + V_A = 1.17\,keV$

$\dfrac{27\,\mu A}{div}$

$\dfrac{26\,\mu A}{div}$

CUP C $E_e + V_A = 0$

CUP G $E_e + V_A = 1.72\,keV$

$\dfrac{267\,\mu A}{div}$

$\dfrac{13\,\mu A}{div}$

CUP D $E_e + V_A = 0.32\,keV$

CUP H $E_e + V_A = 2.30\,keV$

$\dfrac{27\,\mu A}{div}$

$\dfrac{13\,\mu A}{div}$

TIME — CUPS C, E, G : 20 nsec/div
OTHERS : 50 nsec/div
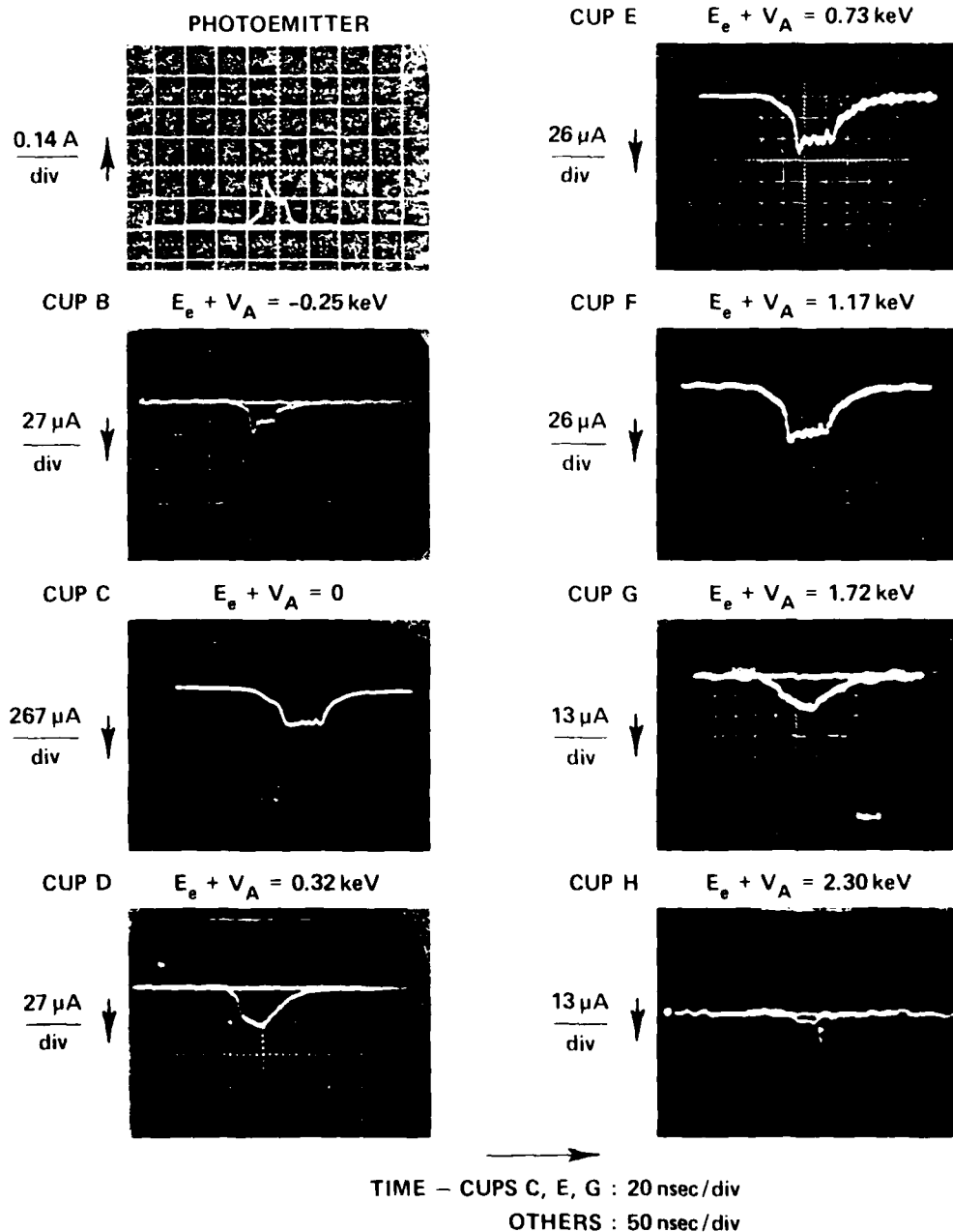
Figure 21   Photoelectron signals from cylindrical aluminum
biased at -650 volt with x-ray intensity 40% of that
in Figure 20; Shot No. 4156 with I_B - 2.3A
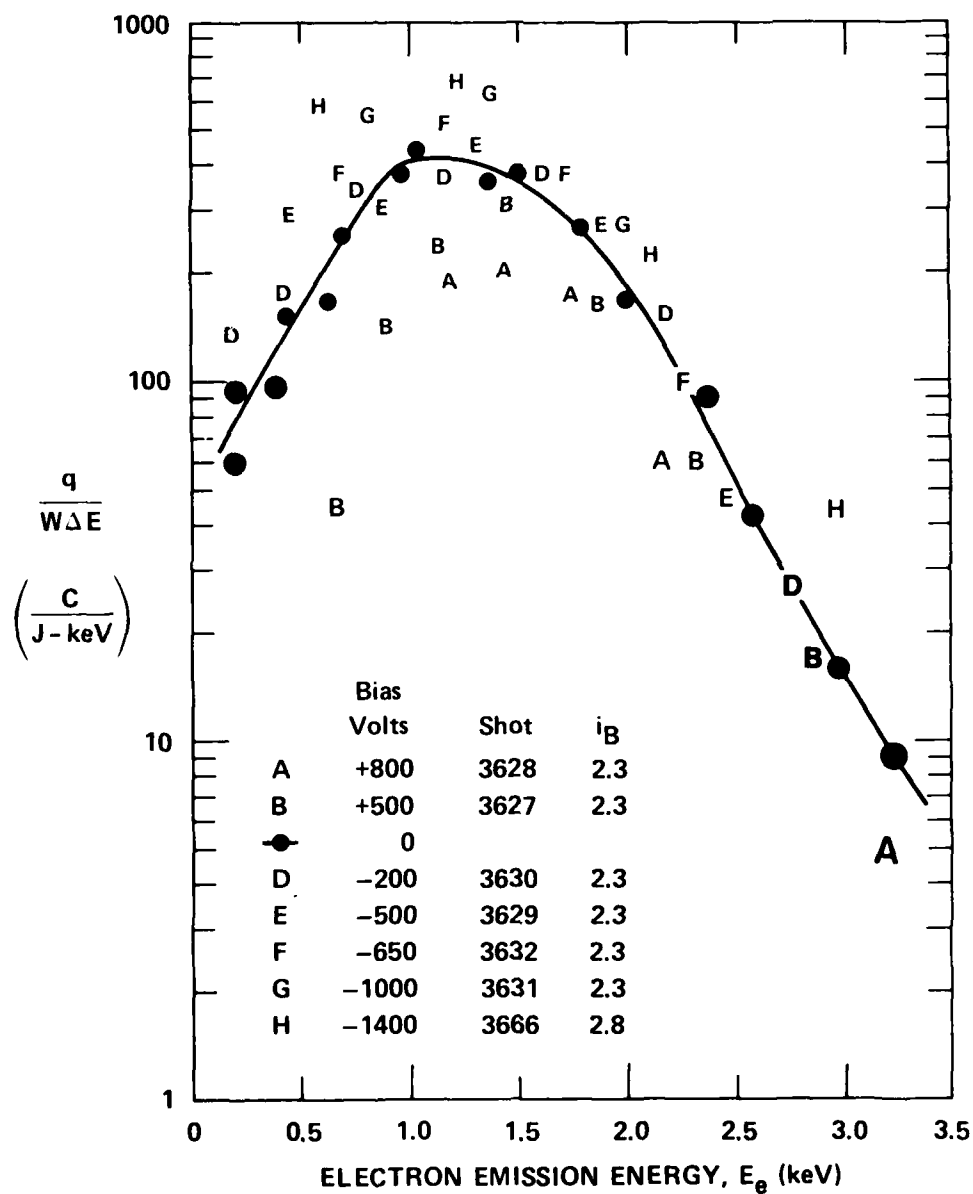
Figure 22   Normalized photoelectron spectral data from gold
            biased at different potentials. Energy scale E_e is
            emission energy with applied voltage subtracted from
            detected energy

a negative bias were much larger at low electron energies and con-
verged to the unbiased results in the 1.0 - 1.5 keV range, but then
diverged sometimes at high energies. The enhanced signals at low-
electron energies were caused by a focusing effect of the applied
electric field; that is, the emission trajectories were deviated
slightly toward the surface normal so that more passed through
the aperture.

The photoemission signals from thick dielectrics on a biased
mounting showed some anomolous behavior. In the case of the 1-mm-
thick glass, the s.c.l. emission of the secondaries differed from
that of conductors shown in Figures 18 and 19. The beginning of
the signals were the same, rising during the initial foot of the
x-ray pulse and dropping to zero at peak x-ray intensity. But
then the difference arose. The secondary-electron signal from the
glass remained near zero for the remainder of the pulse instead of
increasing to a large value when the x-ray intensity was lower.
Such behavior was caused by surface charging of this thick insula-
tor. For this thickness of glass, the magnitude of the emitted
negative charge during the first half of the pulse left the sur-
face at least 1000 volts positive with respect to the biased
photoemitter mount. Therefore, there was no accelerating electric
field.

A quite different behavior was observed in the photoemission
from the solar-cell cover. The secondary electrons were detected
with an average energy only half that of the applied potential.
Since the volume resistivity of the 0.3-mm-thick quartz was ex-
tremely high, a possible effect was electrical conductivity through
the residual gas in the chamber thereby lowering the surface poten-
tial on the cover glass. To check this hypothesis, five fine wires
were laid across the surface of the cover glass and attached to the
biased mounting. Under these conditions, the average energy of the
secondary electrons was increased to about 85% of the applied bias

53

of -970 V. This observation is consistent with the hypothesis, but it is difficult to explain a steady-state current of sufficient magnitude through the poor vacuum.

The secondary-electron yield from the thick Kapton (125 μm) was unexpectedly very low. It was several times smaller than the yields from the thin sheets of Kapton and Mylar that were studied. This probably resulted from a different surface composition but surface charging is also a possibility.

E. TIME RESOLUTION

One of the original PESS design goals was a time resolution of 3 nsec. During the early test series, the time resolution appeared to be at least this as observed on 100-MHz oscilloscopes (rise time of 3.5 nsec). To determine the full capability of the instrument, 500-MHz oscilloscopes with risetimes of 0.8 nsec were used during the November 1977 test series. Some PESS signals were recorded simultaneously using 500-MHz and 100-MHz bandwidths. The higher bandwidth gave only slightly better time resolution as evidenced by slightly deeper valleys between closely-spaced peaks on the signal traces. The slower ocilloscopes recorded the signals with adequate fidelity, because the risetimes of individual peaks were only rarely shorter than 5 nsec. In addition, the coaxial signal cables had more attenuation at higher frequencies.

Two sets of signal traces are reproduced in Figures 23 and 24 for shots taken with unbiased and biased aluminum on a cylindrical support. The signals from Faraday cups E and F and from two XRD channels were recorded on 500-MHz oscilloscopes. Several important observations were made on these signal traces; signals obtained on other shots were in agreement. First of all, the predominant electron emission around 1 keV (cup E) had the same history as observed on the XRD filtered by the standard 19- m Kapton. This is evidence that the PESS did not limit the time resolution of the photoelectron signals generated by the OWL II' x-ray output.
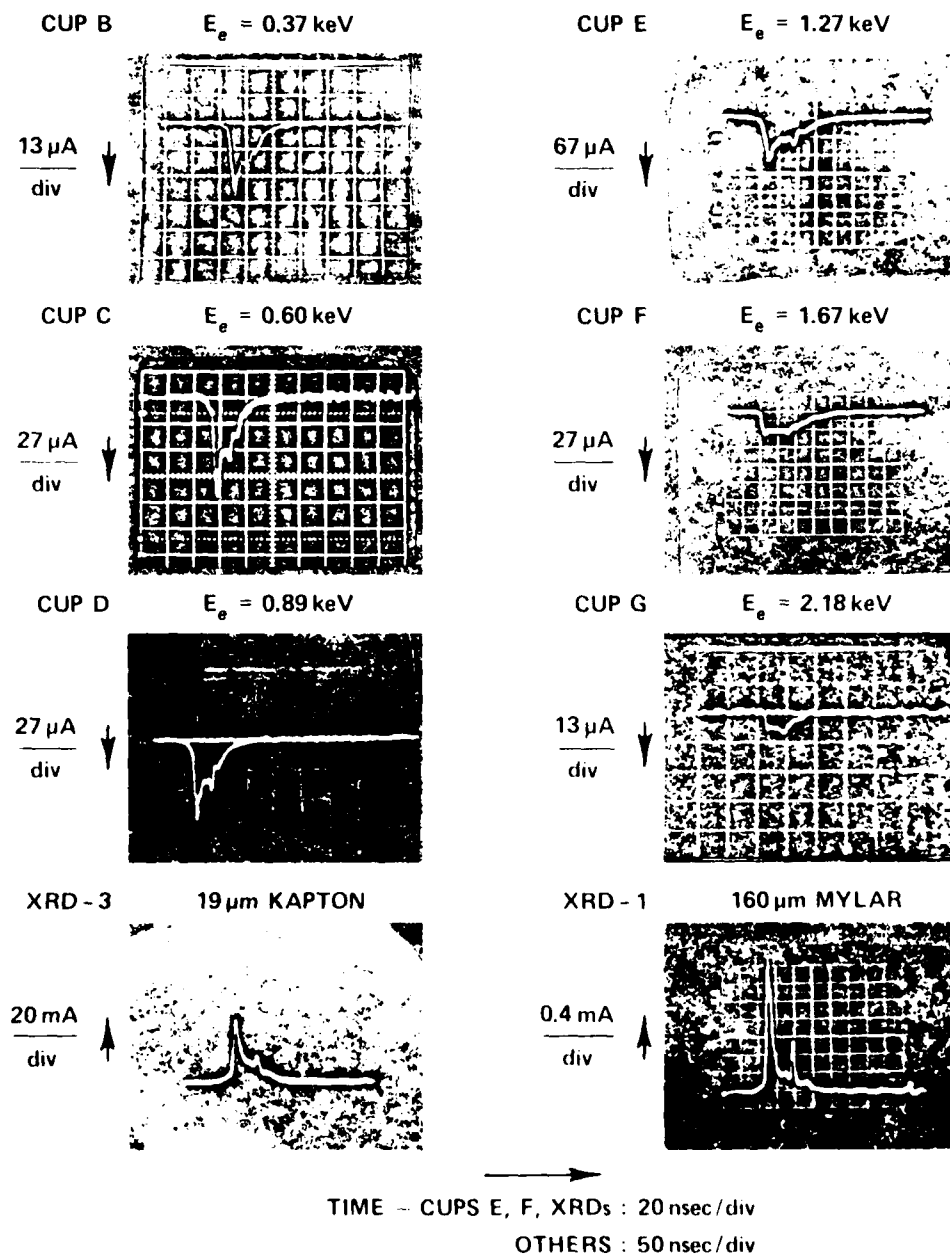
Figure 23. Photoemission signals from unbiased aluminum on hemi-cylindrical support plus corresponding filtered XRD signals for Shot Number 4184. Signals from XRDs and PLSS Cups E and F recorded at 20 nsec/div on 7903 oscilloscopes; other signals recorded at 50 nsec/div

55

CUP C $E_e + V_A = 0$

$\dfrac{267\,\mu A}{div}\;\downarrow$

CUP G $E_e + V_A = 2.55\,keV$

$\dfrac{7\,\mu A}{div}\;\downarrow$

CUP D $E_e + V_A = 0.47\,keV$

$\dfrac{27\,\mu A}{div}\;\downarrow$

CUP E $E_e + V_A = 1.07\,keV$

$\dfrac{27\,\mu A}{div}\;\downarrow$

XRD - 3   19 µm KAPTON

$\dfrac{20\,mA}{div}\;\uparrow$

CUP F $E_e + V_A = 1.73\,keV$

$\dfrac{13\,\mu A}{div}\;\downarrow$

XRD - 1   160 µm MYLAR

$\dfrac{0.4\,mA}{div}\;\uparrow$

TIME — CUPS E, F, XRDs : 20 nsec/div
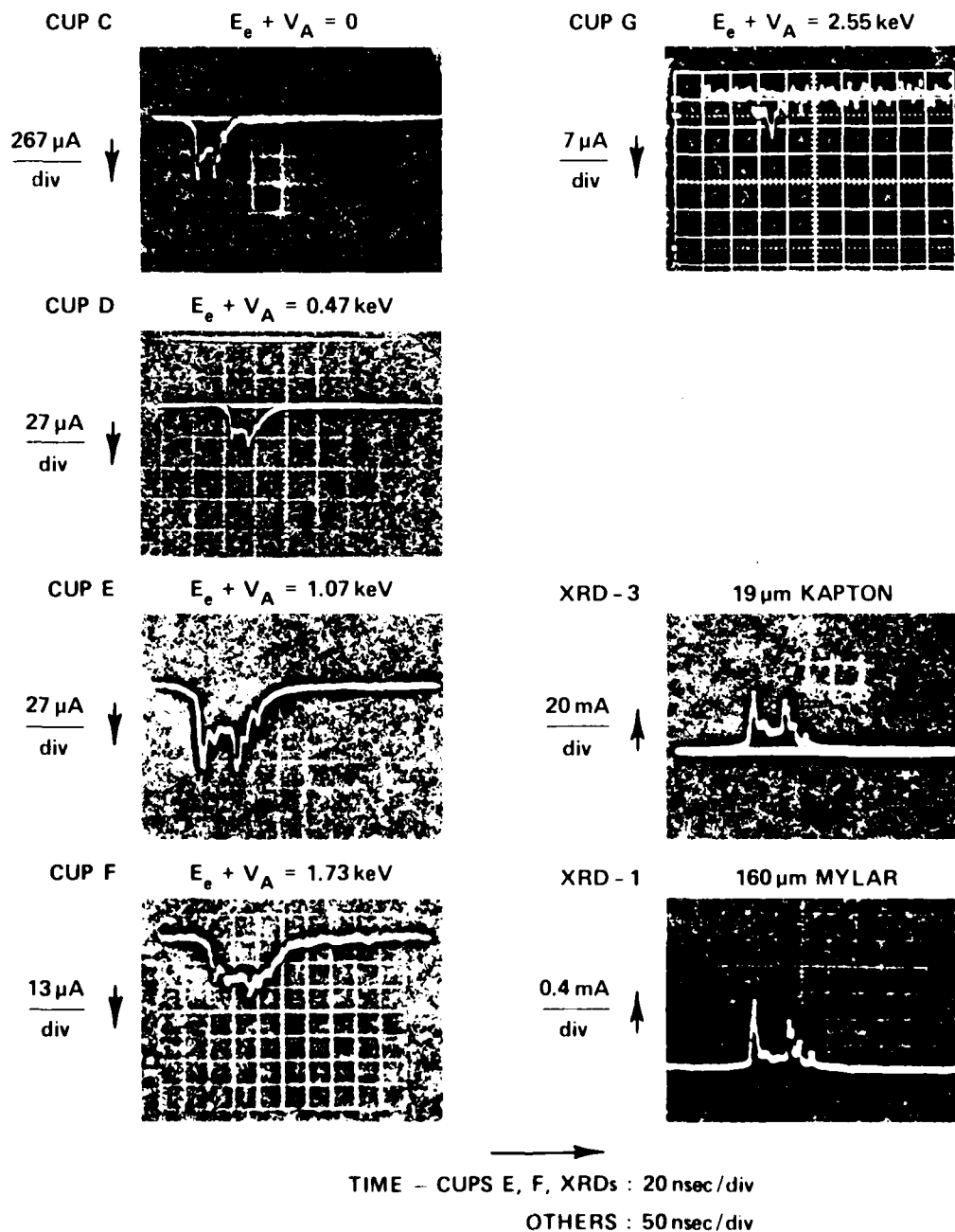
OTHERS : 50 nsec/div

Figure 24   Photoemission signals from aluminum emitter biased at
            -970 volts plus corresponding filtered XRD signals
            for Shot Number 4188. Signals from XRDs and PESS Cups
            E and F recorded at 20 nsec/div on 7903 oscilloscopes;
            other signals recorded at 50 nsec/div.

56

Second, when the x rays were sufficiently attenuated that
secondary emission was not space-charge limited, the secondary
electron emission matched the emission signal around 1 keV. This
can be observed by comparing signals from cups C and E for shot
4188 in above 1.4 keV had a significantly different time history
with less "spikiness" than the lower-energy electrons (compare
signals from cups E and F in Figures 23 and 24). This phenomenon
was already described in the preceeding sections.

The last observation was surprisingly inconsistent with the
XRD signals. As just noted, the higher-energy photoelectrons from
aluminum had peaks greatly reduced in intensity relative to the
broader valley between the peaks. But when the x rays were
filtered by 80 μm and 160 μm of Mylar, the opposite trend was
observed. The narrow peaks dominated the filtered XRD signal with
very low amplitudes in the valleys between the spikes. Detailed
analysis of all experimental methods rules out the possibliity
that the variations in observed signals resulted from the instru-
mentation. Such aspects as electron scattering could not affect
the signals over times greater than a few nanoseconds.

F.   XRD RESULTS

The photoemission from a variety of materials was studied
during the 1979 test series using the XRD array. Although the
integrals of all signals could be recorded on the CAMAC system,
the limited number of oscilloscopes permitted observation of the
time histories of only half the signals on each shot. The empha-
sis in this set of measurements was on determining the total yield
from each material when the x rays were filtered by the standard
two layers of Kapton. Therefore, very little data was obtained
on the time variations of the x-ray signal as a function of filter
thickness, as described in the preceeding section.

57

Besides the Kapton filter, the x radiation was attenuated by the anode screen plus additional screens on some shots. Anode screens had a transmission of either 36%, 90%, 97% or 100% (no screen). When minimum x-ray attenuation was in the line of sight, the largest signals were slightly space charge limited on some shots. But this had an insignificant effect on the integrals of the signals. With the common Kapton filter ahead of all the XRDs, the time histories of the emission signals from different materials were essentially the same on a given shot.

Data from different shots were normalized by dividing the emitted charge by the product IW. The photoemission signal from thick Kapton was less than half that from thin Kapton just as was observed for the secondary electron signal in the PESS.

IV.   ANALYSIS OF SKYNET RESULTS

A.   PRIMARY ELECTRONS

1.   Integrated Yields

The yield of primary electrons was determined from the energy-resolved data from each shot by summing the charges collected by the Faraday cups. This sum was transformed back to the number of emitted primaries by application of appropriate factors for the angular distribution of the emitted electrons, the solid angle subtended by the aperture between emitter and Faraday cups, and the cup collection efficiency. As already discussed in Section II.A.4, the solid angle was 0.023 steradians and the collection efficiency was 0.45.

A suitable factor for the angular distribution rests on the following assumptions: 1) the yield is independent of x-ray angle of incidence, 2) the electron energy spectrum is independent of emission angle, and 3) the number of electrons emitted per steradian follows a cos distribution with respect to the surface normal. The first assumption is valid at the low x-ray energies encountered in these experiments as verified by previous theoretical and experimental results.[6]   The other two assumptions are also based on prior theoretical analyses and are consistent with results given in Section III.C.

In particular, the spectral yield from aluminum foil on a cylindrical form was the same as from aluminum on the flat surface. This is consistent with a cos distribution. It is conceivable that space-charge effects could cause a slight deviation from the cos distribution. However, within the accuracy of the measurements, there was no correlation between the derived yield and the x-ray intensity. On the other hand, as described in Section III.D., more primary electrons were collected by the Faraday cups when the emitter was negatively biased.

All the primary-electron data from the different test series were intercompared and analyzed for sources of uncertainty. The resulting "best" values for the yields of primary electrons above 100 eV are given in Table 1 along with values for the estimated uncertainties. These uncertainty values include the $\pm$ 5% inherent in the calorimeter responses and were also based on the number of data shots, the quality of the data, the reproducibility of the results, and consistency between the results for different materials.

Some values of primary-electron yields were also derived from measurements of the photoemitter current when the emitter was at ground potential. In this derivation, it was assumed that the secondary electrons did not move away from the surface because of heavy space charge limitations. Owing to a lack of recording channels on all but the last test series, limited data were obtained for only a few materials. The resulting yields are also listed in Table 1. There is remarkably good agreement between these values and the Faraday-cup results for most materials--at worst, the values for white thermal paint differed by a factor of 1.5.

In Section VII, several of these primary-yield values are compared with values obtained from steady-state measurements using monochromatic radiation.

2. Spectral Yields

To obtain spectral yields for the primary emission, judgemental best-fit curves were drawn through the spectral data given in Section III.C. The energy scales were modified slightly to account for the actual electron orbits in the PESS. These curves were then normalized to the primary yields given in the preceeding section. The resulting spectral yields are given in Figures 25 and 26. It must be noted that the distributions were smoothed by

Table 1. Primary electron yields, Y_p, derived from summation
of Faraday-cup currents and from net currents off
grounded emitters. Values are "best" yields from
five test series. Units are 10^{13} electrons/joule.

	Faraday Cups	Emitter
Aluminum (Al)	2.0 ± 0.25	2.2 ± 0.5
Al_2O_3	1.4 ± 0.2	--
Gold (Au)	3.2 ± 0.4	--
Silver (Ag)	2.1 ± 0.3	--
Copper (Cu)	1.4 ± 0.2	1.5 ± 0.2
Graphite (C)	0.30 ± 0.08	0.28 ± 0.1
White Thermal Paint	0.90 ± 0.12	1.4 ± 0.3
Glass (SiO_2)	1.1 ± 0.3	--
Solar Cell Cover (MgF_2)	0.90 ± 0.15	1.12 ± 0.1
Mylar (6 μm)	0.43 ± 0.07	0.41 ± 0.1
Kapton (7 μm)	0.55 ± 0.1	0.65 ± 0.1
Kapton (125 μm)	0.90 ± 0.18	1.21 ± 0.1
Teflon (125 μm)	0.95 ± 0.18	0.9 ± 0.4
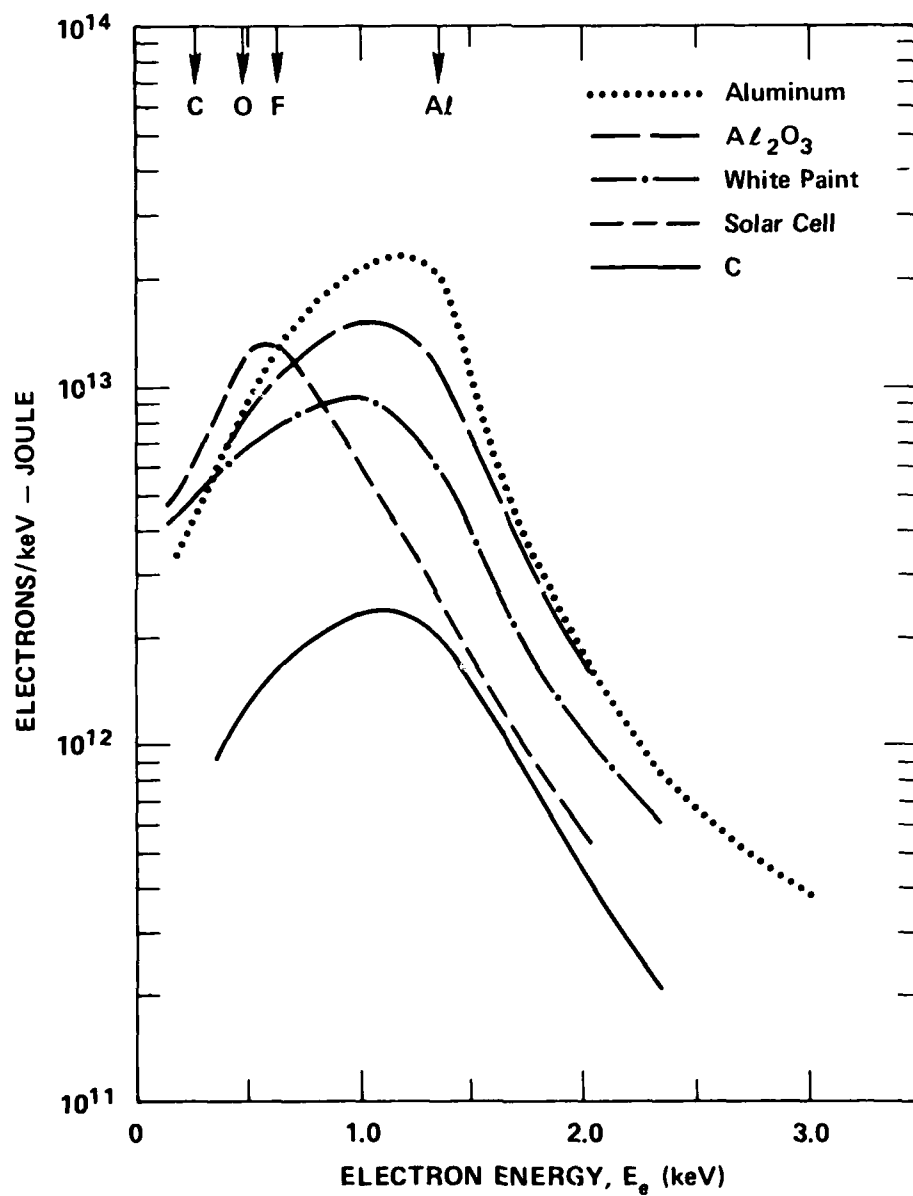
Figure 25   Spectral yields of aluminum, aluminum oxide, white thermal paint, solar cell cover and graphite irradiated by OWL II aluminum-wire spectrum. Uncertainties are discussed in text.
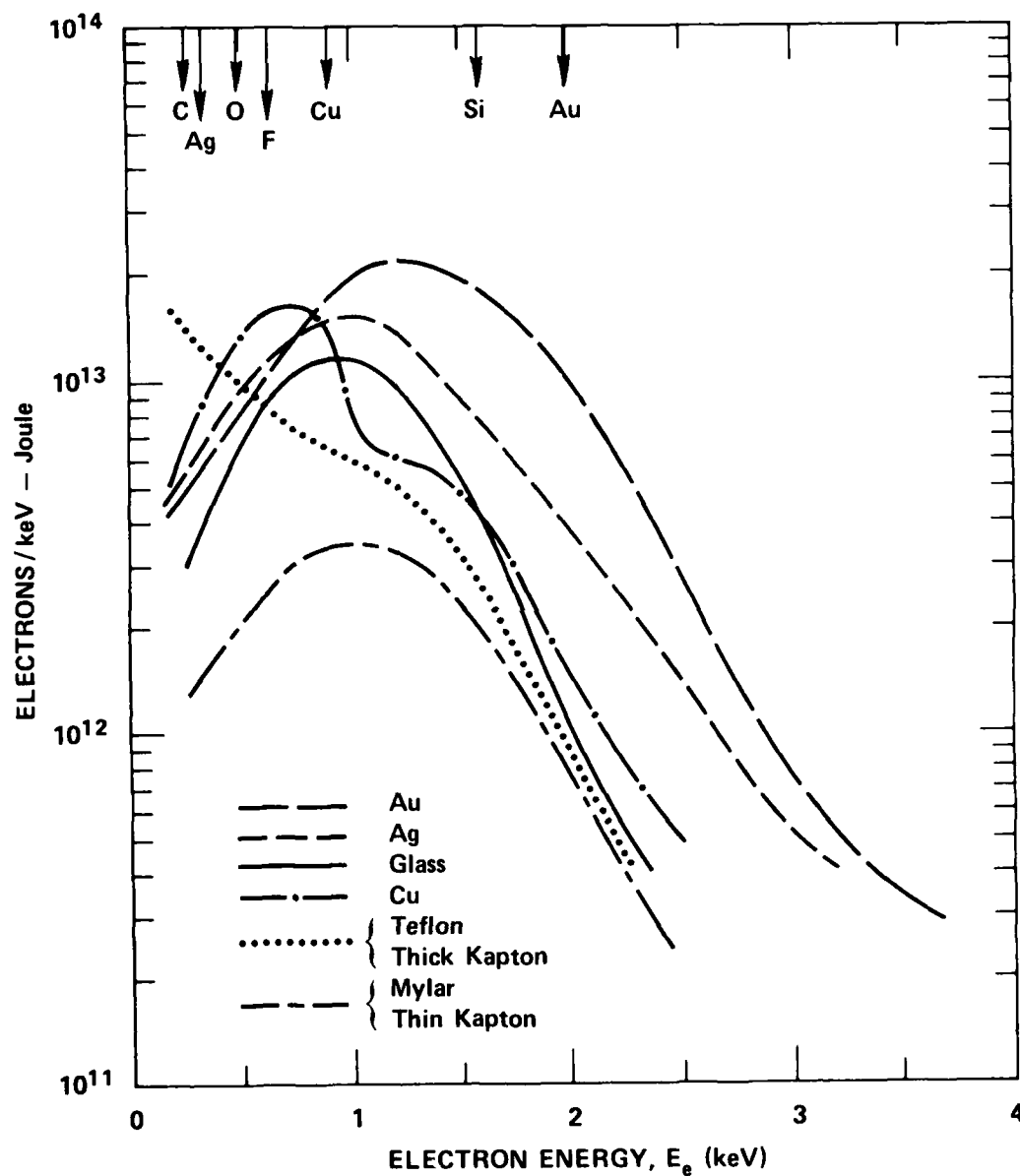
Figure 26   Spectral Yields of gold, silver, glass, copper,
             Teflon/Thick Kapton and Mylar/Thin Mylar irradiated
             by OWL II aluminum-wire spectrum. Uncertainties
             are discussed in text

63

instrumental broadening as well as by the x-ray spectrum. The spectral yields of most materials (Au, Al, Al_2O_3, C, Ag, white thermal paint, thin polymers and glass) peaked in the range from 1.3 down to 0.9 keV. The yields from copper and the solar cell cover peaked at lower energies of 0.7 and 0.6 keV while the thick polymers, Teflon and 125-μm Kapton, did not have a definite peak.

In the vicinity of the peak of each spectral yield, the uncertainty in the accuracy was about the same as for the integrated yield given in Table 1. At both lower and higher energies, the uncertainties were greater. As an example, the estimated uncertainties for aluminum were: ± 60% @ 0.2 kev, ± 30% @ 0.5 keV, ± 10% @ 1.0 keV, ± 30% @ 1.8 kev, and ± 70% @ 2.5 kev.

The absorption of x rays in a photoemitter generates photoelectrons and Auger electrons which lose varying fractions of their energies before emission from the surface. The initial energy of a photoelectron is equal to the difference between the photon energy, E_x, and the appropriate atomic binding energy (absorption edge), $E_{K, L, M, N}$. Auger electrons have energies characteristics of the material. Table 2 is a listing of the important photoemitter elements and the corresponding energies of the relevant absorption edges, principal Auger electrons and photoelectrons generated by 1.65 and 2.25-keV x rays.

The principal Auger-electron energies are indicated in Figures 25 and 26 and there is a good correlation between the location of these energies and the shapes of the spectral yields. In particular, the Auger energies for Al, Cu and F lie just above the peaks in the spectra from aluminum, copper and the solar-cell cover (MgF_2 coated).

64

Table 2. Energies of absorption edges, Auger electrons and photoelectrons for excitation by 1.65 and 2.25 keV X rays. All energies in keV.

Element/Z		Absorption Edge		Auger	Photoelectrons at E_x 1.65	2.25
C	6	K	0.29	0.27	1.36	1.96
O	8	K	0.53	0.50	1.12	1.72
F	9	K	0.69	0.64	0.96	1.56
		L3	0.01	--	1.64	2.24
Mg	12	K	1.31	1.18	0.34	0.94
		L3	0.05	0.04	1.60	2.20
Al	13	K	1.56	1.39	0.09	0.69
		L3	0.07	0.06	1.58	2.18
Si	14	K	1.84	1.61	--	0.41
		L3	0.10	0.09	1.55	2.15
Cu	29	L3	0.93	0.92	0.72	1.32
		M	0.06	0.06	1.60	2.20
Ag	47	M	0.37	0.35	1.28	1.88
		N.	0.01	--	1.6	2.2
Ag	79	M	2.21	2.02	--	0.20
		N	0.33	0.23	1.32	1.92
		O	0.01	--	1.6	2.2

3.   Time Resolved Spectra

In the preceeding section, only time-integrated electron energy spectra were derived because the integrated x-ray spectrum was fairly reproducible while the time history of the x-ray flux changed substantially from shot to shot. Therefore, time-resolved spectra would have to be treated separately for each shot. In addition, the electron energy spectra exhibited only small temporal variations. The notable exception was emission from aluminum plus a similar observation for glass.

As described in Section III.C and shown in Figures 10, 11, 23 and 24, the photoemisison from aluminum had significantly different time histories at different electron energies. The preponderant electron emission collected on cups covering the 0.5 - 1.4 keV range had a common time history with a dominant peak early in time followed by lesser peaks. On the other hand, higher-energy electrons from 1.4 to over 2.3 keV had a smoother time variation, peaking later in time. This hardening of the electron energy spectrum was observed to a much lesser degree in the emission from gold, see Figure 9. Another important observation to be considered was the extreme spikiness in the XRD signal when the x rays were filtered by 160 μm of Mylar, as shown in Figures 23 and 24. This thickness of Mylar had a cut-off transmission of 1% at 2.6 keV.

Most of the x-ray fluence was at energies just above the aluminum K edge at 1.56 keV. Let us consider x-ray energies of 1.65 to 2.25 keV and refer to Table 2. Since the x-ray absorption jump ratio at the Al K edge is 11, ten Auger electrons are generated with energies of 1.39 keV for every electron generated from the L-shell with an energy of 1.6 to 2.2 keV. In addition there will be ten K-shell photoelectrons with energies under 0.7 keV. All these energies are upper limits since the electrons lose energy in the material before being emitted at the surface. The origin of electrons detected in the PESS with energies greater than 1.4

66

keV can be L-shell photoelectrons or K-shell photoelectrons gene-
rated by x rays above 3 keV. The latter possibility is ruled out
by the XRD observations. In addition, a time-varying x-ray spec-
trum must be consistent with the gold photoemission signals.

The x-ray spectrum consisted of several components as des-
cribed in Section III.A. Therefore the signals observed at
different electron energies were a superposition of photoemission
generated by different x-ray spectral fluxes. The time-varying
electron spectrum can be explained by assuming that the He-like
and H-like plasma emit radiation with different time histories;
inherent in this assumption is that the line radiation and con-
tinuum from a given plasma state have the same time variations.
Temporal behaviors, that can explain all the observations, are a
smooth broad pulse for the radiation from the He-like plasma and
sharp spikes for the x-ray emission from the H-like plasma.
The assumed x-ray spectra, photoelectron spectra and time his-
tories of the two plasma states on a representative shot are
shown in Figure 27. Under this assumption, the He-like recombin-
ation radiation interacted with Al L-shell electrons and generated
the electron emission above 1.4 keV, while H-like line radiation
excited the emission peaks superimposed on the signals below 1.4
keV. The H-like continuum produced very little photoemission
from aluminum, but substantial amounts from the gold because of
its larger absorption cross section above 2.2 keV.
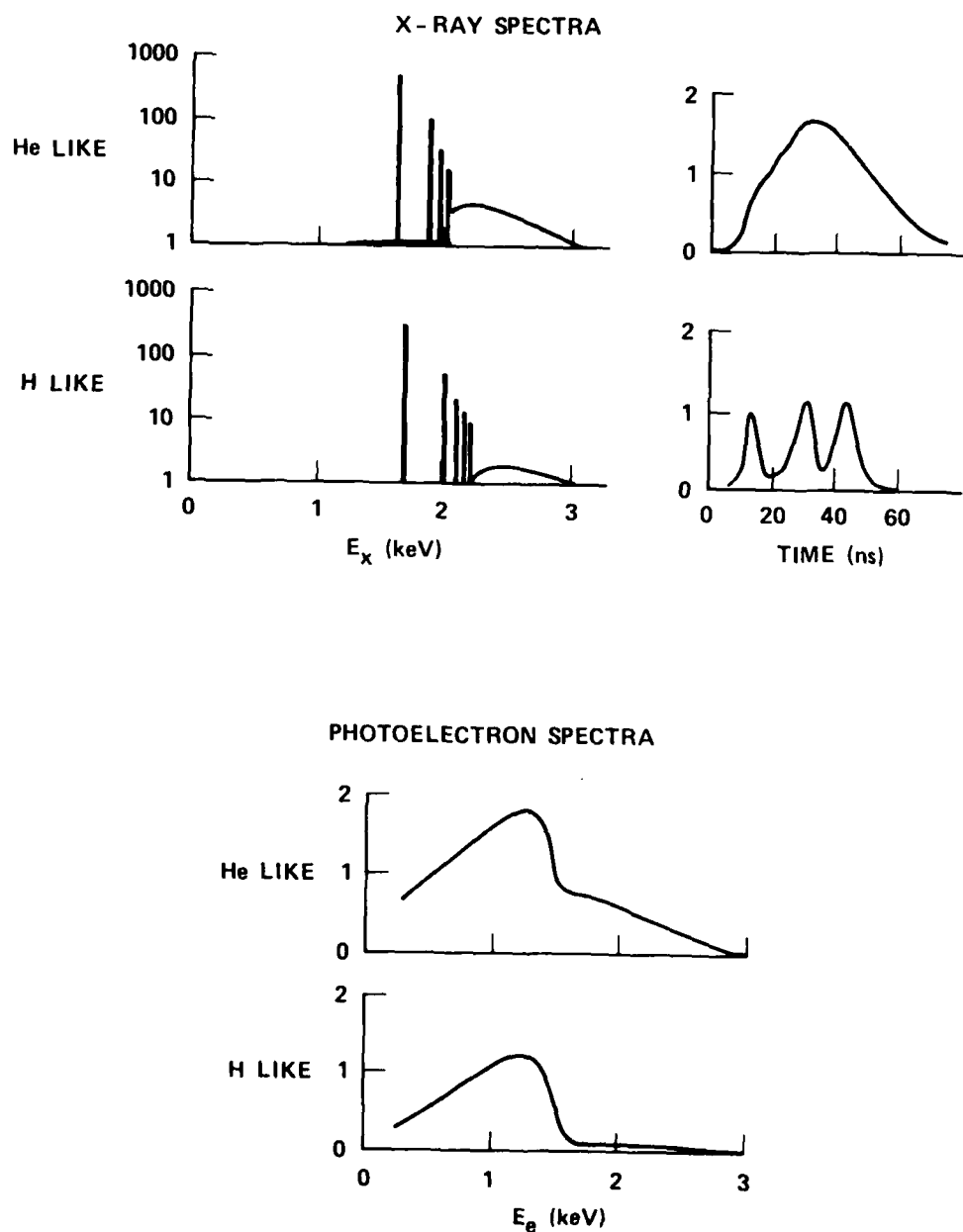
Figure 27   Assumed x-ray spectra, time histories and resulting
             photoelectron energy spectra from aluminum generated
             by typical He-like and H-like plasma components

68

B.   SECONDARY ELECTRONS

1.   Method

Since secondary electrons have very low energies (mostly
0-10 eV), only their yields were determined with no attempt at
energy resolution. Values for secondary-electron yields could
be derived from three different measurements: 1) total emission
from biased XRD cathodes, 2) total emission from the biased PESS
emitters, and 3) collection of accelerated secondaries by a Faraday
cup. The first two measurements were used in a straight-forward
manner to obtain secondary-electrons by subtracting the primary-
electron yields in Section IV.A.1 from the total electron yields.

It turned out that the secondary-electron yields extracted
from the third measurement had a large uncertainty because only a
fraction of the emitted electrons were collected. In the analysis
of primary-electron yields, the electrons were assumed to have a
cosine angular distribution when emitted from a grounded emitter.
However, an applied bias potential altered the trajectories of
lower-energy electrons. In particular, for the case of a flat
emitter, the electric field tended to bend the electron trajec-
tories toward the surface normal so that more electrons passsed
through the aperture. As discussed in Section III.D, there was a
definite enhancement in the number of low-energy primary electrons
detected from a biased emitter. This field-focusing effect was
partially counteracted by space-charge fields that caused the
electrons to diverge. It was already mentioned that there was
space-charge limiting of the secondary emission current, if the x
radiation was not attenuated.

The combined effects of applied electric field and the large space-charge fields were very complicated and difficult to analyze for the actual PESS geometry. Therefore, a sophisticated computational analysis was undertaken by Systems, Science and Software as a subcontract to the overall program. The goals and results of these calculations are given in Section VII.

In spite of the uncertainty in the fraction of emitted secondary electrons collected by the Faraday cups, this type of measurement did provide supplementary information. These results provided relative values of secondary-electron yields from different materials. The spectral-yield data obtained with the emitter biased, such as shown in Figure 22, showed that the magnitude of low-energy enhancement depended slightly on the value of the applied potential. For the bias potentials of -600 to -1000 volts used for most measurements, the detected number of low-energy primary electrons was about twice that observed from a grounded emitter at lower fluxes.

There was a limited amount of data in which the total emission from the biased emitter could be compared with the collected-secondary-electron signal. These results showed that the fraction of secondary electrons passing through the aperture did depend on the x-ray flux--this fraction decreased at higher fluxes. At lower fluxes, the number of secondaries detected was twice that expected for a cosine angular distribution.

Other experimental observations were gleaned using a cylindrical aluminum photoemitter. When this emitter was grounded, the primary-electron spectral yield was the same as that from a flat aluminum surface. Furthermore, the low-energy primary-electron emission from the biased cylindrical surface was still enhanced over that from the grounded emitter. But there was a definite decrease in the observed secondary yield from the biased cylindrial surface. These observations for a cylindrical emitter are

consistent with the field "focusing" the electrons in one direction and "defocusing" in the other direction.

2.   Results

Total yields of secondary plus primary electrons from various materials were derived from the XRD and PESS measurements. Since secondary-electron yields, and thus total yields, are sensitive to surface condition and contamination, care was exercised in selecting the most reliable values. In particular, the total emission from aluminum was observed to have the highest total yields when the surface was fresh. After being left in the system for many shots, the yields were 10 to 50% lower. Thus, the freshness of a surface was an important criterion in weighting the various data. On the other hand, primary-electron yields were not sensitive to this type of contamination.

The resulting "best" values are tabulated in Table 3. For most materials, there was remarkably good agreement between the values obtained in the PESS and in the XRDs. There were substantial differences in the total yields from the thermal white paint and thin Mylar. In the case of the white paint, it is not surprising that the values differed since they were applied differently to the substrates. As to the Mylar results, the samples used in the PESS was aluminized on one side and it may have had some aluminum on the other side. In addition, this sample may have been contaminated. Although contamination reduced the total yield from aluminum, it could increase the yield from other materials.

The biggest discrepancy was the extremely-low total yield from the solar-cell cover mounted in an XRD. In fact, this value was even lower than the primary-electron yield measured in the PESS. A possible explanation is a substantial conductivity

through the "vacuum", as postulated for the biased-emitter observations in the PESS. In the XRD, the gap between solar-cell
surface and grounded screen was very small. Therefore, most of
the applied potential may have been across the thickness of the
quartz so that there was negligible accelerating potential for
the low- energy electrons.

Table 3. Total photoemission yields in units of 10^{13} e/J
measured using pulsed plasma X radiation

Material	XRD	PESS Emitter
Aluminum	9.4 + 0.6	9. + 1.
Gold	--	7.5 + 0.5
Copper	--	5.4 + 0.7
Brass	5.4 + 0.6	--
Graphite	--	1.4 + 0.2
Aerodag	1.45 + 0.15	--
White Paint	3.8 + 0.3	4.4 + 0.6
Glass	2.4 + 0.6	2.5 + 0.6
Solar Cell Cover	0.76 + 0.15	3.5 + 0.5
Mylar (6 μm)	0.9 + 0.1	1.5 + 0.3
Kapton (7 μm)	2.5 + 0.3	2.9 + 0.4
		3.1 + 0.5
Kapton (125 μm)	1.2 + 0.12	1.2 + 0.2
Teflon (125 μm)	1.8 + 0.9	1.9 + 0.4

V. STEADY-STATE YIELD MEASUREMENTS

As a complement to the pulsed measurements described in Sections II, III and IV, photoemission yields were measured using steady-state x radiation. The advantages of these measurements over those using the exploding-wire source were: 1) greater reproducibility, 2) good vacuum conditions, 3) no space-charge effects, 4) greater accuracy, 5) use of monochromatic x rays to determine energy dependences. The experimental arrangement is described followed by the results of the measurements giving total and primary electron yields.

A. EXPERIMENTAL DESIGN

1. X-Ray Source

The low-energy, steady-state x radiation used for these measurements was generated by a DNA calibration facility operated by Science Applications Incorporated (SAI) in Sunnyvale. This facility had a Henke-tube source with a copper anode operated at 16 keV. The copper-anode output spectrum excited characteristic line radiation from eight fluorescers at energies ranging from 1.26 to 5.41 keV. The fluorescent spectra passed alternately through well-matched pairs of Ross filters. A listing of the fluorescer materials and energies of characteristics lines is given in Table 4. The spectral outputs were measured using the standard techniques of a gas proportional counter and a multichannel analyzer. The intensity calibration was normally within 2% and the spectral purity (difference between pass and block filters) was designed to be better than 99%.

Table 4.   Monochromatic X-ray lines used for
steady-state photoemission studies

Fluorescer	Energy (keV)
Mg	1.255
Al	1.488
Si	1.742
Cl (Saran)	2.634
Sc	4.125
Ti	4.551
V	4.948
Cr	5.410

Photoemission currents were measured using a Keithley 610C picoammeter and were displayed on a strip-chart recorder.   The measured currents ranged from 3×10^{-15} to 10^{-12} A and could be determined to within 2% of reading plus 5×10^{-16} A.   The overall accuracy of the measurements was judged to be better than 5% except where limited by signal strength.

2. Yield Apparatus

The yields of primary electrons and primary-plus-secondary electrons (total) were measured using a retarding-potential spectrometer. This "birdcage" apparatus, shown schematically in Figure 28 and by a photograph in Figure 29, had a highly-transparent retarding grid surrounding the photoemitter. The parallel-wire grid was 97% transparent to electrons and was completely transparent to the incident x rays. A low-z coating of Aerodag was sprayed on the chamber walls and the grid to reduce electron backscatter. The photoemitter was a bitruncated circle (two parallel sides) with dimensions of 7 by 10 cm; this was just slightly larger than the pattern of the incident x rays at the chosen distance from the source.

During the development and testing of the apparatus, it was necessary to add two features. One was an apertured magnet near the x-ray source to serve as an electron trap stopping photoelectrons generated in the source region. The other was maintaining the photoemitter assembly at -31 V with respect to the grounded walls in order to inhibit the migration of secondary electrons and low-energy electrons backscattered from the chamber walls to the emitter. This was done by placing an in-line battery between the photoemitter and the picoammeter. The electrical feedthroughs were selected to have negligible leakage currents.

The normalized photoemission current from an aluminum photocathode irradiated by Si-K x rays is plotted in Figure 30 as a function of grid-to-emitter potential, V_G. At positive potentials, the signal was constant providing a clear determination of the total photoemission. On the basis of some simple computer calculations, the minimum potential in front of the photoemitter was estimated to be about 60% of the applied grid bias. For small negative values of V_G, the current decreased rapidly corresponding to the energy

75
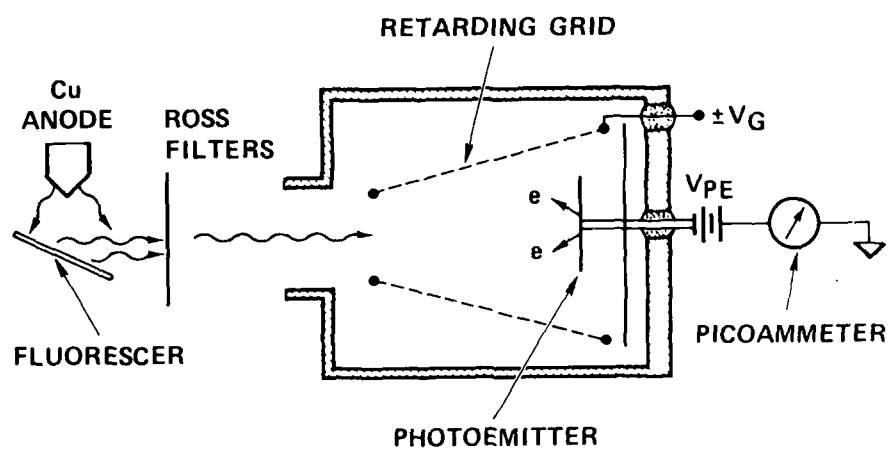
Figure 28   Experimental setup to measure total and primary
x-ray photoyields
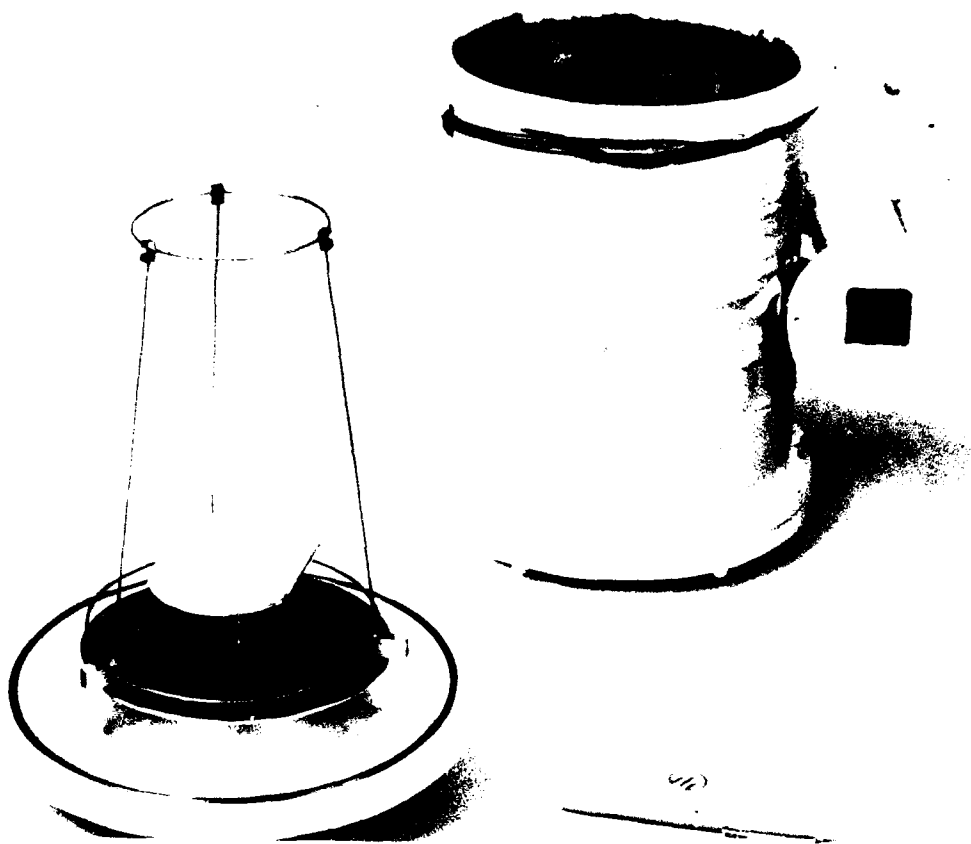
Figure 29   Photograph of birdcage apparatus to measure total
and primary photoemission yields.

NORMALIZED PHOTOEMISSION CURRENT
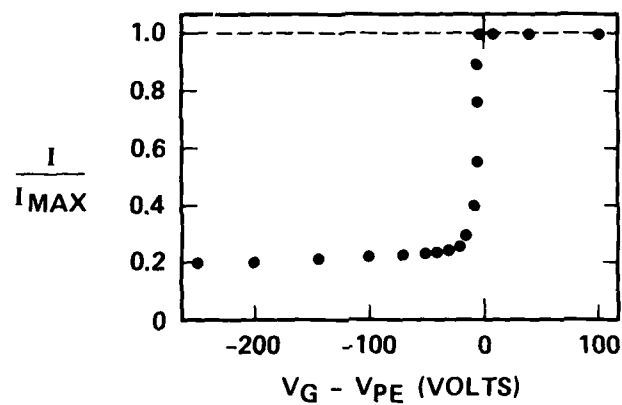
Figure 30   Normalized photoemission current from aluminum as a
             function of retarding potential; x-ray energy was
             1.74 keV

78

distribution of low-energy electrons. At larger biases, a change in V_G from -50V to -100V produced only a 3% decrease in the normalized current, so there was only a slight uncertainty in the primary emission current. The electron flow from the grid was measured to be only 2 to 3% of the primary electron current. Since part of this emission flowed back to the photoemitter when $V_G < 0$, the net effect was only a 1% shift. Measurements of the total photoelectric yield were made with the grid biased at +10V with respect to the photocathode. Primary-electron yields were determined with the grid biased at -50V. In this case, it was estimated that all electrons emitted with kinetic energies under 30 eV were returned to the photocathode assembly. The system was evacuated by a turbo-molecular pump to a pressure of about 2×10^{-6} Torr.

3. Materials Studied

The photoemitter materials studied under this program were aluminum, aluminum oxide, gold, silver, silicon, silicon dioxide, glass, Mylar and Kapton. Several of these photoemitters were from the same sources as used in the PESS measurements. The configurations and compositions are listed below.

1. Aluminum foil. Standard 18-μm Reynolds wrap.
2. Aluminum oxide. Aluminum foil anodized in 3% solution of ammonium citrate, applied voltages of 100 and 200V produced Al_2O_3 thicknesses of 135 nm and 270 nm (1350 and 2700 angstrom).
3. Gold. Coating on copper-clad PC board obtained.
4. Silver. Coating on copper-clad PC board obtained from MRC.
5. Silicon. A 0.5-mm thick sheet cut from a high purity wafer used by the semiconductor industry.
6. Silicon dioxide. The above sheet of silicon was oxidized in a furnace to produce an SiO_2 layer with a thickness of about 200 nm.

7. Glass. Four 1-mm-thick microscope slides mounted side
   by side. The composition was not determined, but most
   likely contained significant amounts of Na_2O, K_2O and/or
   CaO in the SiO_2.
8. Mylar. Thickness of 6 μm, with a nominal composition of
   $C_{10} H_8 O_4$. An Aerodag was applied to the back.
9. Kapton. Thickness of 7 μm and 125 μm were studied with
   the thick sample from MRC. Both samples had been aluminized
   on their backsides.

Where appropriate, all surfaces were cleaned with reagent-grade
methanol.

Some of the materials were dielectrics, having thicknesses of
several micrometers or more. For these samples, it was important
to determine if surface charging affected the results. This effect
was studied experimentally by varying the photon intensity and by
increasing the positive bias on the grid. Analytically, the maxi-
mum surface potential was estimated from the ratio of the emission
current density to the volume resistivity. In all cases, save the
thick Kapton, charging was negligible. For instance, the thin
Kapton and Mylar charged up to no more than 0.4V. The thick Kapton
sample charged up to higher potentials estimated to be about 10V.
When the bias potential was increased from +10V to +300V, the total
emission from this thick Kapton increased by 13%.

B. YIELD RESULTS

The measured primary and total electron yields are tabulated
in Table 5. It is well known that the electron yield is propor-
tional to the energy-absorption cross section, μ, which has an
inverse power-law dependence on photon energy with abrupt increases
at absorption edges. Accordingly, these yield values are displayed

Table 5. Primary and total photo-Auger electron yields in units of 10^{-3} electron/photon

E_x Material	Mg 1.26	Al 1.49	Si 1.74	Cl 2.64	Sc 4.12	Ti 4.55	V 4.95	Cr 5.41
Al	2.45	1.85	8.05	4.10	2.95	2.55	2.35	2.15
Foil	14.3	9.6	36.5	17.1	8.9	7.6	6.6	5.6
Al_2O_3	2.65	2.15	5.05	2.85	1.70	1.55	1.40	1.28
	18.2	13.0	26.5	13.3	5.95	5.00	4.35	3.70
Gold	12.7	11.2	9.7	21.4	19.4	16.6	15.6	14.0
	54.0	43.0	34.0	67.0	52.0	44.5	40.5	34.6
Silver	10.8	9.45	8.7	5.8	15.1	13.6	12.6	11.2
	49.4	41.1	35.6	18.5	43.2	37.7	33.8	29.4
Silicon	1.9	1.6	1.2	5.8	3.45	3.1	2.9	2.6
	5.5	3.6	2.9	13.3	6.7	5.7	5.1	4.6
Glass	2.7	2.35	2.0	2.85	2.2	1.9	1.75	1.55
	19.8	14.6	11.1	12.9	7.4	6.1	5.3	4.5
Mylar	1.95	1.5	1.2	0.77	0.40	0.36	0.33	0.28
(6 μm)	4.45	3.2	2.35	1.25	0.61	0.51	0.45	0.38
Kapton	2.05	1.65	1.85	0.98	0.52	0.45	0.39	0.33
(7 μm)	4.32	3.70	3.92	2.82	1.90	1.71	1.59	1.52
Kapton	1.62	1.39	1.16	0.64	0.41	0.34	0.32	0.28
(125 μm)	5.75	4.3	3.2	1.47	0.76	0.63	0.56	0.48

on logarithmic plots in Figures 31, 32 and 33. In the energy ranges on either side of absorption edges, most of the data are fit by the straight lines drawn on these plots. Most of the small deviations were experimental errors. Some of this data and its analysis were published and compared with other results.[7] There was generally good agreement.

In the case of gold, the data at 2.64 keV fell in the midst of the series of M absorption edges and was therefore expected to fall between the extrapolations of results on either side. Similarly, the two data for glass at 2.64 keV fell below extrapolations of the data at higher energies. This can be explained by the presence of potash or lime which are commonly used in glass -- the absorption edges for potassium and calcium are at 3.61 and 4.04 keV, respectively.

A significant deviation from a straight-line fit was found in the data for aluminum. The primary yield at 2.64 keV definitely fell below a straight line connecting the value at 1.74 keV and the values above 4 keV. Several samples of aluminum foil were measured and the x-ray output was recalibrated to ensure that this was not an experimental error. It was also found that below the aluminum K edge, the yields of the aluminum foil and the anodized aluminum were nearly the same. Such an observation is explained by the normal oxide layer on aluminum which has a thickness of about 5 nm.

There were several interesting aspects to the yield results from the three polymers. The primary yield from the thick (125 μm) Kapton was slightly less than that from Mylar, while the total yield of the Kapton sample was greater than that from the Mylar. For comparison, the primary yield from graphite deposited as Aerodag was the same as the Mylar yield while the total yield was much larger. However, the yields from the thin (7 μm) Kapton exhibited unexpected
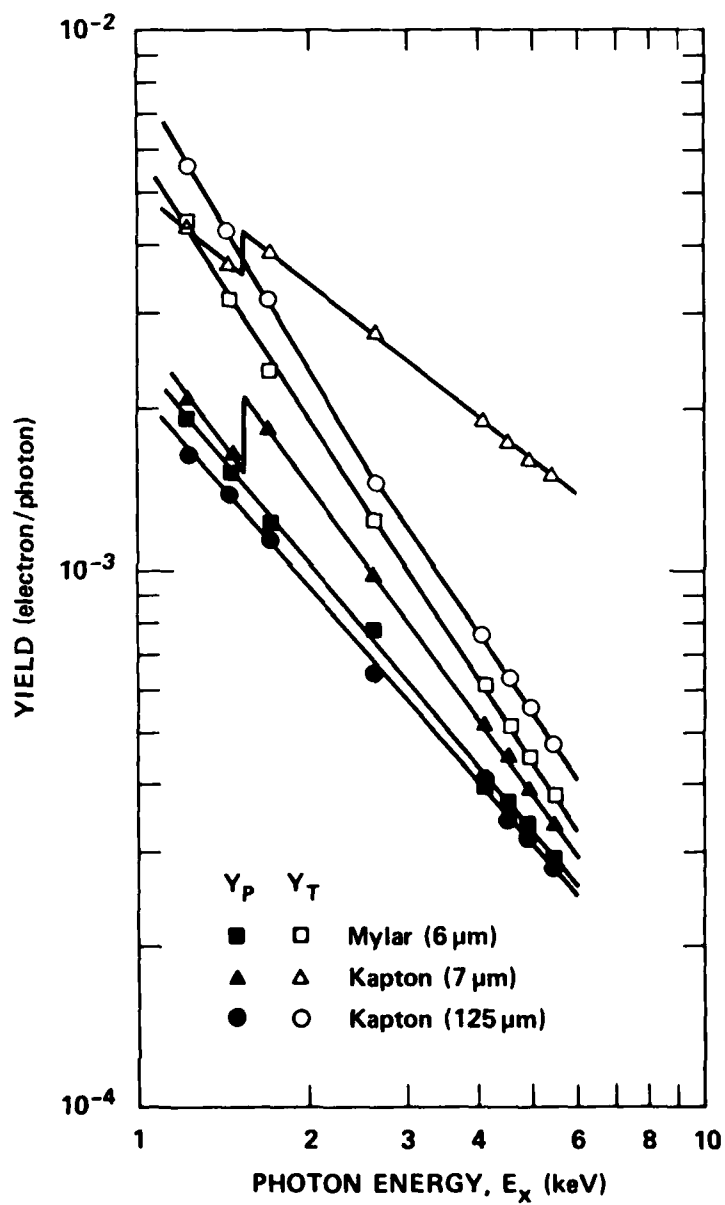
Figure 31   Primary, Y_p, and total, Y_T, photoemission yields
from Mylar and Kapton

83
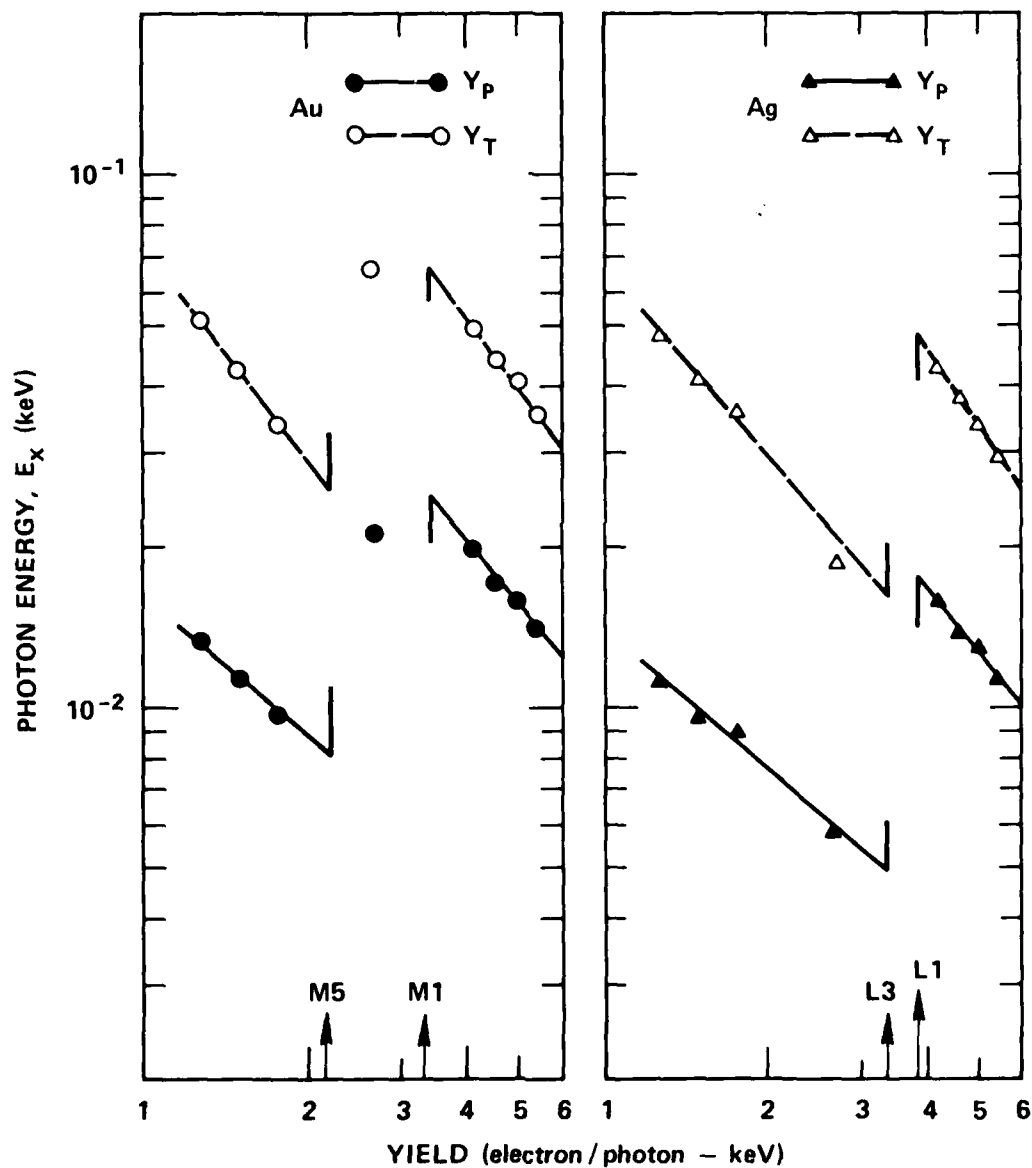
Figure 32   Primary, Y_p, and total, Y_T, photoemission yields from gold and silver
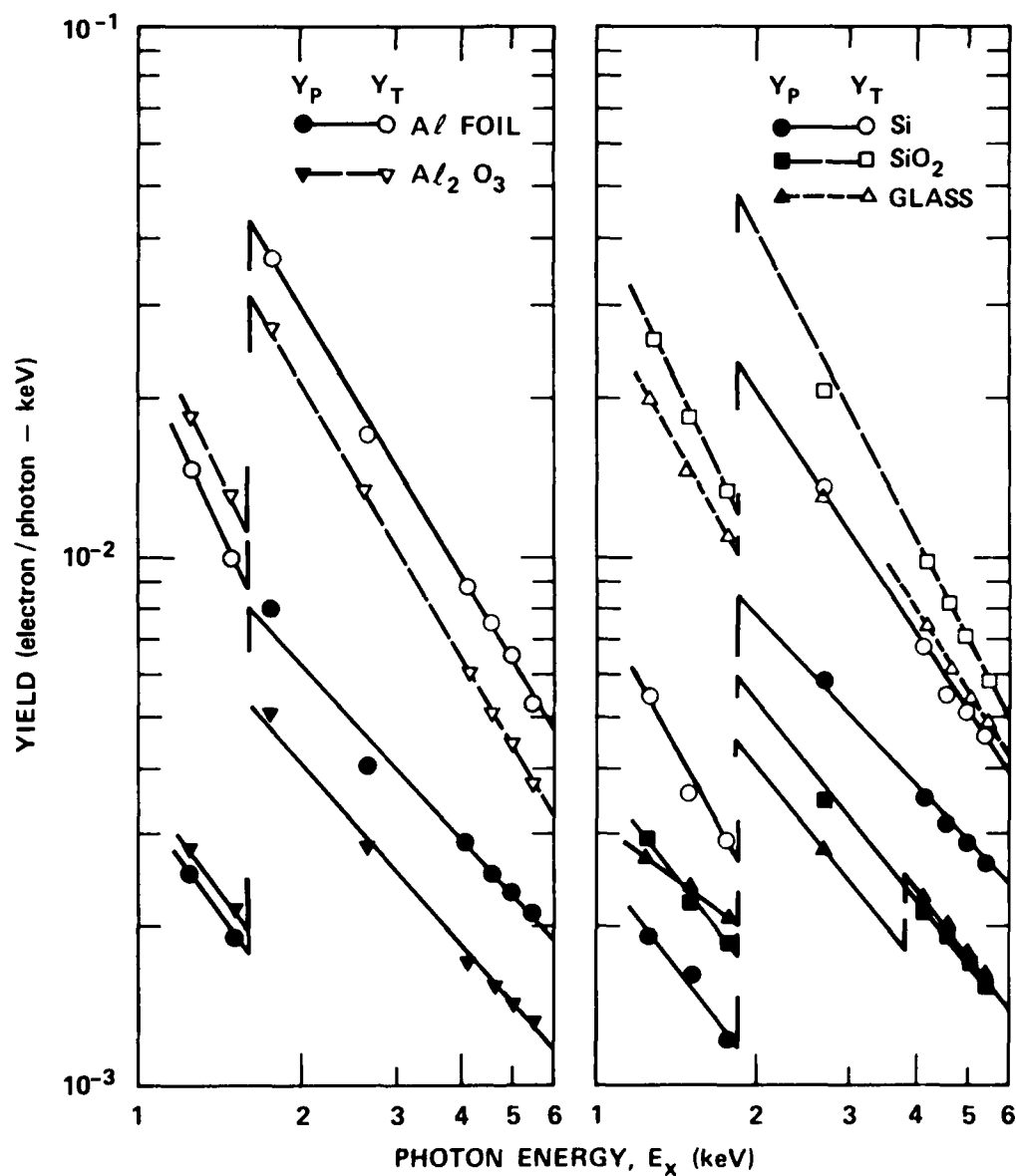
Figure 33   Primary, Y_P, and total, Y_T, photoemission yields
from aluminum foil, anodized aluminum, silicon, silicon
dioxide and glass

behavior. While the primary yield of this thin Kapton was only slightly larger than the Mylar yield at the two lowest photon enegies, there was a significant increase at energies above 1.5 keV. The total yield also had a jump just above 1.5 keV. In addition, the total yield from this thin Kapton sample did not fall off as rapidly with photon energy as all other materials.

An explanation for this observed photoemission from the thin Kapton resides in the aluminizing on the other surface. When the film was rolled up after being aluminized, very small amounts were transferred to the uncoated surface. When it is assumed that this added aluminum (Al_2O_3) needs only have an average thickness of 2 nanometers to account for the 30% jump in the primary yield. It is more difficult to explain the energy dependence of the enhanced total emission. Most likely this transferred aluminum does not form a uniform layer, but is in the form of tiny spots with dimension of 10-30 nm. In this case, the emerging primary electrons will irradiate larger circular spots in the Kapton thereby increasing the secondary-electron generation.

Values for the secondary electron yield, Y_s, were obtained by taking the differences between the total and primary electron yields. Ratios of the secondary and primary yields, Y_s/Y_p, are plotted in Figure 34. The largest ratios were observed for the inorganic dielectrics glass and aluminum oxide while the smallest ratios were found for silicon, Mylar and the thick Kapton. In general, this ratio fell off with increased photon energy. The exception was the thin Kapton which had some aluminum on the surface.
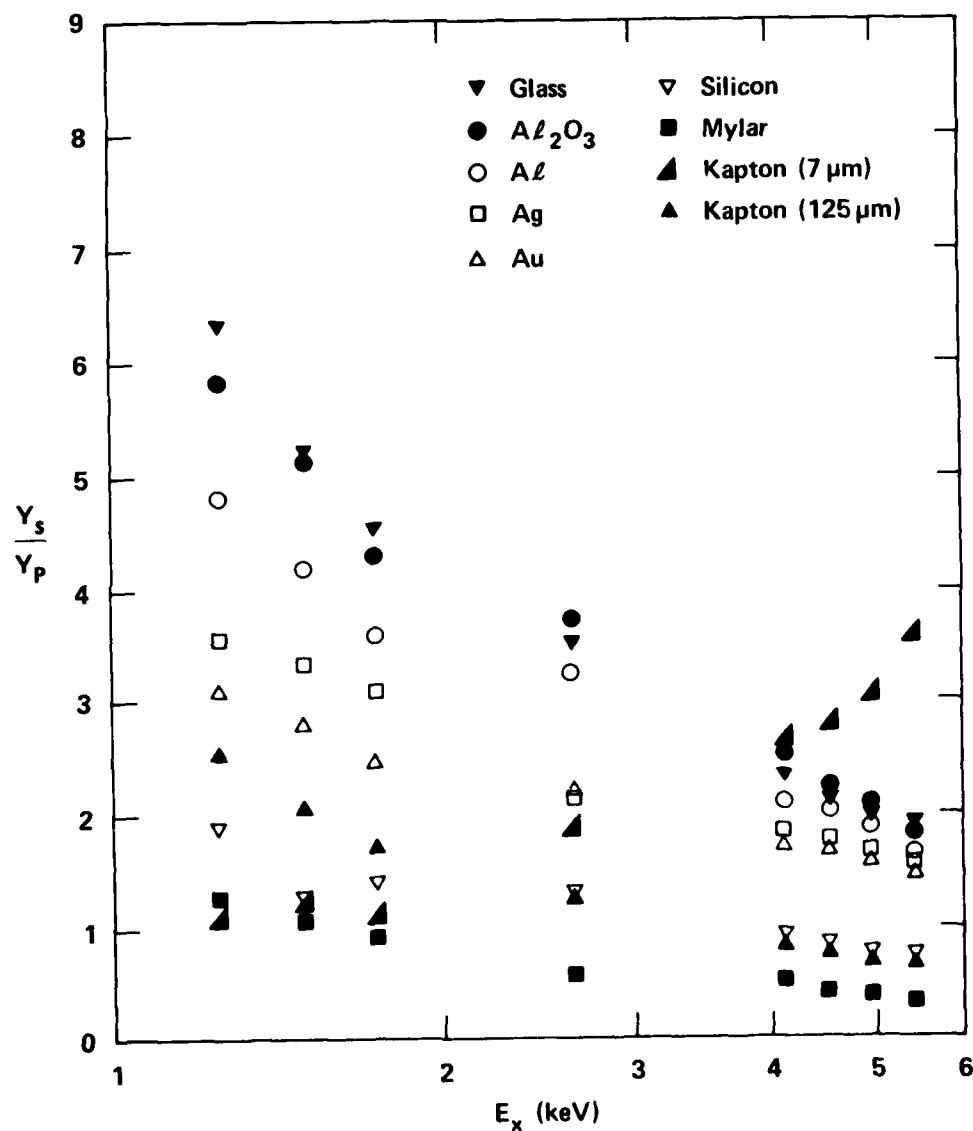
Figure 34   Ratio of secondary electron yield to primary electron yield, $Y_s/Y_p = (Y_T - Y_p)/Y_p$

VI.   STEADY-STATE SPECTRAL MEASUREMENTS

A second phase of the steady-state studies was to develop
suitable instrumentation and measure the energy spectra of photo-
electrons generated by low-energy monochromatic x radiation. The
x-ray source used was the same as described in the previous section
for the steady-state yield measurements.

There are different approaches to determining the energy dis-
tribution of emitted electrons. One method is to use a high-
voltage retarding grid, similar in many respects to the set up
used for the yield measurements. However, the geometry of the re-
tarding grid would have been more complicated than that used to
determine just the primary yield and high voltages would have to
be used. The other method is the use of an electrostatic or magne-
tic energy analyzer with an electron-counting detector. This latter
method was selected for the measurements in this program. The mag-
netic spectrometer (PESS) was used with appropriate modifications.

A.   APPARATUS

To determine the photoelectron energy spectra, the PESS was
modified by replacing the Faraday-cup array with a channeltron
electron multiplier. A schematic diagram of the apparatus is
shown in Figure 35 and a photograph of it is in Figure 36. The
x radiation was incident on the $1.8-cm^2$ beveled photoemitter and
a small fraction of the emitted electrons passed through the aper-
ture into the magnetic analyzer region. Since the transmitted cur-
rent was very small, individual electrons could be counted by the
detector. The electron count rate was measured as a function of
electron energy by varying the magnetic field. As already

COAXIAL FEEDTHROUGH

PHOTOEMITTER

MAGNET COIL
ON VACUUM
CHAMBER

CHANNELTRON
DETECTOR

ELECTRON
APERTURE

e

e

$\odot\,B_z$

$\vdash$— 5 cm —$\dashv$
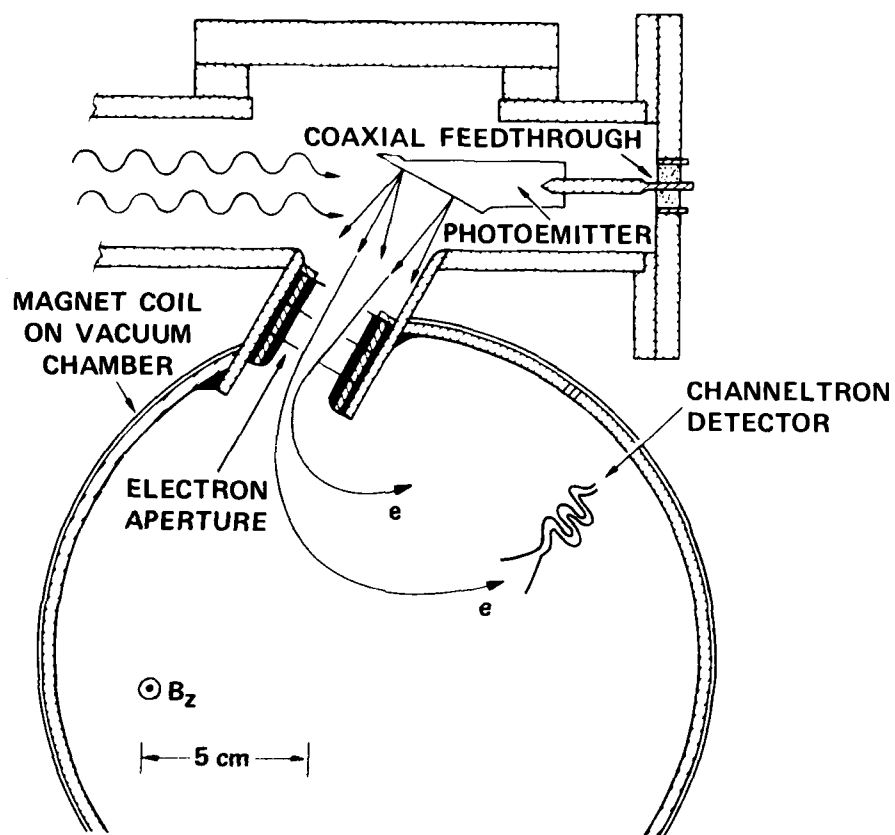
Figure 35   Photoelectron spectrometer system used for steady-
state spectral measurements
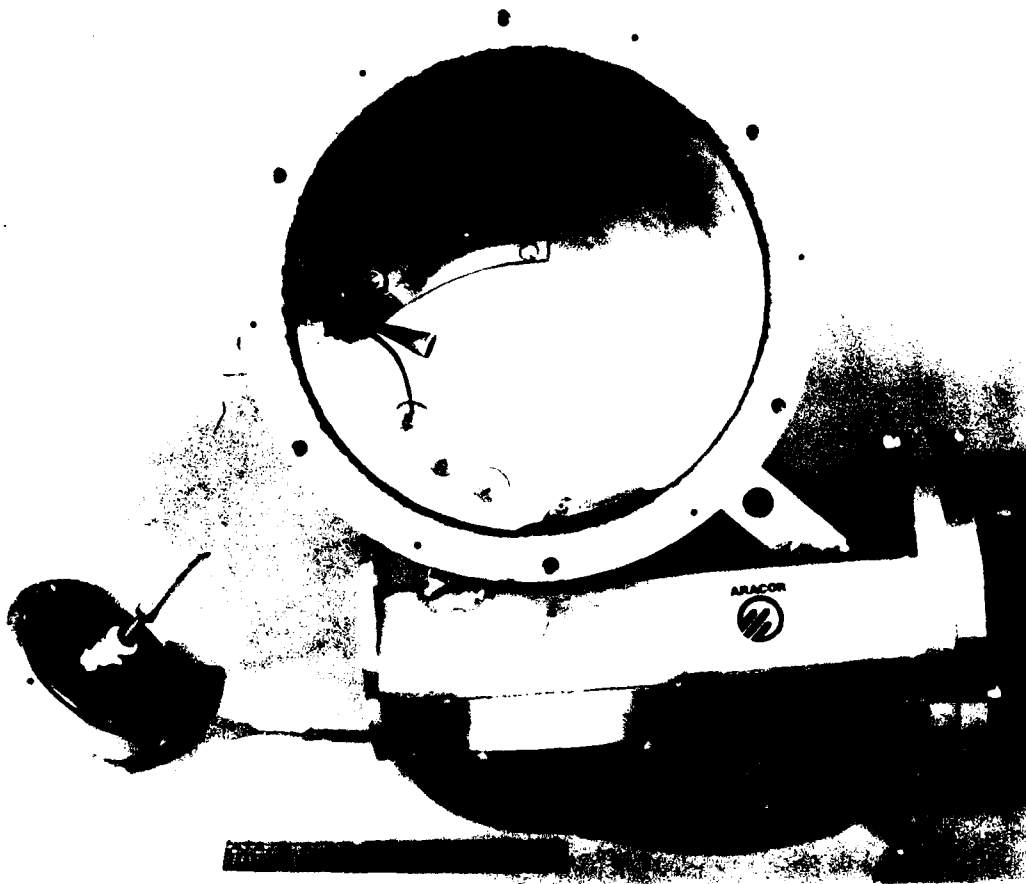
Figure 36   Photograph of PESS with channeltron

described for the yield measurements, the net count rate corres-
ponding to a given x-ray energy was the difference between the
count rates using pass and block x-ray filters. In this experi-
mental set-up, the electron trap was also needed to stop spurious
electrons that originated at the x-ray source.

The detector used for the initial measurements was a Galileo
Model 4039-EIC channeltron, having an entrance aperture 10 mm in
diameter.[8] For subsequent measurements, a new channeltron, Gal-
ileo Model 4028-EIC/B1, was procured which had a rectangular en-
trance 10 mm wide by 25 mm high (parallel to the magnetic field.)
The overall size of this latter detector restricted where it could
be placed in the PESS chamber. Consequently, the electrons tra-
veled orbits averaging only 135° from the aperture to the detec-
tor and the energy resolution was slightly dependent on the angular
distribution of the electrons passing through the aperture.

The channeltrons were operated in a standard way with the
outside of the front entrance cone at ground potential and the
output end at a positive 2.9 or 3.0 kV. Output pulses were trans-
mitted on the high-voltage lead connected to a vacuum feed-through.
These pulses were conditioned by a preamplifier-H.V. unit and then
counted. Discriminator settings on the counter were adjusted to
include all electron counts while rejecting noise. Data for the
energy spectra of primary electrons were generated by measuring
the electron count rate as a function of applied magnet-coil cur-
rent, I_B. To derive spectral yields from the data, calibration
factors were needed for the system energy response (E_ϵ), energy
resolution (ΔE), energy-dependence of the detector response, geo-
metric collection efficiency of the detector and an assumed angular
distribution of the emitted electrons as discussed in Section IV.A.
The energy response and resolution of PESS depended on the geo-
metric configuration of the channeltron with respect to the elec-
tron aperture and upon the magnetic-field calibration.

The energy response and energy resolution of the system were derived both by calculations and experiment. Ideally, the energy resolution, ΔE, in this fixed geometry should have been a constant fraction of the average energy, E_e, of the detected electrons. Electron trajectories in the actual geometry were calculated considering the possible range of angles determined by the photoemitter aperture configuration. Experimentally-derived values for the energy response and resolution were gotten by accelerating low-energy secondary electrons emitted from gold irradiated by 4.12-keV photons. At a fixed setting of the magnetic field current, the electron count rate, C_e, was measured as a function of applied voltage, V_A, on the photoemitter.

The larger, rectangular-aperture channeltron was calibrated using five different magnet-coil currents, I_B, corresponding to nominal electron energies, E_e, of 0.1 to 2.6 keV. The vacuum feedthrough on the PESS photoemitter and the available power supply limited the applied voltage to under 3 keV. These sets of data were normalized through use of the ratio V_A/I_B^2 and are plotted in Figure 37. If the system were perfect, these data sets should have been independent of I_B^2. But two distinct trends were found as I_B was increased: 1) the values of V_A/I_B^2 at peak count rates became larger and 2) the shapes of the plots became pronouncedly asymmetric. Higher-energy primary electrons were also detected as a low-level count rate to the left of the peaks (smaller V_A/I_B^2).

Pertinent aspects of these calibration data are given in Table 6 in which $V_N \equiv V_A/I_B^2$. As I_B was increased, the widths of the peaks, V_N, became narrow while the midpeak position, V_N, shifted upward. This narrowing in the plots can be explained
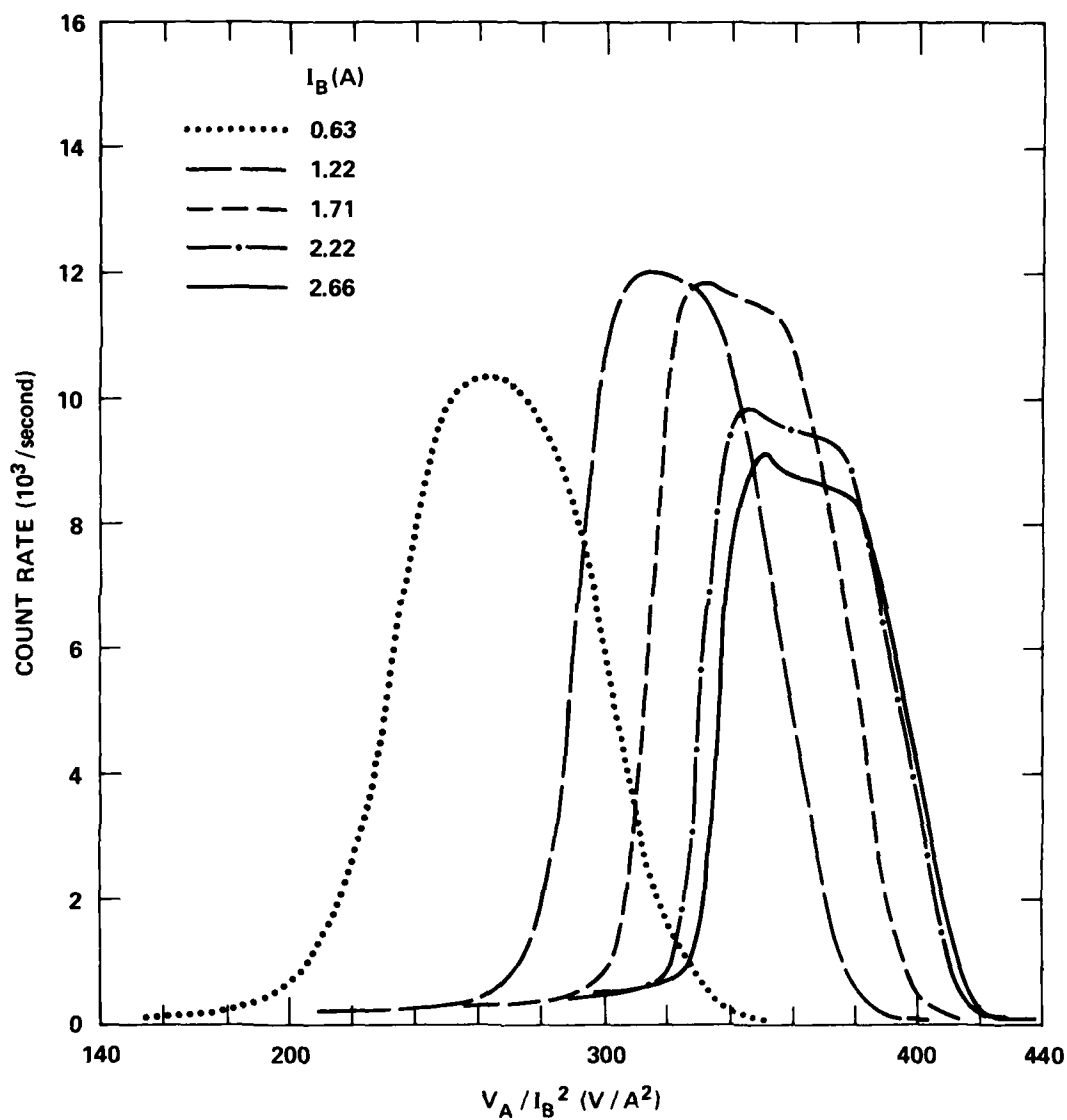
Figure 37 Normalized PESS calibration data with electron count
rate plotted against the ratio V_A/I_B^2 for five
values of I_B

Table 6. Calibration of PESS with Channeltron detector.
Parameter $V_N \equiv V_A/I_B^2$

I_B (A)	0.63	1.20	1.71	2.24	2.66
Peak Count Rate (kc/sec)	10.4	12.0	11.8	9.7	9.0
V_N @ Midpeak	266	322	346	362	367
ΔV_N @ FWHM	72	67	66	65	64
V_A @ Midpeak (V)	106	464	1013	1819	2597
E_e (calculated)	144	523	1061	1821	2568
$P_c \Delta V_N$	749	804	779	631	576
Normalized $P_c \Delta V_N$	0.93	1.00	0.97	0.78	0.72

by the effect of the applied potential on the photoemitter, as mentioned in Section V.B. The secondary-electrons were focused toward the aperture and had a smaller divergence as they passed through, thereby improving the resolution. (The computations of these focused trajectories by SSS are discussed in Section VII). The asymmetric slopes in the data peaks at larger values of I_B were explained by the finite size of the detector aperture. Even with the field focusing of the electron trajectories, the divergence of the electrons along the magnetic field caused them to extend past the top and bottom of the collecting area. As V_A was increased, the orbital radius was larger and there was more spillover.

One problematic aspect was the shift in V_N as I_B was increased. Electron energies were calculated for electron orbits passing through the centers of the aperture and detector; they are compared with the applied voltage at peak count rates in Table 6. There is good agreement only at the higher energies. To explain the discrepancy at smaller I_B, several effects were considered including: stray magnetic field, finite initial energies of the secondary electrons, asymmetrical geometric effects and focusing effects. All of these effects could account for only a quarter of the discrepancy. Finally, at the conclusion of all the spectral measurements, it was discovered that the positive, high-voltage lead to the channeltron had insufficient electrical shielding. The electric field emanating from this wire caused the small perturbation in the trajectories at low electron energies.

An energy resolution ratio, E/E, can be defined as the ratio V_N/V_N. In as much as focusing caused V_N to decrease at larger V_A, an upper limit on the resolution of $E/E < 5.1$ was obtained from the ratio of the maximum values of both V_N and V_N. A value for the energy resolution was also determined from calculations

95

of the range of electron energies intercepted by the detector at a given setting; the derived value was $E/\Delta E = 5.0 \pm 0.2$.

The response of channeltron detectors has been found to be dependent on the energy of the incoming electrons[9] and to be degraded by an ambient magnetic field.[10] A wide range of dependences has been reported, undoubtedly a result of different channeltron geometries and measurement techniques. To determine the influence of a magnetic field on the detection efficiency of the 10-mm-diameter channeltron, its response to x radiation was measured as a function of applied field. It was found that the response dropped off by only 3% at the highest field used for the spectral measurements (40 Gauss), although the response was down by 25% at a field value of 120 Gauss. Channeltrons have a response to electrons of nearly unity at electron energies of several hundred eV. From the results in Table 6, relative efficiencies of the detector were derived and normalized to a maximum value of 0.98 at 0.5 keV. These values are plotted in Figure 38 along with a smooth curve that was fit to the data.

B.   RESULTS

For these determinations of primary-electron energy spectra, the count rate was measured as a function of magnetic-coil current with the photoemitter grounded. The midpoint electron energy, E_e, was calculated from the current, I_B, as given in Table 6. To derive energy spectra, the count rate at each electron energy was divided by $\Delta E = E_e/5$. The spectral yields were then obtained by application of several calibration factors and x-ray intensities were obtained for the location of the photoemitter. The photoemitter area, the solid angle subtended by the electron aperture, and the assumed cosine angular distribution were all the same as used in the analysis of pulsed emission. On the basis of geometry, it was calculated that the height of the rectangular channeltron aperture
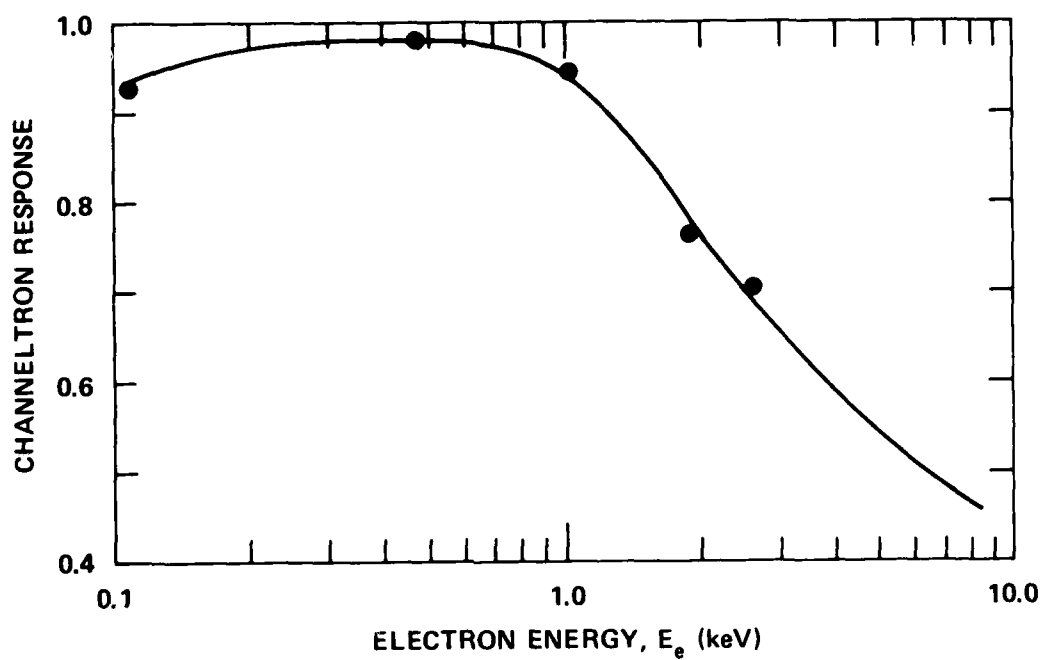
Figure 38   Channeltron detection efficiency as a function of
incident electron energy

97

intercepted 81% of the electron trajectories while the circular-
aperture channel-tron collected 30%. The energy-dependent response
of the rectangular unit to electrons was that shown in Figure 38.

Spectral yields from gold were measured at four photon ener-
gies of 1.49, 2.64, 4.12 and 5.41 keV. Aluminum foil was studied
at 1.49, 1.74, 4.12 and 5.41 keV, and aluminum oxide was studied
at 5.41 keV. The resulting spectral yields are presented in
Figures 39, 40, and 41. All these displayed emission spectra
were rounded and broadened by the instrumental broadening. The
number of counts accumulated for each data point ranged from 50
to 20,000 so that statistical fluctuations provided a significant
error on some data. In particular, the data obtained for aluminum
at 1.49 and 1.74 were initial results using the smaller channel-
tron[11]; both the number of data points and count rates were
quite limited.

The energy spectra of emitted electrons results from a fold-
ing together of the initial electron energies and energy losses
in the emitter, while the measured shapes also reflected the in-
strumental broadening. Initial energies of the emitted Auger elec-
trons and photoelectrons are given in Table 7 for gold, aluminum
and oxygen. If significant carbon contamination were present, its
Auger peak would be at 0.27 keV. Smooth curves were fit through
the data consistent with the appropriate photoelectric and Auger
electron energies to maintain consistency between the results at
different photon energies. At electron energies below 0.5 keV,
the curves were shifted slightly toward lower energies to account
for the small perturbation caused by the high voltage lead to the
channeltron. The few maverick data points falling well away from
the curves are attributed to statistical fluctuations. In all
cases, the spectral yields became very large at low electron energies
under 0.15 keV. It was not determined if this was a real feature
of the spectra or were scattered electrons. Both gold and aluminum

98
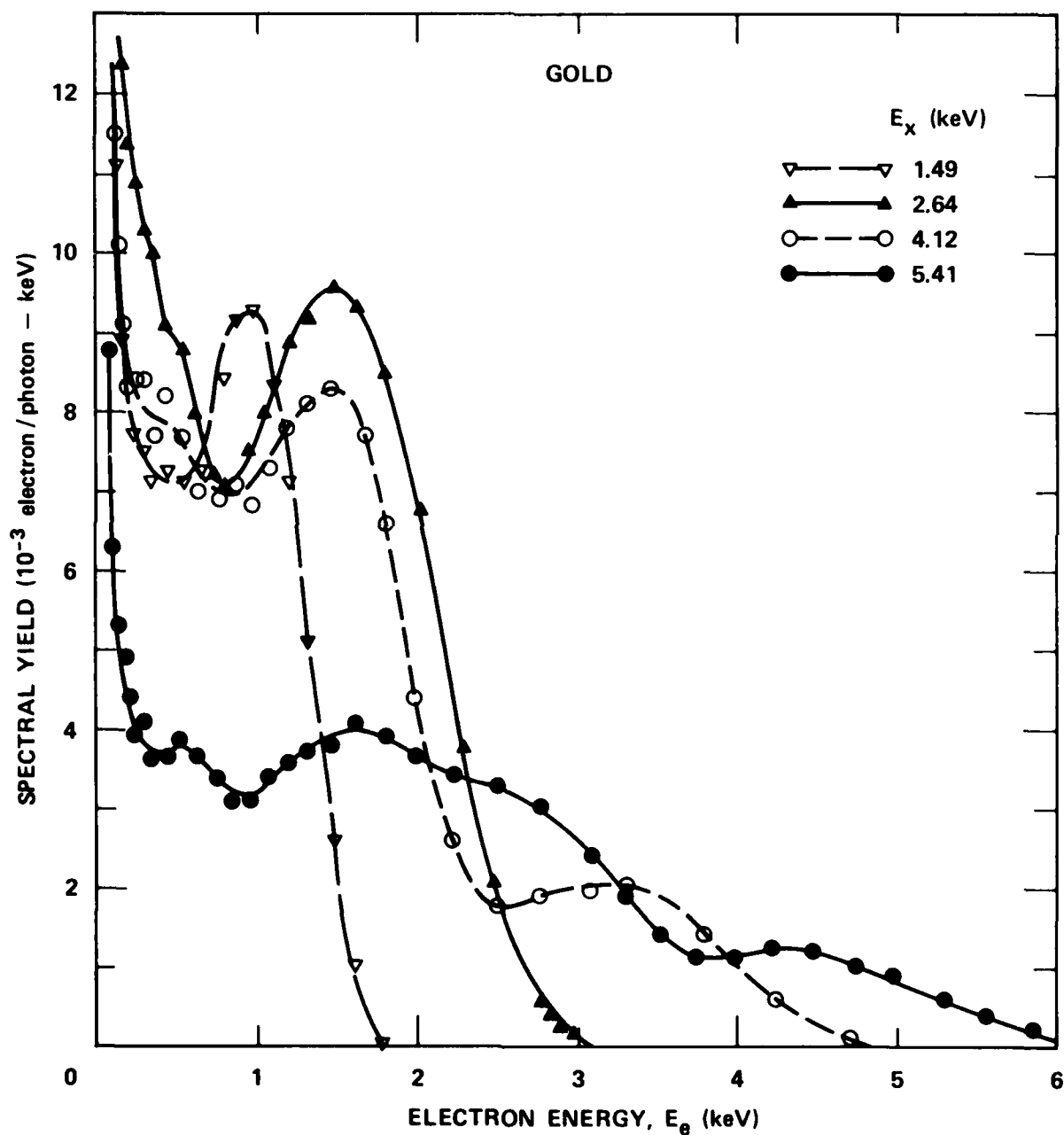
Figure 39   Photoemission spectral yields of primary electrons
             from gold at x-ray energies of 1.49, 2.64, 4.12 and
             and 5.41 keV

99
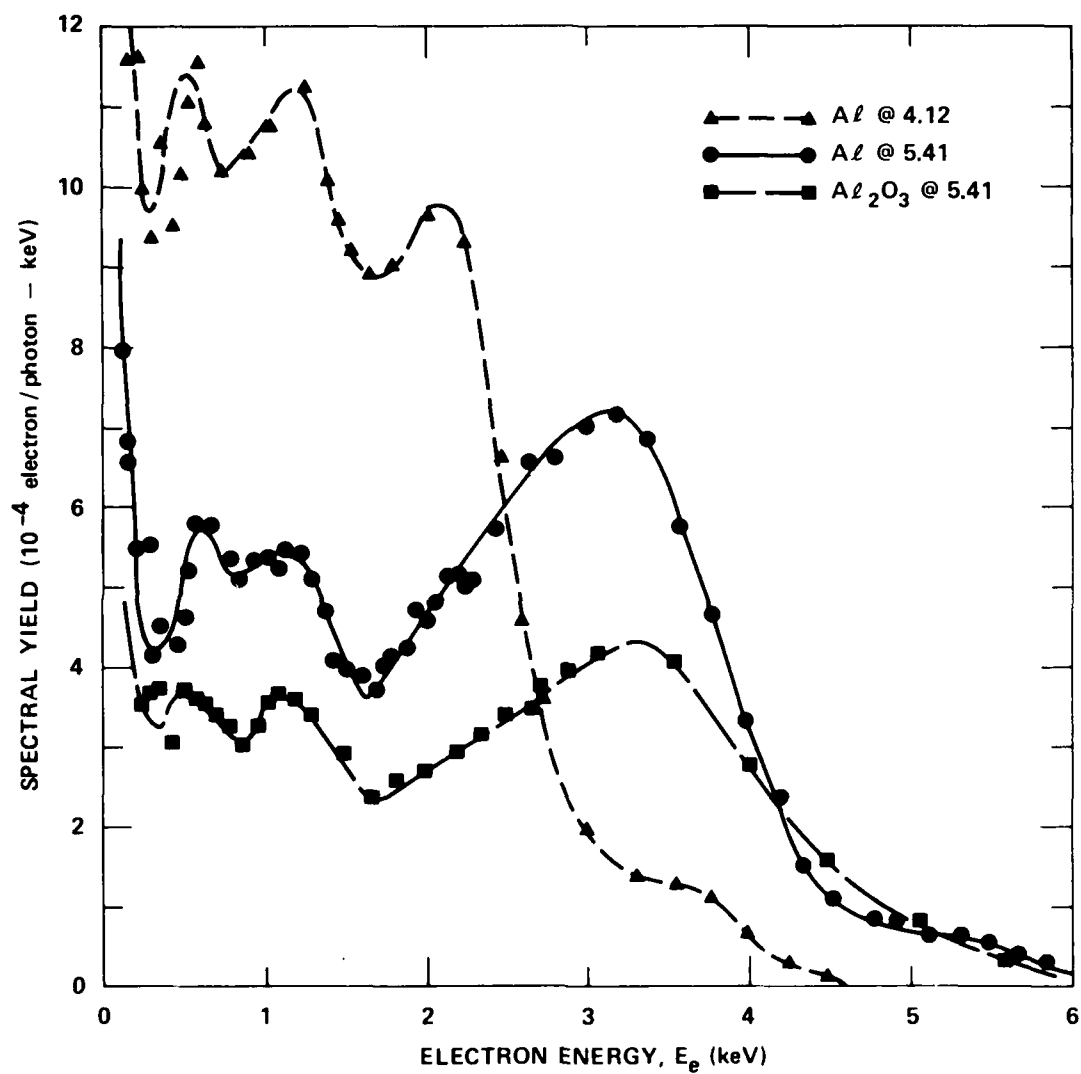
Figure 40   Photoemission spectral yields of primary electrons from aluminum foil and anodized aluminum at x-ray energies of 4.12 and 5.41 keV

100
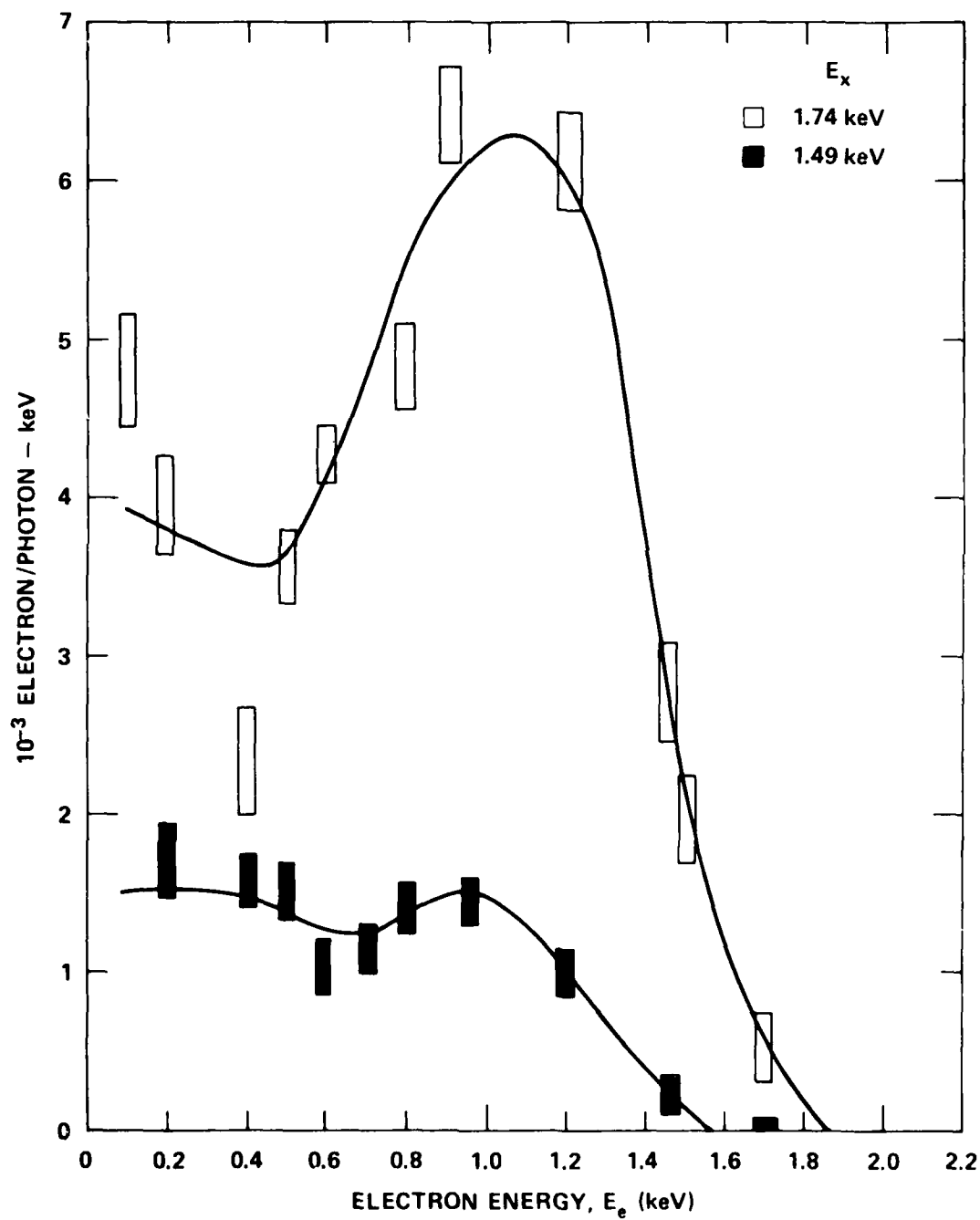
Figure 41   Photoemission spectral yields of primary electrons
from aluminum foil at x-ray energies of 1.49 and
1.74 keV

101

Table 7. Predominant energies of Auger electrons and photo-
electrons from gold and aluminum foil irradiated
by monochromatic X-rays

Auger Electron Energies (keV)

Au	0.02	0.04	0.07	0.15	0.24	0.35
	1.52	1.77	2.02	2.11		

Al	0.04	0.07	1.34	1.39
O	0.50			
C	0.27			

Average Photoelectron Energies (keV)

Element	– Shell	Photon Energy (keV)				
		1.49	1.74	2.64	4.12	5.41
Au	– M	-	-	0.43	1.9	3.3
		-	-	0.34	1.8	3.2
Au	– N	1.1	1.4	2.3	3.7	5.0
Au	– O	1.4	1.6	2.5	4.0	5.3
Al	– K	-	0.18	1.08	2.56	3.85
Al	– L	1.42	1.67	2.57	4.05	5.34
O	– K	0.96	1.21	2.11	3.59	4.88
O	– L	1.48	1.73	2.63	4.11	5.40

do have strong Auger-electron peaks at about 40 and 70 eV. On the
other hand, at very-low magnetic fields, high-energy electrons
could hit the chamber wall and be scattered to the detector.

The spectral yields were integrated to obtain values of pri-
mary-electron yields which are listed in Table 8. For comparison,
the values determined from the birdcage steady-state measurements
are also listed. These integrated spectral yields are in very good
agreement considering the uncertainties in several of the calibra-
tion factors. Only in the case of Al_2O_3 at 5.41 keV was there
a discrepancy of greater than 10%. Slightly better agreement would
be achieved if the channeltron response fell off less with electron
energy above 2 keV than that shown in Figure 38. That would reduce
the spectral yields at the higher energies.

Table 8.   Primary-electron yields from integrated
           spectral yields at given X-ray energies

Yields in Units of 10^{-3} electron/photon

Emitter	E_x (keV)	PESS	Birdcage
Gold	1.49	11.6	11.1
	2.64	19.3	21.4
	4.12	19.3	19.4
	5.31	13.8	13.9
Al foil	1.49	2.0[*]	1.9
	1.74	7.5[*]	7.9
	4.12	2.8	2.85
	5.41	2.3	2.1
Al_2O_3	5.41	1.6	1.28

[*]Data obtained with small channeltron

103

VII   PESS CALIBRATION COMPUTATIONS

In the initial development and usage of the PESS, the photo-
emitter was grounded and the primary electrons were assumed to
follow straight-line trajectories in the region between the photo-
emitter and the aperture. When the goals were extended to deter-
mine the yield of secondary electrons generated by the pulsed
x radiation, it was recognized that the orbits could be greatly
altered by the combined effects of space-charge fields and the
applied potential accelerating the low-energy secondaries.

In order to calibrate the response of the PESS under these
conditions, electron trajectories were computed by Systems, Science
and Software Incorporated (SSS) under subcontract. The scope of
these computations included modeling the complicated geometry of
the PESS, developing a suitable computer program, and calculating
the Faraday-cup currents for several sets of experimental parameters.
This computer program had to handle properly the distributions of
electron energies and emission angles, the finite area of the emit-
ter, and the time-dependent flux.

The computer used for the calculations was a CDC 7600 located
at the Air Force Weapons Laboratory. In spite of the high-speed
capabilities of such a computer, the accuracy of the calculations
was limited because of the huge size of the parameter space. Even
with the development of sophisticated weighting factors, it was
found that a large number of values were needed to approximate the
electron velocity distribution, the spatial distribution and time
steps. A large fraction of the effort was devoted to modeling and
computing space-charge-limited currents such as shown in Figures
18 and 19. Considering the complexity of the problem, the computed
signals agreed very well with the measured currents on a qualita-
tive basis. However, there were significant quantitative differ-
ences as shown in Figure 42; the computed current signals were com-
pared with the measured currents obtained on Shot No. 3632 shown in
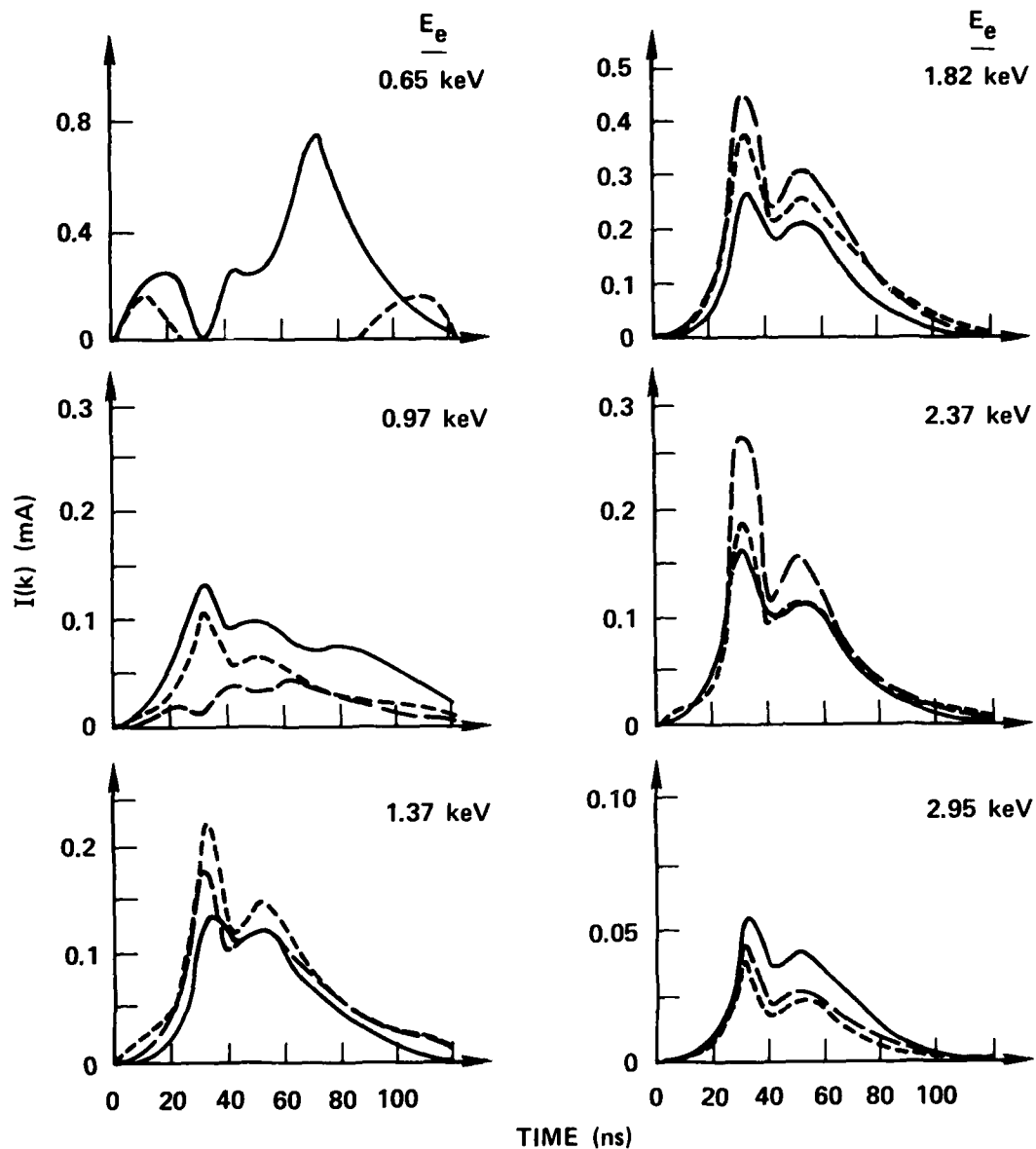
Figure 42   Comparison of measured photoelectron currents in
             Faraday cups (solid) with computations using 10
             energy bins (dashed) and 23 energy bins (dash-dot).
             Measurements were for gold biased at $V_A = -650$
             volts; energies of electrons detected at each cup
             were $E_e - V_A$

Figure 18. The biggest discrepancy was in the third cup detecting
the accelerated secondary electrons, which was of major interest.
It did not appear feasible to push the computations to a greater
accuracy without consuming unreasonable amounts of computer time.
In the meantime, alternate experimental techniques were exploited
for determining the secondary electron yields.

The remainder of the SSS effort was redirected to analyzing
the influence of the applied potential, V_A, on electron trajec-
tories for the case of no space charge effects, which was appli-
cable to the steady-state spectral measurements. For these com-
putations, the secondary electrons were assumed to be emitted
with an energy of 5 eV. To establish the influence of the applied
electric field, two types of angular emission were studied: 1) all
electrons emitted normal to the surface and 2) a cosine distribu-
tion. The fraction of the total emitted electrons passing through
the aperture as a function of applied potential is given in Table 9.
At $V_A = 0$ the fraction for normal emission is just the ratio of
aperture area to emitter area, while for cosine emission the frac-
tion is $1/\pi$ times the solid angle subtended by the aperture. For
normal emission, the applied field causes the electron trajectories
to diverge so that fewer pass through the aperture. But for a
cosine emission, the field focuses the trajectories so a much larger
fraction pass through. The calculations showed a factor of four
increase when $V_A/E_e = 36$. Unfortunately, emitted secondary
electrons have a range of energies from 0 to 20 eV and it would
be necessary to sum over the energy distribution to obtain an
accurate calibration factor for the PESS. This energy distribu-
tion was not known and was expected to be different for each
material. In another vein, if the angular distribution of trans-
mitted electrons were known as a function of position in the aper-
ture, the PESS energy resolution could be calculated. However,
the size of the spatial grid zones was too large to provide an
accurate angular distribution of electrons passing through the
aperture.

Overall, these calculations turned out to be more difficult than many other types of SGEMP/photoemission computations because only a small fraction of the emitted electrons were detected. In addition, the computations needed to be accurate to 10% since the experiments were set up to give accuracies better than 20%.

Table 9. Computed fraction of secondary electrons passing through PESS aperture as a function of applied potential, V_A. The initial electron energy was assumed to be 5 eV for both normal emission and a cosine distribution

V_A (eV)	Normal	Cosine
0	0.37	0.0067
-5	0.14	0.0098
-10	0.10	0.0109
-30	--	0.0151
-180	--	0.0265

VIII COMPARISON OF RESULTS

An important phase of this program was the intercomparison
of the results from the pulsed measurements, steady-state measure-
ments and DNA-sponsored computations of photoemission spectral
yields. The SKYNET experimental results are compared with the
steady-state results first. Then these are compared with the
computational values.

A.   PULSED AND STEADY-STATE YIELDS

To compare the yields from the pulsed-radiation data with
the yields from the steady-state studies, the OWL II' exploding-
wire spectrum was modeled by assuming 40% of the energy at 1.65
keV, 50% at 2.0 keV and 10% at 2.5 keV. The resulting values of
the primary and total yields, in units of 10^{13} electrons per
joule, are listed in Table 10.

Within the stated uncertainties, there was good agreement
between most of the primary-electron yields. The slightly lower
values for the pulsed x-ray data may have been caused by space-
charge effects on the lowest energy electrons. Exceptions to the
good agreement were found for silver, copper and thick Kapton.
The low values obtained from the samples of silver and copper
during the SKYNET measurements may have been the result of con-
tamination; these materials were studied less than many others.
As for the very large primary yield observed from the thick Kapton
during these pulsed x-ray experiments, there was no explanation
found. The extra electrons appeared mostly at lower energies,
as shown in Figure 26.

The total yield values from the pulsed and steady-state measurements were also in good agreement considering the sensitivity of secondary emission to surface composition. A surprising result was the large total yield from 7- m Kapton observed during the SKYNET experiments using different samples mounted on XRDs and in the PESS. This enhanced yield might have been caused by a different distribution of aluminum on the surface.

The spectral yields of photoelectrons from aluminum and gold measured during the pulsed-plasma experiments are consistent with the spectra obtained during the steady-state studies. No attempt was made to synthesize a spectral yield from the monochromatic-x-ray spectral data, as was done in comparing the yields in Table 10, since this would have required a substantial effort beyond the scope of the present program.

Table 10. Comparison of yields from pulsed measurements and steady-state measurements. The steady-state values were derived by modeling the plasma radiation as 40% at 1.65 keV, 50% at 2.0 keV and 10% at 2.5 keV.

Yields (10^{13} Electrons/Joule)

Material	Primary		Total	
	Pulsed	Steady State	Pulsed	Steady State
Aluminum	2.1 ± 0.3	2.35	9.4 ± 0.6	10.8
Al_2O_3	1.4 ± 0.3	1.54	--	8.2
Gold	3.2 ± 0.4	3.45	7.5 ± 0	11.6
Silver	2.1 ± 0.3	2.73	--	10.7
Copper	1.5 ± 0.3	2.71[*]	5.4 ± 0.6	9.7[*]
Glass	1.1 ± 0.3	1.04	2.4 ± 0.6	5.3
Carbon (Aerodag)	0.30 ± 0.1	0.39	1.4 ± 0.2	1.63
Mylar (6 m)	0.42 ± 0.08	0.39	0.9 ± 0.1	0.77
Kapton (7 m)	0.60 ± 0.1	0.56	2.7 ± 0.5	1.24

[*]Values derived from data obtained under an AFOSR Program.

B.   EXPERIMENTAL AND THEORETICAL YIELDS

As a complement to this program, DNA sponsored theoretical
work at Science Applications, Incorporated, (SAI), Vienna,
Virginia, to develop a computer code for calculating spectral
yields generated by soft x rays. This code was used to compute
spectral yields from relevant materials using the OWL II' x-ray
spectrum and at selected monochromatic energies. The integrated
yields of primary electrons are compared with the corresponding
experimental values in Table 11.

For the most part, the computed values agreed reasonably well
with the measured values; the variations ranged from a few percent
up to a factor of two. The largest discrepancies were found for
silver and SiO_2. The computed yields from gold appear to agree
well with the steady-state measurements and disagree with the EWR
results. This might be explained by the neglect of sub-keV Auger
electrons in the computations.

In addition to the integrated yields, the spectra of emitted
electrons can be compared. For the exploding-wire radiator spec-
trum, Strickland and Lin have, in references 1 and 2, compared
their computed spectral yields from Al, Au, Aq and C with the
measured results given in Figures 25 and 26. There was good
agreement for aluminum with the experimental spectrum smoothed
by the instrumental broadening. In the case of gold, the compu-
ted primary yield was larger by 50% as given in Table 11. This
increase in spectral yield was mostly between 1.5 and 2.1 keV when
the instrumental broadening was taken into account. As reflected
in the integrated yields given in Table 11, the computed spectral
yield from carbon was in good agreement with the measured spectrum,
while the silver spectrum was low by about a factor of two over
the entire energy range.

Table 11.   Ratios of computed primary-election yields
(SAI) to measured values (ARACOR) for both
OWL II' exploding wire radiator (EWR) and
monochromatic X-rays.

			X-Ray Energy (keV)				
Material	EWR	1.26	1.49	1.74	2.64	4.12	5.41
Aluminum	1.15	NA	0.74	1.10	1.30	NA	1.24
Al_2O_3	0.87	NA	0.79	1.03	1.04	NA	1.30
SiO_2	NA	NA	NA	0.57*	0.84*	NA	0.67*
Gold	1.52	0.94	NA	1.06	1.26	0.83	0.88
Silver	0.63	NA	0.54	NA	0.45	0.73	0.81
Carbon	1.05	NA	0.86*	NA	NA	NA	0.76*

NA = Not available

*Measured under AFOSR Program

111

In the case of monochromatic x radiation, it turned out that there were only a few common cases between the experimental and theoretical spectral yields. One relevant comparison between the measured and computed results is shown in figure 43 for aluminum oxide irradiated at 5.41 keV. The experimental results are presented twice, once as given in Figure 40 and again with the instrumental broadening empirically unfolded from the data. These experimental and theoretical spectra are in fair agreement, but the computations gave more photoemission in the 2 to 5 keV range and less in the 0.2 to 1.2 keV portion. The spectral yield from aluminum irradiated at 5.41 keV had similar variations between the theoretical and measured results. Apparently the thin layer of oxide on the surface had only a slight effect on the emission, although the oxygen Auger peak was observed.

For the cases of gold irradiated at 4.12 and 5.41 keV, the computed spectral yields were 30 to 50% greater than the experimental yields near the photo- and Auger-emission peaks. And, as with aluminum, the spectra dropped off more rapidly at lower energies. In addition, the computed spectra stopped at 0.5 keV and thus missed Auger peaks of gold at lower energies.
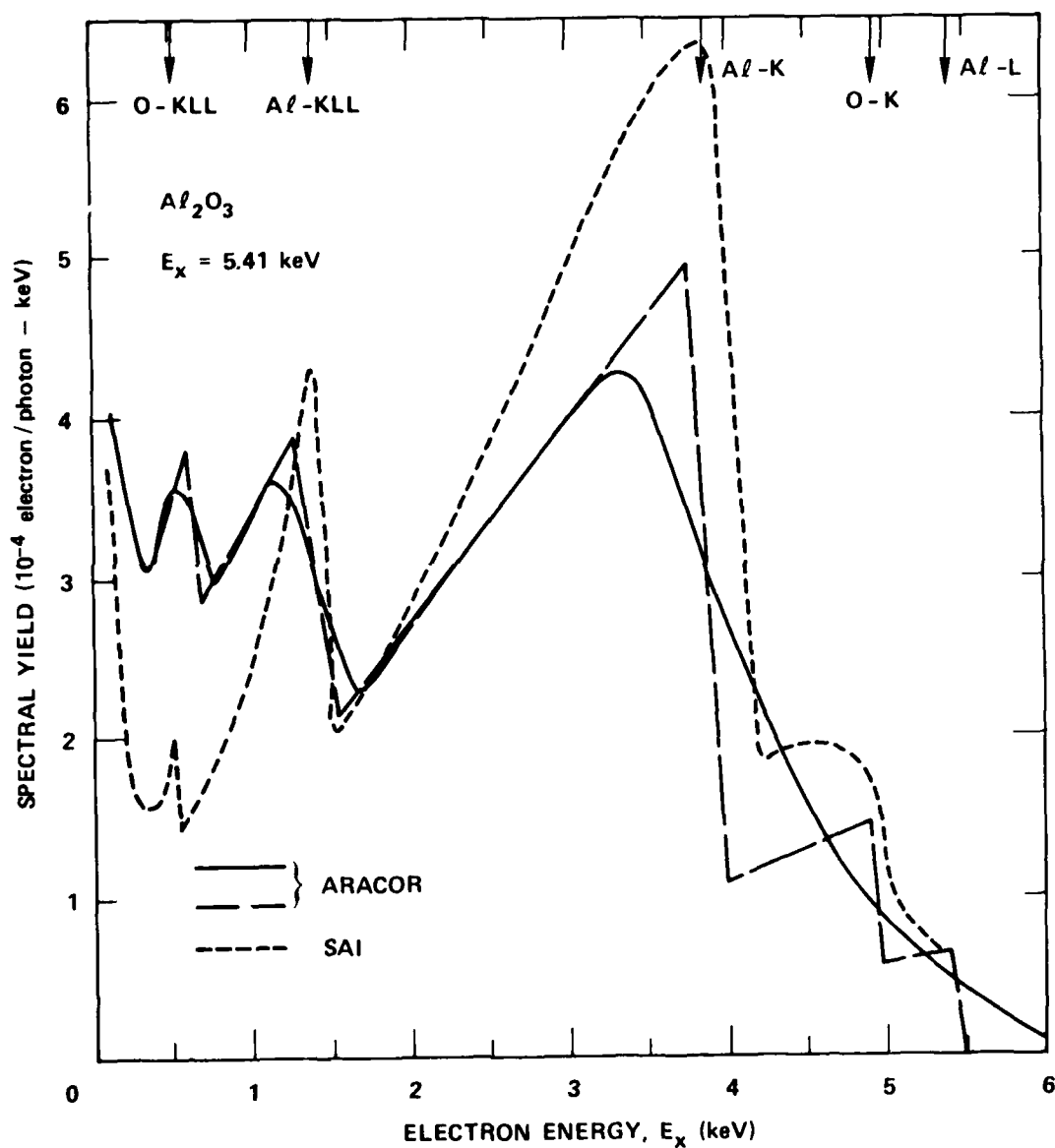
Figure 43   Comparison of experimental and theoretical primary-
electron spectral yields from aluminum oxide irradia-
ted at 5.41 keV.   Solid curve is the data shown in
Figure 40 while the dashed curve is the measured
results after unfolding instrumental broadening

IX CONCLUSIONS AND RECOMMENDATIONS FOR FUTURE WORK

The overall goal of this program was to characterize x-ray-generated photoelectron emission which is the driving term for SGEMP effects. To accomplish this goal, instrumentation was developed and used for both pulsed and steady-state measurements. A magnetic photoelectron spectrometer system, PESS, proved to be a reliable instrument for determining the time-resolved energy distributions and fluxes of primary electrons generated by pulsed-plasma x radiation. The total photoemission yield generated by the pulsed radiation was measured using x-ray diodes. The primary-electron yields and secondary-electron yields, generated by monochromatic steady-state x radiation, were accurately determined using a retarding-potential spectrometer. The PESS was also modified to obtain photoelectron spectral yields using the steady-state x radiation.

These instruments were used to determine photoelectron yields and spectra from several materials relevant to SGEMP analyses and typical of spacecraft surfaces. In addition to the numerous series of SKYNET measurements conducted on the PI OWL II' facility, the PESS was also used on the higher-power DNA Backjack 4 facility at Maxwell Laboratories, Incorporated (MLI). The results of these measurements, that were done as a subtask to MLI as part of the DNA Advanced Concepts Program, demonstrated the usefulness of the PESS for measuring photoelectron spectral fluxes generated by higher-energy x radiation in the 4-6 keV range. During SKYNET experiments the PESS was shown to have a time-resolution capability of better than 2 nanoseconds. A valuable byproduct of the pulsed measurements was the demonstrated capability of the PESS to resolve the time histories of radiation from different plasma states.

The steady-state measurements provided a data base of photo-emission yields from several relevant conducting and dielectric materials at x-ray energies in the 1-6 keV range. To confirm the accuracy and reliability of the PESS operation, the pulsed x-ray results were compared with these steady-state yield values. Good agreement was found in the primary-yield results for several materials, including the conductors aluminum, gold and carbon, and the thin insulators Al_2O_3, glass, Mylar and Kapton. Reasonably good agreement was also obtained in the total-yield values. The spectral yields from gold and aluminum, measured using pulsed radiation, were consistent with the steady-state results at four different x-ray energies.

However, there were some important unresolved questions. The primary-electron yield from the thick Kapton, that was measured using the pulsed radiation, was twice as large as expected and this extra emission was mainly at lower electron energies. The primary-electron spectral yield from the 125-μm-thick Teflon sample was about the same as from this thick Kapton. But there are not yet any steady-state measurements on Teflon for comparison. Another unexplained result was the large secondary-electron yield from the thin Kapton measured during the pulsed experiments.

The overall results of this program indicate that the photoemission characteristics of all relevant satellite materials should be measured. The theoretical values of spectral yields are in reasonable agreement with the measured values; the differences were no more than a factor of two for those materials that could be compared. But, even though a computer code can adequately predict the spectral yield of some common materials, the surface composition and behavior of other materials may be unknown to a substantial degree. This is particularly important with respect to dielectric materials and coatings.

Data that needs to be acquired and results that need re-solving include the following.

1. Investigations of the substantial differences in pulsed photoemission from the different thicknesses of Kapton. It should be determined if the differences arose from different material properties or from surface charging in the experimental apparatus.

2. Steady-state measurements of primary-electron and secondary-electron yields from the thick Teflon, thermal white paint and solar-cell cover glass, all of which were measured under pulsed illumination

3. Steady-state measurements of spectral yields from Kapton, Mylar, Teflon, solar-cell cover glass and carbon. The spectral yield of carbon would extend the data base for photoemission-computer-code development so that there was a large energy range with no absorption edges. This would also be a reference for comparing the photoemission from the spacecraft dielectric materials.

The results of the measured photoemission currents from the biased and unbiased photoemitter suggests this as a convenient method to monitor both the primary and total electron yields gen-erated by intense pulsed x radiation. This technique needs to be refined and exploited during future SGEMP-effects programs.

The anomalies occuring during the pulsed irradiation of some important dielectrics, such as Kapton, suggest that surface charging and other effects could complicate the overall SGEMP response of a spacecraft in other ways. For instance, the magni-tude of secondary - electron emission from a dielectric can play an important role in the initiation of surface breakdown across a charged dielectric. This can be determined by suitably-designed experiments.

116

REFERENCES

1. D. J. Strickland and D. L. Lin, "Soft X-ray Photoemission Properties for the Newly Modeled Materials Gold, Silver, Copper, and Carbon," DNA Final Report (January 1979).

2. D. J. Strickland and D. L. Lin, "The Photoemission Spectrum for an Exploding Wire Radiator Source Incident on Al and Au", IEEE Trans. Nucl. Sci. NS-25, 1571 (1978) and "Photoemission From Ag and C for an Exploding Wire Radiator Source", IEEE Trans. Nucl. Sci. NS-26, 4984 (1979).

3. Colloidal suspension of graphite manufactured by Acheson Colloids Co., Port Huron, Michigan.

4. Manufactured by Amplica, Incorporated, Newbury Park, California.

5. M. J. Bernstein, "Photoelectron Energy Spectra Generated by Low-Energy X Rays from Intense Plasmas", IEEE Trans. Nucl. Sci., NS-24, 2512 (1977).

6. J. N. Bradford, "Absolute Yields of X-Ray Induced Photo-emission from Metals," IEEE Trans. Nucl. Sci. NS-19, 167 (1972).

7. M. J. Bernstein and J. A. Smith, "Primary and Secondary Photo-electron Yields Induced by Soft X Rays", IEEE Trans. Nucl. Sci. NS-26, 4978 (1979).

8. Manufactured by Galileo Electro-Optics Corporation, Sturbridge, Massachusetts.

9. G. Paschmann, et. al., "Absolute Efficiency Measurements for Channel Electron Multipliers Utilizing a Unique Electron Source", Rev. Sci. Instrum. 41, 1706 (1970).

10. Y. B. Hahn, et. al., "Channeltron Gain in Magnetic Fields," Rev. Sci. Instrum. 43, 695 (1972).

11. M. J. Bernstein and J. A. Smith, "Photoelectron Spectral Yields Generated by Monochromatic Soft X Radiation," IEEE Trans. Nucl. Sci. NS-25, 1577 (1978).

DISTRIBUTION LIST

DEPARTMENT OF DEFENSE

Assistant to the Secretary of Defense
Atomic Energy
    ATTN: Executive Assistant

Director
Defense Intelligence Agency
    ATTN: DB-4C

Defense Nuclear Agency
2 cy ATTN: RAEV
4 cy ATTN: TITL

Defense Technical Information Center
12 cy ATTN: DD

Field Command
Defense Nuclear Agency
    ATTN: FCLMC
    ATTN: FCPR

Field Command
Defense Nuclear Agency
Livermore Division
    ATTN: FCPRL

Interservice Nuclear Weapons School
    ATTN: TTV

Joint Chiefs of Staff
    ATTN: J-5 Nuclear Division
    ATTN: C3S Evaluation Office

Director
Joint Strat Tgt Planning Staff
    ATTN: JLA
    ATTN: JLTW-2

National Communications System
Department of Defense
    ATTN: NCS-TS

Undersecretary of Def for Rsch & Engrg
    ATTN: AE
    ATTN: Strategic & Space Systems (OS)

DEPARTMENT OF THE ARMY

BMD Advanced Technology Center
Department of the Army
    ATTN: ATC-O

BMD Systems Command
Department of the Army
    ATTN: BDMSC-H

Deputy Chief of Staff for Rsch Dev & Acq
Department of the Army
    ATTN: DAMA-CSS-N

Electronics Tech & Devices Lab
U.S. Army Electronics R&D Command
    ATTN: DRSEL

U.S. Army Communications Sys Agency
    ATTN: CCM-AD-LB

DEPARTMENT OF THE ARMY (Continued)

Harry Diamond Laboratories
Department of the Army
    ATTN: DELHD-N-RBC, R. Gilbert
    ATTN: DELHD-I-TL

U.S. Army Foreign Science & Tech Ctr
    ATTN: DRXST-IS-1

U.S. Army Missile R&D Command
    ATTN: RSIC

DEPARTMENT OF THE NAVY

Commanding Officer
Naval Research Laboratory
    ATTN: Code 6707, K. Whitney
    ATTN: Code 7550, J. Davis
    ATTN: Code 6701

Officer in Charge
Naval Surface Weapons Center
    ATTN: Code F31

Strategic Systems Project Office
Department of the Navy
    ATTN: NSP

DEPARTMENT OF THE AIR FORCE

Air Force Geophysics Laboratory
    ATTN: PH, C. Pike

Air Force Weapons Lab
Air Force Systems Command
    ATTN: SUL
    ATTN: NT
    ATTN: NXS
2 cy ATTN: DYC

Ballistic Missile Office
Air Force Systems Command
    ATTN: MNNH
    ATTN: MNRTE
    ATTN: MNNG

Deputy Chief of Staff
Research, Development & Acq
Department of the Air Force
    ATTN: AFRDQI

Headquarters Space Division
Air Force Systems Command
    ATTN: SKF

Rome Air Development Center
Air Force Systems Command
    ATTN: ESR, E. Burke

Strategic Air Command
Department of the Air Force
    ATTN: NRI-STINFO Library
    ATTN: XPFS

DEPARTMENT OF ENERGY CONTRACTORS

Lawrence Livermore National Laboratory
    ATTN: Tech Information Dept Library

Los Alamos National Scientific Laboratory
    ATTN: MS 364

Sandia National Laboratories
Livermore Laboratory
    ATTN: T. Dellin

Sandia National Laboratories
    ATTN: 3141

OTHER GOVERNMENT AGENCIES

Central Intelligence Agency
    ATTN: OSWR/STD/MTB, A. Padgett

NASA
Lewis Research Center
    ATTN: N. Stevens
    ATTN: C. Purvis
    ATTN: Library

DEPARTMENT OF DEFENSE CONTRACTORS

Aerospace Corp
    ATTN: Library
    ATTN: V. Josephson

AVCO Research & Systems Group
    ATTN: Library A830

Boeing Company
    ATTN: P. Geren

Ccmputer Sciences Corp
    ATTN: A. Schiff

Dikewood Industries, Inc
    ATTN: Technical Library

Dikewood Industries, Inc
    ATTN: K. Lee

EG&E Wash Analytical Services Ctr, Inc
    ATTN: Library

Ford Aerospace & Comm Corp
    ATTN: A. Lewis
    ATTN: Tech Library

General Electric Co
Space Division
    ATTN: J. Peden

General Electric Company—TEMPO
    ATTN: W. McNamara
    ATTN: DASIAC

Hughes Aircraft Company
    ATTN: Technical Library

Hughes Aircraft Company
    ATTN: E. Smith
    ATTN: W. Scott
    ATTN: A. Narevsky

TRW Defense & Space Sys Group
    ATTN: D. Clement
    ATTN: Technical Info Center

DEPARTMENT OF DEFENSE CONTRACTORS (Continued)

Institute for Defense Analyses
    ATTN: Classified Library

IRT Corp
    ATTN: B. Williams
    ATTN: Library
    ATTN: N. Rudie

JAYCOR
    ATTN: E. Wenaas
    ATTN: Library

JAYCOR
    ATTN: R. Sullivan

Johns Hopkins University
Applied Physics Lab
    ATTN: P. Partridge

Kaman Sciences Corp
    ATTN: W. Rich
    ATTN: Library
    ATTN: N. Beauchamp
    ATTN: D. Osborn

Lockheed Missiles & Space Co, Inc
    ATTN: Dept 85-85

McDonnell Douglas Corp
    ATTN: S. Schneider

Mission Research Corp
    ATTN: C. Longmire
    ATTN: R. Stettnner

Mission Research Corp
    ATTN: B. Goplen

Mission Research Corp-San Diego
    ATTN: V. Van Lint
    ATTN: Library

R & D Associates
    ATTN: S. Siegel
    ATTN: Tech Information Center
    ATTN: L. Schlessinger
    ATTN: R. Schaefer
    ATTN: P. Haas

Rockwell International Corp
    ATTN: Library

Science Applications, Inc
    ATTN: W. Chadsey

Pacific-Sierra Research
    ATTN: H. Brode

Spire Corp
    ATTN: R. Little

SRI International
    ATTN: Library

Systems, Science & Software, Inc
    ATTN: A. Wilson
    ATTN: Library

DATE